# Oxidoreductase and Chaperone Activities Co-opted by Nonenveloped Polyomaviruses During Entry

by

Christopher P. Walczak

A dissertation submitted in partial fulfillment
of the requirements for the degree of
Doctor of Philosophy
(Cellular and Molecular Biology)
in the University of Michigan
2014

Doctoral Committee:

Professor Billy Tsai, Chair
Professor Robert S. Fuller
Professor Michael J. Imperiale
Associate Professor Akira Ono
Assistant Professor Daniel Southworth

**Acknowledgements**

I would like to express my gratitude and appreciation for my mentor Bill Tsai. He has gone to great lengths in teaching me how to think about and do research. His inspiring positivity and enthusiasm for his lab's research couldn't be more ideal for someone in training. Bill has put in a fantastic amount of mentorship throughout my training and has always made time for helpful discussions. I would also like to thank my committee members for their important discussions and guidance.

It has been an excellent experience working with members of the Tsai lab over the years. Together, everyone has made the lab a cooperative, relaxed and fun environment. I feel very fortunate for this. I would like to specifically thank Taka Inoue for his technical help and guidance from the very start.

Finally, I would like to thank my friends and family for their love and support. I would like to especially thank my Dad who has been incredibly supportive throughout my entire life. Very special thanks to my wife/soulmate/genetomate Beth for her never-ending encouragement.

Data presented in Figures 2-2C, 2-2E, 2-2G and 2-5C was generated by Billy Tsai. Figure 3-3G was generated by Takamasa Inoue and Figures 3-4C-E, 3-5 and 3-6 were generated with Madhu Sudhan Ravindran.

## TABLE OF CONTENTS

## LIST OF FIGURES

## CHAPTER 1: Introduction

Viruses are remarkably diverse in the ways they enter a host-cell and cause infection. Membrane coated viruses (i.e. enveloped) enter a host-cell by first binding to a receptor at the plasma membrane. Subsequently, an exposed viral fusion peptide interacts with the cellular components to induce membrane fusion events, which deliver the viral particle or genetic material into the host (1).

Nonenveloped viruses represent a class of pathogens with entry mechanisms profoundly different from enveloped viruses (2). How nonenveloped viruses, containing a proteinacious capsid surface, cross a limiting host-cell membrane is poorly understood. This step in entry, referred to as membrane penetration, is absolutely required for the human pathogenesis caused by several viruses including reovirus, parvovirus, adenovirus and polyomavirus (2).

The necessity of conformational changes or ‘activation’ of viral particles is a reoccuring theme among nonenveloped viruses (2). Host-factors present at specific cellular locations are responsible for inducing these conformational changes. Therefore, nonenveloped viruses need to first be internalized and trafficked to the appropriate region within the cell. For example, rotavirus and adenorvirus are endocytosed and targeted to endosomes (3, 4). For endosome membrane penetration these viruses are activated by proteases or the low pH environment. Structural changes within the capsid permit virus binding to the limiting membrane or release of viral components with lipolytic properties, which ultimately results in the disruption of membrane integrity.

While general principles are known, in many cases the mechanism of membrane penetration is poorly understood. With improved mechanistic insight, this entry

step could be subjected to therapeutic intervention. The research presented in this thesis focuses on understanding membrane penetration by polyomaviruses (Pys).

Human infection by polyomaviruses is nearly ubiquitous but generally remains subclinically latent (5). Several human polyomaviruses are known to cause disease, particularly individuals with weakened immune systems. For example, the very elderly, organ transplant recipients and AIDS patients are susceptible to diseases caused by BK polyomavirus (BKPyV), JC polyomavirus (JVPyV) or Merkel Cell polyomavirus (MCPyV). Affecting a spectrum of host-tissues, Py infections can lead to a diversity of severe pathologies.

BKPyV lytic infection of kidney epithelial cells most prominently causes polyomavirus nephropathy (PVN) in patients receiving renal transplants. Patients with PVN have a 90% chance of allograft loss due to tissue necrosis (6). Approximately 5% of AIDS patients are afflicted by JCPyV lytic infection of oligodendrocites resulting in progressive multifocal leukoencephaloptahy (PML) (7). PML is a rapid neurodegenerative disease resulting in dementia, paralysis and death. Finally, MCPyV was discovered in Merkel Cell Carcinoma (MCC) and appears to play a causal role this rare and very lethal skin cancer (8). As with other human Pys, infection by MCPyV appears to be very common, therefore the factors controlling cellular transformation and the onset of disease warrant intense investigation.

Currently, therapeutics aimed at stopping Py infections and consequences thereof are limited. When patients undergoing organ transplants encounter complications due to reactivated Py infection, the most common course of action is to reduce immunosupressive treatment. This treatment plan can lead to rejection of the transplant organ.

In a laboratory setting mouse polyomavirus (mPyV) and simian virus 40 (SV40) have been used as models to study events during cellular entry. mPyV and SV40 serve as useful models of this family in part due to the ease of their production and their detailed structural characterization. As with other nonenveloped viruses, understanding the virion structure of Pys is essential for unraveling their mechanisms of entry.

**Key Structural Features of Polyomaviruses**

Three primary capsid proteins VP1, VP2 and VP3, comprise the viral particle of most Pys including mPyV and SV40 . MCPyV and perhaps a subset of other related Pys appear to lack VP3 (9). VP1 is the major capsid protein that forms the outer layer of the virus in an icosahedral geometry (10, 11). Each virus contains 360 copies of VP1 that are arranged as 72 pentamers (Figure 1-1A). The icosahedral geometry constructed from pentameric building blocks requires that not all VP1 pentamers share equivalent environments and chemical interactions. 60 pentamers are coordinated by six pentamers and 12 pentamers are surrounded by five pentamers, yielding multiple distinct pentamer interfaces (Figure 1-1B). For example, particularly strong contacts are made at the interface between pentavalent and hexavalent pentamers (11).

Interactions between pentamers are maintained by the C-terminal sequences of VP1. This region is referred to as the C-terminal arm, because it extends away from each pentamer to invade and dock with the core of a neighboring pentamer (Figure 1-2A) (10-12). This interpentameric interaction drives the assembly of pentamers into full capsids, which are then stabilized by additional chemical forces. For example, highly conserved acidic residues on VP1 coordinate calcium ions to help fasten a VP1 arm into a target pentamer.

Covalent disulfide linkages also contribute to overall capsid integrity. SV40 and mPyV contain seven and six cysteine residues respectively. SV40 has no intrapentameric disulfides but does have two interpentameric bonds (Figure 1-

2A). These disulfides are produced by C9 and C104 of one pentamer interacting with the same residues of an adjacent pentamer (i.e. C9-C9 and C104-C104 bonds) (10, 13). No other disulfides on infectious SV40 exist, however, C87 and C207 are important for folding and assembly and may form transient linkages. Crystallography data obtained for mPyV reveals only an intrapentameric disulfide between C19 and C114 (Figure1-2B). Similar to the effect of the aforementioned calcium ions, the positioning of this bond contributes to interpentameric stabilization by reducing the flexibility of the interlocking C-terminal arms. As the C114 residue of mPyV is analogous to C104 of SV40 and is instead used for an intrapentameric bond, it has been assumed that no interpentameric disulfides are present for mPyV. However, structural data are absent for mPyV at the disordered N-terminus of VP1, which contains C11 and C15 (12).

The minor capsid proteins VP2 and VP3 share identical sequences except for an N-terminal extension in VP2 (118 additional residues in the case of SV40). This VP2 N-terminus is myristolyated, hydrophobic and has alpha helical secondary structure. These proteins are buried underneath the VP1 pentamer surface with one VP2 or VP3 associating with a VP1 pentamer (14). Nearly every stage of the life cycle is influenced by the minor capsid proteins including particle assembly, genome packaging and entry. VP2 and VP3 also make contacts with the viral genome.

The ~5 kb dsDNA genome of Py is packaged as a minichromosome with cell-derived histones. This genetic material must reach the nucleus for infection and viral replication to occur. Nonstructural viral proteins capable of modulating intracellular signaling are produced by the host cell's transcription and translation machinery. Large T-antigen (TAg) is the first of these viral proteins expressed and promotes viral DNA synthesis and progression of the cell cycle from the nucleus.

While the complex structure of Py virions confers a resistance to the harsh extracellular milieu, many of the stabilizing forces described above are reversed during the course of host cell entry. This process is referred to as capsid uncoating or disassembly and is necessary for productive infection. As with other nonenveloped viruses, Pys rely on host factors to undergo uncoating at the precise time and cellular localization (2).

**Internalization and Sorting From Endosomes**

To cause infection, the dsDNA genome of Pys must be delivered from outside the host-cell to the cell nucleus. The study of how polyomaviruses enter host cells has historically focused primarily on two members of this family mPyV and SV40. However, the entry of human polyomaviruses such as BKPyV and JCPyV has also been interrogated (15-17). The entry pathway described below can be subdivided into distinct stages. 1) ganglioside receptor attachment at the plasma membrane 2) endocytosis and retrograde transport 3) ER arrival with subsequent conformational changes 4) ER membrane penetration into the cytosol and 5) nuclear import.

The entry of Pys has been studied for over 25 years. A landmark study of SV40 by Kartenbeck et al was the first to describe the unique endocytosis and trafficking of polyomaviruses (18). Although it was unclear at the time, their finding that SV40 particles become localized to the ER is now accepted to be the productive and infectious entry pathway of polyomaviruses. Brefeldin A (BFA) treatment disrupts COPI vesicle formation required for retrograde trafficking to the ER and potently blocks infection of mPyV, SV40, BKPyV and JCPyV(16, 17, 19, 20). Secondly, perturbing ER homeostasis in a variety of ways decreases infection. While this mode of entry is also utilized by some bacterial toxins, trafficking to the ER by Pys is unique among viruses (21).

To enter a cell, most polyomaviruses use direct contact between VP1 and glycolipid receptors called gangliosides on the plasma membrane (22-25). SV40

uses a ganglioside called GM1 and mPyV can use both GD1a and GT1b (24). While some glycoproteins serve to promote cell surface attachment of Pys or as nonproductive decoy receptors (26), gangliosides are well documented to be the entry receptors necessary for productive infection. This is most clearly evident from infection studies utilizing cell lines which lack complex gangliosides and are infected very poorly by Pys. When these cells are provided with purified gangliosides that can be incorporated into the cell surface, infectivity is dramatically restored (24, 27). This restored infectability is concomitant with increased ER localization, as gangliosides appear to drive not only internalization but subsequent vesicle sorting to the ER (28). As gangliosides span only one leaflet of a membrane bilayer, future studies must address the mechanism underlying how a ganglioside-bound virus transduces signals to direct these trafficking events.

The endocytosis of SV40 and mPyV is mostly lipid raft/caveolae-dependent, clathrin-independent (27), however as with other steps in entry there are apparent differences among cell types (29). Notably, JCPyV utilizes a clathrin-dependent entry pathway (30, 31), which is probably related to its apparent use of non-ganglioside entry receptors (32-34). During internalization of viral particles actin molecules undergo transient breakdown and recruitment at the site of endocytosis, where viruses pack tightly in plasma membrane derived tubules (35). Tyrosine kinase activity is also important for endocytosis of Pys (35). Contrary to previous accounts (36), endocytosed SV40 particles do not travel through a pH neutral organelle referred to as the caveosome. The presence of this organelle is an artifact of overexpressed caveolin-1 protein, the primary constituent of caveolae (37, 38). Instead, SV40 and other Pys are slowly transported in a microtubule-dependent retrograde manner through endosomes and lysosomes (28, 39). Pys are not observed in any Golgi compartments during entry, suggesting a Golgi-independent route or rapid viral transit through this organelle (27). Instead, the viral particles are sorted to the smooth ER approximately 5-6 h post-infection in most cell types (13, 28, 36, 39).

**Penetration of the Endoplasmic Reticulum Membrane for Arrival to the Cytosol**

The ER membrane is the limiting cellular membrane that must be breached for Pys to gain access to the cytosol and nucleus. Penetration of the ER membrane could allow direct access to the nucleus, however, several lines of evidence support a model whereby Pys primarily enter the cytosol prior to the nucleus (discussed below). Nonetheless, the ER contains several cellular factors which are co-opted by Pys to accomplish the task of membrane penetration. Intriguingly, these cellular factors are those which normally function in protein quality control (PQC) or aid in protein folding and biogenesis.

The first step in membrane penetration involves the detachment of Pys from gangliosides allowing the virus to be deposited into the lumen of the ER. How this is accomplished is unclear. Upon release into the ER lumen, redox reactions are responsible for partial disassembly of the viral particle. In the case of SV40, a protein disulfide isomerase (PDI) family member called ERp57 is critical for this event (13). ERp57 is normally involved in assisting the folding and maturation of nascent glycoproteins in conjunction with the lectins calnexin (CNX) and calreticulin (CRT) (40). However, ERp57 acts independently of these factors when utilized by SV40. Using an unpaired Cys on VP1, ERp57 acts as an isomerase to disrupt the interpentameric disulfide bonds. This reaction effectively produces new intrapentameric disulfides and releases a subset of VP1 pentamers from the viral particle. The canonical PDI is also important for infection but does not reduce or isomerize disulfide bonds on SV40 during entry. Instead, it may use chaperone activity to promote exit from the ER. The partial uncoating imparted by PDI-mediated reactions, and possibly other factors, results in the exposure of the minor coat proteins VP2 or VP3 (19, 41, 42). As these viral proteins contain hydrophobic moieties that can integrate into the ER

membrane, their exposure enables capsid binding to the ER membrane (43, 44). The process of membrane integration initiates nonenveloped virus membrane penetration.

The capsid of mPyV has a different disulfide bond arrangement than SV40. Therefore, an outstanding question is whether mPyV also uses PDI family members for their oxidoreductase activities. In contrast to SV40, a PDI family member known as ERp29 is co-opted by mPyV to promote infection (43). ERp29 has no documented redox activity but uses chaperone activity to maintain the proper oligomerization state and export of secreted ER proteins (45). In the context of mPyV, ERp29 uses its chaperone function to unfold the VP1 C-termini that stabilize the capsid structure (43). ERp29 requires its C-terminal substrate binding domain and the ability to dimerize to induce these conformational changes to mPyV (46, 47). Importantly, *in vitro* studies reveal that ERp29 exposes the normally buried VP2 capsid protein, allowing the virus to bind to and perforate the ER membrane (48). The *in vitro* assay utilized for the unbiased identification of ERp29 required the use of mPyV that was pretreated with DTT for detection of full unfolding activity (43). Presumably this chemical reductant disrupts viral disulfide bonds that expose or loosen the C-terminal arm for complete unfolding by ERp29. Therefore, the use of an ER reductase or isomerase was hypothesized to be important in mPyV infection. In agreement with this, PDI downregulation blocks mPyV infection in HeLa cells but it was not tested whether PDI engage the virus directly (49).

The research presented in Chapter 2 further explores the requirement of oxidoreductase activities during mPyV infection. Findings from this study suggest that the PDI family members ERp57, PDI and ERp72 are important for mPyV infection. Additionally, ERp57 and PDI are capable of disrupting disulfides on mPyV that are necessary for ERp29-mediated VP1 unfolding. Therefore, PDI family members work in a coordinated fashion to initiate membrane penetration.

After PDI-mediated priming events which lead to VP2 exposure (48), the abundant ER-resident Hsp70 chaperone, BiP, is also critical for Py exit from the ER (44, 50). Loss of function approaches depleting BiP levels from the ER are expected to induce massive cellular stress because BiP is required for protein translocation and folding. However a direct role for BiP in the ER exit of Pys is supported by the detection of physical BiP-SV40 interactions (50). BiP is currently the only ER resident protein known to form a stable complex with Pys in cells. Disrupting the function of BiP cochaperones, which regulate BiP binding activity, also decreases virus arrival to the cytosol without preventing exposure of VP2 (50). BiP is hypothesized to minimize nonproductive interactions by shielding hydrophobic regions of the virus that are not buried in the ER membrane during penetration.

Once hydrophobic Pys have engaged the ER membrane they are recognized by a PQC system known as ER-associated degradation (ERAD) (51). The highly organized process of ERAD begins with the recognition of misfolded or unassembled protein subunits by lumenal chaperones or membrane proteins. The aberrant substrate protein is targeted to specialized machinery on the ER membrane for retrotranslocation into the cytosol for subsequent ubiquitination and proteasomal degradation. Treatment with proteasome inhibitors strongly inhibits successful Py entry (13, 15, 16, 20), originally suggesting the importance of the ERAD pathway in membrane penetration. Proteasome inhibition stalls ERAD and leads to substrate accumulation at all stages of the pathway. Under these conditions ERAD factors, which would otherwise engage Pys, are saturated with misfolded proteins that fail to be degraded normally.

Importantly, siRNA knockdown screens have identified a subset of ERAD membrane proteins that are critical for Py infection, specifically during the ER-to-cytosol transport stage of entry. It is unclear whether Pys breach the ER membrane directly or utilize a large protein channel. Due to their localization, a

thorough characterization of the ER membrane proteins used by Pys is central to understanding the precise mechanism of membrane penetration.

The presence of the ERAD membrane proteins Derlin-1, Derlin-2 and Sel1L is important for entry of Pys. siRNA knockdown of Derlin-1 and Sel1L decreased SV40 infection by approximately 50% (13). Knockdown of Sel1L blocks infection of JCPyV similarly (17). Derlin-1-YFP and Derlin-2-YFP overexpression negatively affects some ERAD pathways by perturbing the structure of endogenous Derlins to which they oligomerize with (52). Overexpression of these variants also perturbs BKPyV and mPyV infection respectively (16, 53). The exact role these proteins serve during membrane penetration remains to be clarified. During ERAD, Derlin proteins recruit cytosolic p97, an ATPase which provides a driving force in the dislocation of substrates into the cytosol (54, 55). Sel1L is a scaffolding protein that allows targeting of misfolded glycoproteins to its primary binding partner, the E3 ubiquitin ligase, Hrd1 (56, 57). The finding that p97 and Hrd1 are not important for SV40 infection further muddles the exact role for Derlins and Sel1L (44). Without supporting evidence highlighting a particular action these factors carry out, the effects produced by their loss of function could be indirect, as with proteasome inhibition.

Recently, some mechanistic insight has been obtained for how ERAD components facilitate membrane penetration. A study by Gieger et al identified important details surrounding the initial recognition of membrane bound SV40 by ERAD machinery (44). Analyses *in vitro* confirmed that conformational changes occur to SV40 that permit membrane binding, with the exposure of VP2 being of primary importance. The N-terminus of VP2 having alpha helical and hydrophobic characteristics becomes integrated with membranes. Yet a conserved charged Glu (E17) residue is also present near the N-terminus of VP2. Mutation of this residue abolishes the ability of SV40 to cause infection entirely. E17 of VP2 is hypothesized to be the signal recognized by a membrane component called BAP31 to initiate retrotranslocation. BAP31, which is

implicated in numerous processes including ERAD, contains two charged residues within a transmembrane domain that are complimentary to E17 in VP2. Therefore, BAP31 may weakly interact with membrane embedded virus electrostatically. Interestingly, virions containing VP2 induced a drastic reorganization of BAP31 into discrete foci containing virus. The functional significance of these structures is not understood and warrants further investigation.

A study by Goodwin et al also identified ER membrane proteins critical for the ER membrane penetration of Pys: DnaJB14 (B14), DnaJB12 (B12) and DnaJC18 (C18) (50). These three factors share 40-50% sequence identity, span the ER membrane once and contain a highly conserved J domain in the cytosol. J domain containing proteins, termed J proteins, typically function as cochaperones to stimulate the ATPase regulated substrate binding of Hsc70s (58). Whether a functional J domain of B14, B12 and C18 is required to facilitate Py infection is not known. B14 and B12 are both implicated in the ERAD of the membrane substrates (59-61). C18 has not been studied in the context of ERAD and may be less important than B14 and B12 for Py infection.

The research presented in Chapter 3 focuses on characterizing the role of B14 and B12 in SV40 membrane penetration. The findings reveal that B14 and B12 are in fact unified with BAP31 in promoting SV40 exit from the ER. Importantly, these J proteins serve to recruit Hsc70 and another cytosolic chaperone called small glutamine-rich tetratricopeptide repeat-containing protein alpha (SGTA) to the ER membrane. Cell based assays suggest that chaperone recruitment and their interactions with SV40 are important for the completion of membrane penetration.

Membrane penetration is completed upon cytosol arrival. Contributing to the enigma of membrane penetration are results from a characterization of cytosol localized viral particles obtained during entry. Remarkably, some SV40 particles

can be observed directly and biochemically to reach the cytosol as large, intact and containing all capsid components (20). Other particles within the cytosol are smaller and have a profoundly distorted shape. Thus, Pys are hypothesized to penetrate the ER membrane intact before they undergo more severe disassembly due to the cytosol's reducing potential and low calcium concentration. This scenario is in line with SV40's genome becoming exposed only upon cytosol arrival (42). Hsc70 chaperones are also known to disassemble mPyV *in vitro* and may assist in this process during entry (62).

Microinjection and biochemical studies support a model whereby SV40 utilizes the cytosolic arrival and classical nuclear import mechanisms for transport of its genome into the nucleus. The microinjection of antibodies against VP1 or VP3 into the cytosol blocks expression of virally encoded TAg in the nucleus (i.e. nuclear import and infection) (63). Cells with SV40 particles microinjected into the cytosol begin to express the viral protein large T-antigen (TAg) successfully within several hours, a widely used experimental readout for infection. When the 'naked' viral genome is microinjected into cells, TAg expression is inefficient, indicating capsid proteins contribute to the nuclear import of the viral genome to which they associate with. Moreover, importin family proteins can be detected in complex with SV40 during entry (64).

Pronounced disassembly in the cytosol is predicted to be important for several reasons. The subviral particle produced in the cytosol would present exposed NLS of capsid proteins and not exceed the size limit of the nuclear pore complex. Moreover, a disassembled particle would permit access of cellular machinery to the viral genome during transcription. *In vitro* experiments notwithstanding, host proteins that aid in this process in cells are unknown.

Why do Pys take such an elaborate path into the host-cell? Clearly, the ER provides an ideal environment for oxidoreductase and chaperone-mediated conformational changes. Also trafficking to the ER and penetrating 'late' allows

for the particles to arrive in the cytosol near the center of the cell, close to the nucleus (65). In some instances, this allows the capsid to avoid the crowded cytoplasmic environment as much as possible. Some portions of the ER, however, are observed near the plasma membrane. It is unclear whether Pys traffic to specific regions or subdomains of the smooth ER for efficient entry. As such a low percentage of virions reach the cytosol, ER membrane penetration appears to be a rate-limiting step of entry. A mechanistic understanding of this transport step could reveal therapeutic targets for preventing diseases caused by human Py infection.

The extensive use of protein quality control factors during membrane penetration by Pys deviates from the mechanisms used by other nonenveloped viruses. This could be in large part due to the unique delivery of Pys to the ER, whereas parvovirus and adenovirus penetrate the endosomal membrane (2). Conformational changes to parvovirus and adenovirus are still critical for pore formation and membrane disruption, however activation events are instead triggered by low pH or proteases (2, 3, 66). In contrast to endosomes, permanent lysis of the ER would cause cell death. Because of this, ER membrane penetration may be a more organized process with additional mechanistic complexity.

This thesis divides the ER-to-cytosol transport step into two stages. Details surrounding the initiation or priming events allowing Pys to bind the ER membrane is presented in Chapter 2. Data presented in Chapter 3 demonstrate that membrane penetration is completed by recruitment of cytosolic chaperones. Finally, conclusions drawn from this research and future directions are presented in Chapter 4.

## FIGURES

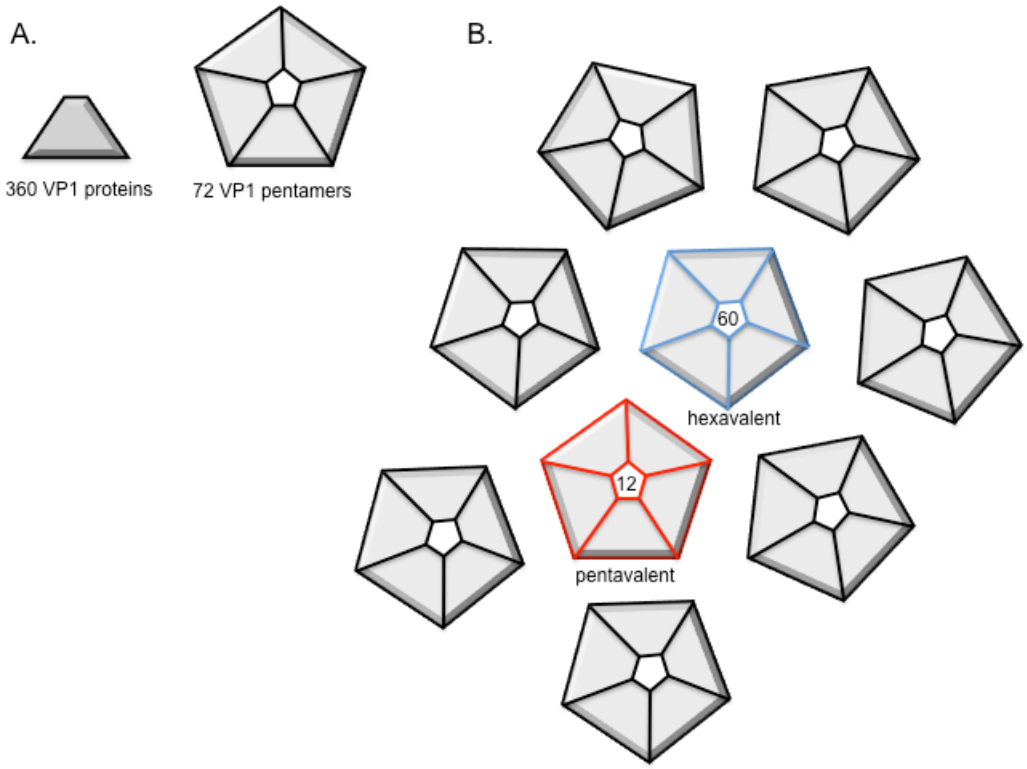


**Figure 1-1. VP1 is the major capsid protein of Pys and has complex arrangement.**

(A) Depiction of VP1 proteins, which assemble from 360 copies into 72 pentamers per virus. One VP2 or VP3 minor capsid protein is buried beneath each pentamer (not shown).

(B) VP1 pentamers have multiple distinct interfaces. 60 pentamers are surrounded by six other pentamers and are referred to as hexavalent (blue). The remaining 12 pentamers, referred to as pentavalent, are surrounded by five pentamers (red).

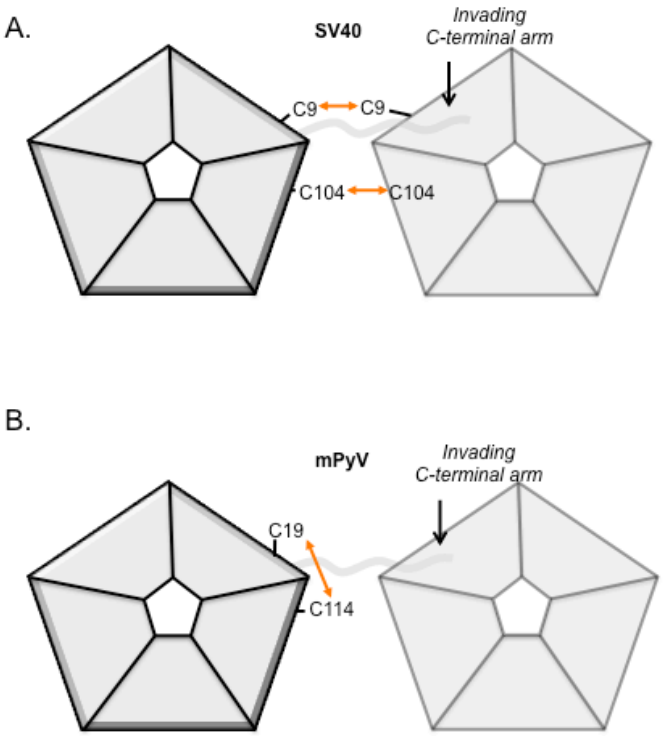


**Figure 1-2. Known interpentameric interactions of model Pys, SV40 and mPyV.**

(A) SV40 contains two types of interpentameric disulfide bonds with cysteine residues in position 9 and 104 interacting with the same residues of a neighboring pentamer i.e. C9-C9 and C104-104 (orange arrows). Due to the distinct pentamer interfaces these disulfide bonds are not always present, for example C104 can also exist in a reduced state. Every C-terminus of VP1 (gray wavy line) extends away from one pentamer, enters a neighboring pentamer and makes hydrophobic contacts.
(B) mPyV lacks known interpentamer disulfides. C114, which is analogous to C104 of SV40, forms an intrapentamer linkage with C19 (orange arrows). This bond strengthens the C-terminus, which again interacts with an adjacent pentamer.

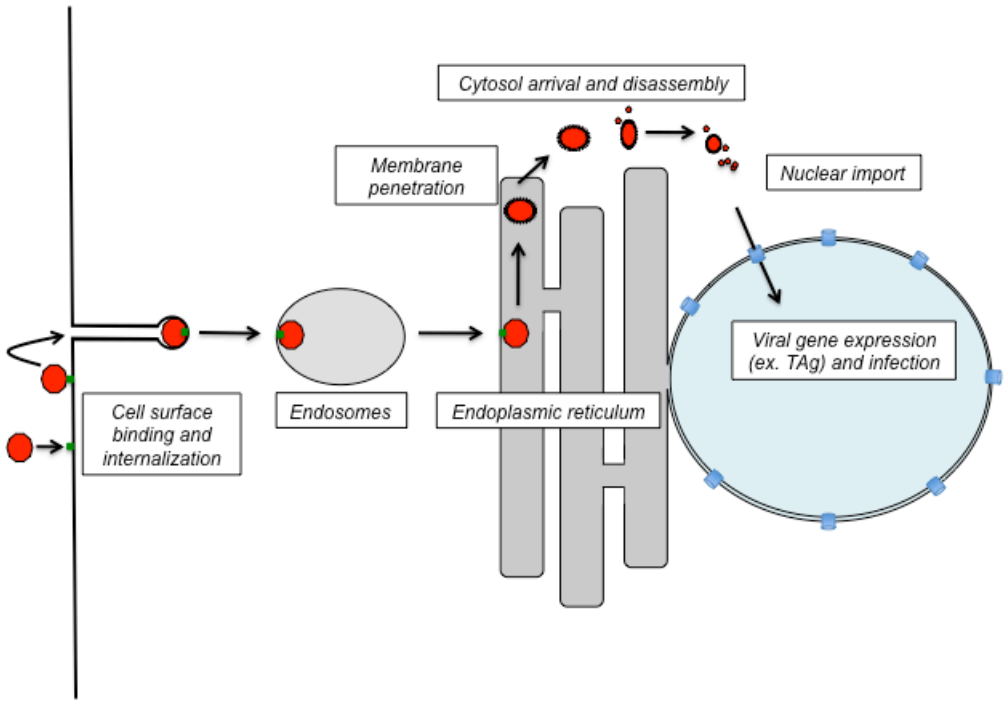


**Figure 1-3. Cellular entry pathway of Pys.**

Pys (red) bind to ganglioside receptors (green) on the plasma membrane to induce endocytosis (far left). Viral particles traffic through endosomes and lysosomes before being sorted to the endoplasmic reticulum (ER). From the ER, conformational changes imparted to the virus permits membrane penetration into the cytosol, where particles arrive large and intact. The reducing conditions, low calcium concentration and presence of chaperones within the cytosol cause disassembly into subviral particles which enter the nucleus using the nuclear pore complex (blue). Viral gene expression stimulates replication and propagation of new viruses.

## REFERENCES


1. Earp LJ, Delos SE, Park HE, & White JM (2005) The many mechanisms of viral membrane fusion proteins. *Curr Top Microbiol Immunol* 285:25-66.

2. Tsai B (2007) Penetration of nonenveloped viruses into the cytoplasm. *Annu Rev Cell Dev Biol* 23:23-43.

3. Wiethoff CM, Wodrich H, Gerace L, & Nemerow GR (2005) Adenovirus protein VI mediates membrane disruption following capsid disassembly. *J Virol* 79(4):1992-2000.

4. Baker M & Prasad BV (2010) Rotavirus cell entry. *Curr Top Microbiol Immunol* 343:121-148.

5. Jiang M, Abend JR, Johnson SF, & Imperiale MJ (2009) The role of polyomaviruses in human disease. *Virology* 384(2):266-273.

6. Binet I*, et al.* (1999) Polyomavirus disease under new immunosuppressive drugs: a cause of renal graft dysfunction and graft loss. *Transplantation* 67(6):918-922.

7. Berger JR (2003) Progressive multifocal leukoencephalopathy in acquired immunodeficiency syndrome: explaining the high incidence and disproportionate frequency of the illness relative to other immunosuppressive conditions. *Journal of neurovirology* 9 Suppl 1:38-41.

8. Feng H, Shuda M, Chang Y, & Moore PS (2008) Clonal integration of a polyomavirus in human Merkel cell carcinoma. *Science* 319(5866):1096-1100.

9. Schowalter RM & Buck CB (2013) The Merkel cell polyomavirus minor capsid protein. *PLoS Pathog* 9(8):e1003558.

10. Liddington RC*, et al.* (1991) Structure of simian virus 40 at 3.8-A resolution. *Nature* 354(6351):278-284.

11. Stehle T, Gamblin SJ, Yan Y, & Harrison SC (1996) The structure of simian virus 40 refined at 3.1 A resolution. *Structure* 4(2):165-182.

12. Stehle T, Yan Y, Benjamin TL, & Harrison SC (1994) Structure of murine polyomavirus complexed with an oligosaccharide receptor fragment. *Nature* 369(6476):160-163.

13. Schelhaas M*, et al.* (2007) Simian Virus 40 depends on ER protein folding and quality control factors for entry into host cells. *Cell* 131(3):516-529.

14. Chen XS, Stehle T, & Harrison SC (1998) Interaction of polyomavirus internal protein VP2 with the major capsid protein VP1 and implications for participation of VP2 in viral entry. *EMBO J* 17(12):3233-3240.

15. Bennett SM, Jiang M, & Imperiale MJ (2013) Role of cell-type-specific endoplasmic reticulum-associated degradation in polyomavirus trafficking. *J Virol* 87(16):8843-8852.

16. Jiang M, Abend JR, Tsai B, & Imperiale MJ (2009) Early events during BK virus entry and disassembly. *J Virol* 83(3):1350-1358.

17. Nelson CD, Derdowski A, Maginnis MS, O'Hara BA, & Atwood WJ (2012) The VP1 subunit of JC polyomavirus recapitulates early events in viral trafficking and is a novel tool to study polyomavirus entry. *Virology* 428(1):30-40.

18. Kartenbeck J, Stukenbrok H, & Helenius A (1989) Endocytosis of simian virus 40 into the endoplasmic reticulum. *J Cell Biol* 109(6 Pt 1):2721-2729.

19. Norkin LC, Anderson HA, Wolfrom SA, & Oppenheim A (2002) Caveolar endocytosis of simian virus 40 is followed by brefeldin A-sensitive transport to the endoplasmic reticulum, where the virus disassembles. *J Virol* 76(10):5156-5166.

20. Inoue T & Tsai B (2011) A large and intact viral particle penetrates the endoplasmic reticulum membrane to reach the cytosol. *PLoS Pathog* 7(5):e1002037.

21. Tsai B & Qian M (2010) Cellular entry of polyomaviruses. *Curr Top Microbiol Immunol* 343:177-194.

22. Gilbert J*, et al.* (2005) Ganglioside GD1a restores infectibility to mouse cells lacking functional receptors for polyomavirus. *J Virol* 79(1):615-618.

23. Erickson KD, Garcea RL, & Tsai B (2009) Ganglioside GT1b is a putative host cell receptor for the Merkel cell polyomavirus. *J Virol* 83(19):10275-10279.

24. Tsai B*, et al.* (2003) Gangliosides are receptors for murine polyoma virus and SV40. *EMBO J* 22(17):4346-4355.

25. Low JA, Magnuson B, Tsai B, & Imperiale MJ (2006) Identification of gangliosides GD1b and GT1b as receptors for BK virus. *J Virol* 80(3):1361-1366.

26. Qian M & Tsai B (2010) Lipids and proteins act in opposing manners to regulate polyomavirus infection. *J Virol* 84(19):9840-9852.

27. Gilbert J & Benjamin T (2004) Uptake pathway of polyomavirus via ganglioside GD1a. *J Virol* 78(22):12259-12267.

28. Qian M, Cai D, Verhey KJ, & Tsai B (2009) A lipid receptor sorts polyomavirus from the endolysosome to the endoplasmic reticulum to cause infection. *PLoS Pathog* 5(6):e1000465.

29. Damm EM*, et al.* (2005) Clathrin- and caveolin-1-independent endocytosis: entry of simian virus 40 into cells devoid of caveolae. *J Cell Biol* 168(3):477-488.

30. Pho MT, Ashok A, & Atwood WJ (2000) JC virus enters human glial cells by clathrin-dependent receptor-mediated endocytosis. *J Virol* 74(5):2288-2292.

31. Querbes W, Benmerah A, Tosoni D, Di Fiore PP, & Atwood WJ (2004) A JC virus-induced signal is required for infection of glial cells by a clathrin- and eps15-dependent pathway. *J Virol* 78(1):250-256.

32. Assetta B*, et al.* (2013) 5-Ht2 Receptors Facilitate Jc Polyomavirus Entry. *J Virol*.

33. Neu U*, et al.* (2010) Structure-function analysis of the human JC polyomavirus establishes the LSTc pentasaccharide as a functional receptor motif. *Cell host & microbe* 8(4):309-319.

34. Elphick GF*, et al.* (2004) The human polyomavirus, JCV, uses serotonin receptors to infect cells. *Science* 306(5700):1380-1383.

35. Pelkmans L, Puntener D, & Helenius A (2002) Local actin polymerization and dynamin recruitment in SV40-induced internalization of caveolae. *Science* 296(5567):535-539.

36. Pelkmans L, Kartenbeck J, & Helenius A (2001) Caveolar endocytosis of simian virus 40 reveals a new two-step vesicular-transport pathway to the ER. *Nat Cell Biol* 3(5):473-483.

37. Hayer A*, et al.* (2010) Caveolin-1 is ubiquitinated and targeted to intralumenal vesicles in endolysosomes for degradation. *J Cell Biol* 191(3):615-629.

38. Parton RG & Howes MT (2010) Revisiting caveolin trafficking: the end of the caveosome. *J Cell Biol* 191(3):439-441.

39. Engel S*, et al.* (2011) Role of endosomes in simian virus 40 entry and infection. *J Virol* 85(9):4198-4211.

40. Oliver JD, van der Wal FJ, Bulleid NJ, & High S (1997) Interaction of the thiol-dependent reductase ERp57 with nascent glycoproteins. *Science* 275(5296):86-88.

41. Daniels R, Rusan NM, Wadsworth P, & Hebert DN (2006) SV40 VP2 and VP3 insertion into ER membranes is controlled by the capsid protein VP1: implications for DNA translocation out of the ER. *Mol Cell* 24(6):955-966.

42. Kuksin D & Norkin LC (2012) Disassembly of simian virus 40 during passage through the endoplasmic reticulum and in the cytoplasm. *J Virol* 86(3):1555-1562.

43. Magnuson B*, et al.* (2005) ERp29 triggers a conformational change in polyomavirus to stimulate membrane binding. *Mol Cell* 20(2):289-300.

44. Geiger R*, et al.* (2011) BAP31 and BiP are essential for dislocation of SV40 from the endoplasmic reticulum to the cytosol. *Nat Cell Biol* 13(11):1305-1314.

45. Das S*, et al.* (2009) ERp29 restricts Connexin43 oligomerization in the endoplasmic reticulum. *Mol Biol Cell* 20(10):2593-2604.

46. Rainey-Barger EK, Mkrtchian S, & Tsai B (2007) Dimerization of ERp29, a PDI-like protein, is essential for its diverse functions. *Mol Biol Cell* 18(4):1253-1260.

47. Rainey-Barger EK, Mkrtchian S, & Tsai B (2009) The C-terminal domain of ERp29 mediates polyomavirus binding, unfolding, and infection. *J Virol* 83(3):1483-1491.

48. Rainey-Barger EK, Magnuson B, & Tsai B (2007) A chaperone-activated nonenveloped virus perforates the physiologically relevant endoplasmic reticulum membrane. *J Virol* 81(23):12996-13004.

49. Gilbert J, Ou W, Silver J, & Benjamin T (2006) Downregulation of protein disulfide isomerase inhibits infection by the mouse polyomavirus. *J Virol* 80(21):10868-10870.

50. Goodwin EC*, et al.* (2011) BiP and Multiple DNAJ Molecular Chaperones in the Endoplasmic Reticulum Are Required for Efficient Simian Virus 40 Infection. *MBio* 2(3).

51. Olzmann JA, Kopito RR, & Christianson JC (2012) The Mammalian Endoplasmic Reticulum-Associated Degradation System. *Cold Spring Harbor perspectives in biology*.

52. Bernardi KM, Forster ML, Lencer WI, & Tsai B (2008) Derlin-1 facilitates the retro-translocation of cholera toxin. *Mol Biol Cell* 19(3):877-884.

53. Lilley BN, Gilbert JM, Ploegh HL, & Benjamin TL (2006) Murine polyomavirus requires the endoplasmic reticulum protein Derlin-2 to initiate infection. *J Virol* 80(17):8739-8744.

54. Ye Y, Meyer HH, & Rapoport TA (2001) The AAA ATPase Cdc48/p97 and its partners transport proteins from the ER into the cytosol. *Nature* 414(6864):652-656.

55. Ye Y*, et al.* (2005) Recruitment of the p97 ATPase and ubiquitin ligases to the site of retrotranslocation at the endoplasmic reticulum membrane. *Proc Natl Acad Sci U S A* 102(40):14132-14138.

56. Christianson JC, Shaler TA, Tyler RE, & Kopito RR (2008) OS-9 and GRP94 deliver mutant alpha1-antitrypsin to the Hrd1-SEL1L ubiquitin ligase complex for ERAD. *Nat Cell Biol* 10(3):272-282.

57. Mueller B, Lilley BN, & Ploegh HL (2006) SEL1L, the homologue of yeast Hrd3p, is involved in protein dislocation from the mammalian ER. *J Cell Biol* 175(2):261-270.

58. Kampinga HH & Craig EA (2010) The HSP70 chaperone machinery: J proteins as drivers of functional specificity. *Nature reviews. Molecular cell biology* 11(8):579-592.

59. Sopha P*, et al.* (2012) A novel mammalian ER-located J-protein, DNAJB14, can accelerate ERAD of misfolded membrane proteins. *Cell Struct Funct* 37(2):177-187.

60. Grove DE, Fan CY, Ren HY, & Cyr DM (2011) The endoplasmic reticulum-associated Hsp40 DNAJB12 and Hsc70 cooperate to facilitate RMA1 E3-dependent degradation of nascent CFTRDeltaF508. *Mol Biol Cell* 22(3):301-314.

61. Yamamoto YH*, et al.* (2010) A novel ER J-protein DNAJB12 accelerates ER-associated degradation of membrane proteins including CFTR. *Cell Struct Funct* 35(2):107-116.

62. Chromy LR, Oltman A, Estes PA, & Garcea RL (2006) Chaperone-mediated in vitro disassembly of polyoma- and papillomaviruses. *J Virol* 80(10):5086-5091.

63. Nakanishi A, Clever J, Yamada M, Li PP, & Kasamatsu H (1996) Association with capsid proteins promotes nuclear targeting of simian virus 40 DNA. *Proc Natl Acad Sci U S A* 93(1):96-100.

64. Nakanishi A, Shum D, Morioka H, Otsuka E, & Kasamatsu H (2002) Interaction of the Vp3 nuclear localization signal with the importin alpha 2/beta heterodimer directs nuclear entry of infecting simian virus 40. *J Virol* 76(18):9368-9377.

65. Lozach PY, Huotari J, & Helenius A (2011) Late-penetrating viruses. *Curr Opin Virol* 1(1):35-43.

66. Farr GA, Zhang LG, & Tattersall P (2005) Parvoviral virions deploy a capsid-tethered lipolytic enzyme to breach the endosomal membrane during cell entry. *Proc Natl Acad Sci U S A* 102(47):17148-17153.

## CHAPTER 2: PDI Family Members Act Distinctly and Coordinately to Facilitate Murine Polyomavirus Infection

### INTRODUCTION

Penetration of the host-membrane represents a decisive step in virus infection. For enveloped viruses that are surrounded by a lipid bilayer this process requires fusion of viral and host membranes, resulting in the delivery of the inner viral particle across the limiting membrane (1, 2). A mechanistic understanding of membrane penetration by nonenveloped viruses is less clear but appears to be fundamentally different. Common principles governing this important process have emerged from several studies within the past two decades.

One central principle involves the ability of the nonenveloped virus to undergo productive conformational changes. These structural changes to the viral capsid may generate a hydrophobic viral particle or release an internal virus peptide harboring intrinsic lytic activity (often called a lytic peptide) buried inside the native virus (3). Disruption of the limiting membrane by this peptide enables virus transport across the membrane. In both instances, the critical trigger for virus transport is the conformational change the viral particle experiences. These structural alterations often occur as a result of concerted or sequential actions among numerous cellular factors acting upon the virus. How the distinct functions of each contributing cellular factor are coordinated to produce the final, penetration-competent capsid is unclear but is likely to be unique to the native structure of the capsid. For efficiency during entry the majority of conformational changes should be imparted precisely at the site of membrane penetration.

For successful infection of a host-cell, the nonenveloped murine polyomavirus (mPyV) binds to the gangliosides GD1a or GT1b and is transported in a retrograde manner to the endoplasmic reticulum (ER) (4-8), where the virus penetrates the ER membrane to access the cytosol. mPyV is ultimately transferred into the nucleus, where transcription and replication of the viral genome leads to propagation of new viral particles. As with other nonenveloped viruses, recent studies imply that the membrane penetration of Pys is a complex event requiring conformational changes within the capsid structure (9-11).

The mPyV capsid is comprised of 360 copies of the major coat protein VP1, which are arranged in a icosahedral geometry of 72 pentamers enclosing a dsDNA genome (12). Twelve of the pentamers are surrounded by five other pentamers (i.e. five-coordinated), while the remaining 60 pentamers are surrounded by six other pentamers (i.e. six-coordinated). Each pentamer associates with a single copy the minor coat protein VP2 or VP3, which are buried from the surface of a native virion (13).

Three reversible forces stabilize the architecture of the viral capsid. First, the C-terminus of VP1 (C-terminal arm) invades a neighboring pentamer (12, 14, 15). These hydrophobic surface contacts effectively stabilize interpentamer interactions. Second, intrapentamer disulfide bonds between cysteine 19 of one monomer and cysteine 114 of another monomer further stabilize the VP1 capsid by ‘clamping down’ on the C-terminal arms (14). Interestingly, the analogous residues in the related simian virus 40 (SV40) form interpentameric disulfide bonds(14). While the X-ray structure of mPyV indicates that C273 and C282 exist unbonded with free thiols, this structure does not provide information on the remaining C11 and C15 residues located at the disordered N-terminus of VP1 (12). C11 and C15 may be fully reduced, form inter- or intrapentameric disulfide bonds or exist as a mixed population dependent on their positioning in relation to neighboring pentamers. Finally, calcium ions are coordinated by acidic residues in VP1 that contribute further to stabilize the capsid (16). Thus, local unfolding of

the VP1 C-terminal arm, disulfide bond disruption, and removal of calcium ions are reactions that destabilize Pys, initiating the uncoating process that prepares the virions for ER membrane penetration.

The host activities responsible for these structural disruptions, however, have not been fully defined. In the case of SV40, the ER-resident PDI family member ERp57 has been reported to isomerize interpentameric disulfide bonds into intrapentameric linkages resulting in the release of a subset of pentamers (17). This modification to VP1 by ERp57 is critical for infection and may contribute to the exposure of internal VP2 or VP3 proteins. For mPyV, an ER resident PDI-like protein called ERp29 was identified to be necessary for infection (11). ERp29 functions to produce conformational changes to VP1 that unfold the C-terminal arms of VP1 and expose the hydrophobic VP2 without global disassembly of the capsid (18). Due to the hydrophobicity of VP2, this remodeling event permits membrane binding by mPyV (11). Interestingly, siRNA downregulation of ERp29 does not appear to inhibit SV40 infection (17). Collectively, these results indicate that PDI protein requirements and virus priming reactions (i.e. viral conformational changes) may vary among different species of polyomaviruses.

In this study, using a combination of cell infection studies and *in vitro* biochemistry, we identify a network of ER-resident protein disulfide isomerase (PDI) proteins called ERp57, PDI, and ERp72 that facilitate infection and act on mPyV's disulfide bonds *in vitro*. Additionally, our data reveal an important role of the previously uncharacterized VP1 C11 and C15 residues during entry.

## MATERIALS AND METHODS

### Reagents

Crude and purified mPyV, NIH 3T3 cells and “M1” VP1 antibody were generously provided by T. Benjamin (Harvard Medical School, Boston, MA). Polyclonal “I-58” VP1 antibody was provided by R. Garcea (University of Colorado, Boulder, Colorado), the polyclonal antibody against ERp29 was a gift from S. Mkrtchian (Karolinska Institutet, Stockholm, Sweden), the polyclonal antibody against ERp57 was a gift from S. High (University of Manchester, Manchester, England), and the polyclonal antibody against Derlin-1 was a gift from T. Rapoport (Harvard Medical School, Boston, MA). The monoclonal antibody against BiP was purchased from BD Biosciences (San Jose, CA). The polyclonal antibody against PDI was purchased from Santa Cruz Biotechnology (Santa Cruz, CA). The polyclonal antibody against ERp72 was purchased from Assay Designs (Ann Arbor, MI). Dulbecco’s modified Eagle’s medium (DMEM), Optimem, Lipofectamine 2000, and 0.05% trypsin-EDTA were purchased from Invitrogen (Carlsbad, CA). Fetalclone III (FC) was purchased from HyClone (Logan, UT). Complete Mini EDTA-free protease inhibitor cocktail tablets were purchased from Roche (Indianapolis, IN). The cross-linking reagent dithiobis succinimidylpropionate (DSP) was purchased from Pierce Biotechnology (Rockford, IL). Reduced and oxidized glutathione, Proteinase K, trypsin, DTT, NEM and anti-FLAG M2-agarose were purchased from Sigma (St. Louis, MO). Calmodulin was purchased from Calbiochem. Micro Bio-Spin P-30 Tris Chromatography Columns were purchased from Bio Rad.

### siRNA Knockdown

Stealth RNAi negative control duplexes (low or medium GC % duplex) were purchased from Invitrogen. Duplex siRNAs corresponding to a segment of mouse PDI (siRNA #1 5’-GCA ACA ACU UUG AGG GUG AUU-3’; 5’-UCA CCC UCA AAG UUG UUG CUU-3’, siRNA #2 5’-GCA ACA ACU UUG AGG GUG AUU-3’; 5’-UCA CCC UCA AAG UUG UUG CUU-3’), mouse ERp57 (siRNA #1 5’-CCA

GCA ACU UGA GAG AUA ATT-3'; 5'-UUA UCU CUC AAG UUG CUG GCT-3', siRNA #2 5'-GCC AGC AAC UUG AGA GAU AUU-3'; 5'-UAU CUC UCA AGU UGC UGG CUU-3'), and mouse ERp72 (siRNA #1 5'-GCA GUU UGC UCC AGA AUA UTT-3'; 5'-AUA UUC UGG AGC AAA CUG CTT-3', siRNA #2 5'-UGA CAA AGA UAC AGU GCU AUU-3'; 5'-UAG CAC UGU AUC UUU GUC AUU-3') were synthesized by Invitrogen. 100 nM (ERp57 siRNA #2, ERp72 siRNA #2) or 200 nM duplexed siRNAs (ERp57 siRNA #1, ERp72 siRNA #1, PDI siRNA #1 and #2) were transfected into 15-30% confluent NIH 3T3 cells using Lipofectamine 2000 according to the manufacturer's protocol. Negative control duplexes were transfected similarly at 100 nM or 200 nM concentrations. Protein expression was assessed by SDS-PAGE and immunoblot analysis at 72 h post-transfection. Infection assays were initiated 72 h post-transfection.

**XBP1 Splicing Assay**

Detection of XBP1 splicing was performed as described previously in reference (19). The forward and reverse primers used were 5' GAA CCA GGA GTT AAG AAC ACG 3' and 5' AGG CAA CAG TGT CAG AGT CC 3' respectively.

**Infection Assays**

Cells treated with the indicated siRNA were plated on glass coverslips 48 h post-transfection at a density of $3 \times 10^4$ cells/well in a 6-well plate. At 72 h post-transfection, crude mPyV (100 PFU/cell) was added to cells in fresh DMEM plus 10% FC. The infected cells were incubated at 37°C for 24 h, washed with PBS, provided with fresh DMEM plus 10% FC, and allowed to incubate for an additional 24 h. Cells were then fixed and stained with a rat monoclonal antibody against mPyV large T antigen and a rhodamine-conjugated donkey anti-rat IgG (Jackson ImmunoResearch, West Grove, PA). In each experiment, at least 500 cells per condition were scored for the absence or presence of nuclear large T antigen expression using standard immunofluorescence microscopy as before (20). A Nikon epifluorescence microscope (Model Eclipse TS100, Melville, NY) equipped with a TexasRed emission filter and a 40× objective was used.

**Production of Recombinant PDI, ERp57, and ERp72**

PDI proteins were expressed and purified as before(21). Full length mouse PDI, human ERp57, and mouse ERp72 containing N-terminal $His_6$ tag were expressed from pQE30 (Qiagen) constructs in *Escherichia coli* strain BL21-pro (Clontech) for 2-4 h at 37°C upon induction with isopropyl thio-β-galactoside (1 mM, Invitrogen). Cells were lysed by incubation in buffer containing 1% Triton X-100, 300 mM KOAc, 250 mM sucrose, 2mM $Mg(OAc)_2$ 50 mM HEPES (pH 7.5) and protease inhibitors, followed by sonication. Lysates were centrifuged, and the resulting supernatant fractions were applied to a nickel nitrilotriacetic acid-agarose column (Qiagen) in the presence of imidazole (20 mM, Sigma). The His-tagged proteins were eluted from the column with imidazole (100, 300 or 500 mM). Eluates containing purified proteins were dialyzed extensively overnight in PBS, frozen in liquid nitrogen and stored at -80°C.

**mPyV Reduction and Isomerization Assays**

Reaction mixtures were incubated for 1 h at 37°C containing the indicated components. Each reaction mixture was subjected to nonreducing SDS-PAGE followed by immunoblotting with an antibody against VP1. In Figure 2B-D, untreated purified Py (100 ng) was incubated in the presence or absence of ERp57 (8 mM), ERp72 (6 mM), or PDI (5 mM). ERp57 (heat-treated) denotes protein heated for 1 h at 95°C prior to incubation with Py. NEM treated ERp57, ERp72 and PDI denotes protein reacted with NEM (10 mM) for 2 h at 37°C followed by overnight dialysis against PBS to remove excess NEM. In Figure 2-3C-D reaction mixtures were treated as in Figure 2-2B-D except virus used was either mock treated or NEM treated as indicated. Where indicated, DTT (5 mM) was added to the reaction mixtures.

**Acid Pre-treatment of mPyV**

WT Py was pre-treated with acidic conditions (pH 5) or neutral conditions (pH 7) as before (6).

**Alkylation of mPyV**

Crude or purified Py was alkylated with NEM (10 mM) for 2 hrs at 37°C or mock-treated. Excess NEM was removed efficiently with subsequent buffer exchange using a spin column (Bio Rad) according to the manufacturer's protocol.

**Trypsin Digestion Assays**

An ER lumenal extract was produced from dog pancreatic microsomes by three freeze-thaw cycles followed by centrifugation of the microsomes at 50,000 x g for 30 min to remove the membrane material. Contents in the supernatant represent soluble proteins in the ER lumen, referred to as an ER lumenal extract. Trypsin digestion assays were performed similarly to those described previously(11). For experiments using crude virus, virus was pretreated with DTT (3 mM) and EGTA (10 mM) for 20 min at 37°C followed by the addition of the ER lumenal extract or BSA (1 mg/ml) and continued incubation for 1 h at 37°C. Reaction mixtures were then treated with or without trypsin (0.25 mg/ml) for 30 min at 4°C. The reaction was stopped by the addition of TLCK (1 mM) for 10 min at 4°C. Samples were analyzed by reducing SDS-PAGE followed by immunoblotting with a VP1 antibody.

For experiments using purified mPyV, an ER lumenal extract enriched for ERp29 was used as described in (11, 18, 22). This extract was pretreated with DTT (1 mM) for 1 h at 37°C followed by 3-6 hr dialysis against PBS to remove excess DTT. Calmodulin was also dialyzed against PBS to remove trace amounts of protease inhibitors. Purified mPyV (50 ng) was first incubated with the indicated protein (10 mM) and EGTA (10 mM) for 1 h at 37°C. An ER lumenal extract (1 mg/ml) was then added to the reaction mixtures and incubated for 30 min at 37°C. Trypsin (0.25 mg/ml) was added next and the incubation proceeded for 30 min at 4°C. The reaction was stopped by the addition of TLCK (1 mM) for 10 min at 4°C. Samples were analyzed by reducing SDS-PAGE followed by immunoblotting with a VP1 antibody.

**Construction of N-terminally FLAG-tagged rat ERp29**

The cDNA of ERp29 was amplified by PCR using a 5'-primer containing the FLAG-tag sequence with pcDNA3.1(+)-rat ERp29 as a template (18). The fragment was inserted into modified pcDNA3.1 (Invitrogen) that contains the ERp29 signal sequence.

**Chemical Cross-linking and Co-immunoprecipitation Analyses**

NIH 3T3 cells were grown to 80-90% confluency on a 10 cm dish before being transfected with constructs expressing rat ERp29 or N-terminally FLAG-tagged rat ERp29 using Lipofectamine 2000 according to the manufacturer's protocol. At 48 h post-transfection, cells were harvested, pelleted and washed twice with PBS. Where indicated cells were treated with the DSP crosslinker or mock treated. DSP dissolved in DMSO (25 mM) was diluted to a concentration of 1 mM into 1.5 ml of PBS, which was used to resuspend cells followed by incubation for 1 h at 4°C. Cells were pelleted and the DSP removed. After washing with PBS, cells were lysed for 30 min at 4°C in a buffer containing 1% Triton X-100 for DSP treated cells or 1% deoxyBigChap for mock treated cells. Cells were centrifuged at 16,000 x g for 15 min and 10% of the supernatant was taken as input. A 30 ml slurry of an anti-FLAG M2 agarose was equilibrated and added to the remaining supernatant and incubated overnight at 4°C. Agarose was pelleted and the supernatant removed before extensive washing. Samples were subjected to SDS-PAGE followed by immunoblotting with the appropriate antibody.

**Mutagenesis of Py and Analyses of WT and Mutant Viruses**

The WT mPyV genome (RA strain) cloned into a PBS vector was generously provided by T. Benjamin (Harvard Medical School, Boston, MA) and used as a template for PCR-based site directed mutagenesis with a QuickChange II site-directed mutagenesis kit from Stratagene (La Jolla, CA). Desired mutations were confirmed by sequencing. The viral genomes were removed from the PBS construct by restriction digest and religated in a dilute reaction. Purified WT or

mutant genomes were transfected into 80-90% confluent NIH 3T3 cells using Lipofectamine 2000 according to manufacturer's protocol. After 24 h, cells were washed and provided with fresh media containing penicillin-streptomycin (Invitrogen). Media containing viral particles was collected 5-7 days post-transfection and used for subsequent infection and *in vitro* experiments. Media containing viral particles was subjected to reducing or nonreducing SDS-PAGE and immunoblotting with an antibody against VP1. Infection assays were performed essentially as described above, treating cells with equal amounts of crude WT or mutant virus as determined by VP1 signal in immunoblots.

**Proteolytic Analyses of WT, Alkylated and mPyV mutants**

Crude WT, mutant, alkylated or mock-treated mPyV was incubated for 30 min at 4°C with various concentrations of proteinase K as indicated. Samples were subjected to reducing SDS-PAGE followed by immunoblotting with an antibody against VP1.

**Native Agarose Electrophoresis of WT and Mutant mPyV**

Crude WT or mutant viruses were mixed with sample-loading buffer without reducing agent or SDS and loaded onto a 0.4% agarose gel. Electrophoresis in 50 mM Tris-acetate (pH 8.1) was carried out at 4°C for at least 3.5 h, replacing the running buffer frequently.

## RESULTS

### Downregulation of ERp57, ERp72, and PDI reduces mPyV infection

We sought to investigate the role of PDI proteins in mPyV infection as they may assist in capsid remodeling events with their oxidoreductase activities. Due to their high levels of expression, we chose to assess the importance of three PDI family members called ERp57, ERp72 and PDI in the entry of mPyV. Each of these PDI family members were individually downregulated in the murine fibroblast NIH 3T3 cells using siRNAs against ERp57, PDI, and ERp72. Immunoblot analysis was first performed using transfected cell lysates at the time of virus addition. In cells treated with the ERp57-specific siRNA **#**1, the ERp57 level decreased with only a subtle increase in expression of PDI and ERp72. (Figure 2-1A, first, second, third, and fourth panel, compare lane 2 to 1). Downregulation of ERp57 did not cause detectable upregulation of two prominent unfolded protein response (UPR) markers BiP and Derlin-1 (23) (Figure 2-1A, 5$^{th}$ and 6$^{th}$ panels, compare lane 2 to 1), indicating that loss of ERp57 did not cause profound ER stress. ERp72 (Figure 2-1A, second panel, lane 3) and PDI (Figure 2-1A, third panel, lane 4) were also downregulated with similar efficiency and specificity. Again, in these cases, BiP and Derlin-1 expression was also not increased. (Figure 2-1A, 5$^{th}$ and 6$^{th}$ panels, compare lanes 3 and 4 to 1).

To further assess whether knockdown of the PDI proteins (using siRNA #1) causes ER stress leading to UPR induction, we monitored the splicing of the XBP1 transcription factor mRNA (19)(Figure 2-1B). In contrast to incubating cells with the known ER stress inducers DTT and tunicamycin (Figure 2-1B, compare lanes 2 and 3 to 1) siRNA-mediated knockdown of ERp57, ERp72 or PDI did not result in splicing of XBP1 (Figure 2-1B compare lanes 4-6 to 2-3). Collectively this data indicates that the three PDI family proteins can be effectively down-regulated without inducing detectable levels of ER stress.

Using the above knockdown conditions, mPyV infection was measured with immunofluorescence microscopy by quantifying the percentage of cells positive for expression of the virus-encoded large T antigen. When compared to scrambled siRNA treated cells, infection was reduced by approximately 40% when each PDI protein was individually knocked down with siRNA #1 (Figure 2-1C, siRNA#1). A similar block in infection was observed when a second distinct set of siRNAs was used to downregulate ERp57, ERp72 and PDI (Figure 2-1C, siRNA#2). When simultaneous downregulation of all three PDI family proteins was attempted, cells appeared unhealthy in their overall morphology and number compared to the scrambled transfected control. When two PDI family members were simultaneously downregulated in all combinations using siRNA #1 (Figure 2-1D, top three panels), ER stress remained undetectable (Figure 2-1D, 4th, 5th, and 6th panels; Figure 2-1E). Under these double knockdown conditions, infection was reduced by at least 60% in all combinations (Figure 2-1F). The average infection decrease is significantly different when comparing single and double knockdown experiments (Figure 2-1G). We conclude that efficient mPyV infection requires multiple PDI family members including PDI, ERp57 and ERp72.

**ERp57, PDI, and ERp72 disrupt disulfide bonds on mPyV *in vitro***

PDI was previously implicated in the infection of HeLa cells by mPyV but it is not known if PDI or PDI-like proteins act directly on the virus (9). Several PDI family members are well documented to oxidize, reduce or isomerize disulfide bonds (24). Therefore, we tested our hypothesis that some PDI family members could act directly on mPyV by disrupting viral disulfide linkages. Mammalian PDI, ERp57, and ERp72 were expressed in bacteria with N-terminal His tags and purified to homogeneity (Figure 2-2A, lanes 1-3). We first examined the activity of ERp57. Purified mPyV was incubated in the presence or absence of ERp57 and subjected to nonreducing SDS-PAGE and immunoblotting with an antibody against VP1. In reactions lacking ERp57, immunoblotting for VP1 did not detect any bands (Figure 2-2B, lane 1). This is indicative of the presence of only unmodified virus, which fully intact is too large to migrate into the gel. By

contrast, band patterns corresponding approximately to the sizes of VP1 monomer (42 kDa), trimer (126 kDa), pentamer (210 kDa), and higher oligomers were observed when mPyV was incubated with ERp57 (Figure 2-2B, compare lane 2 to 1). No pattern was detected when ERp57 was incubated in the absence of virus (Figure 2-2B, lane 5), demonstrating that the signals observed in the presence of virus are virus-derived products.

When ERp57 was denatured with heat prior to incubation with the virus, the various Py-derived species were not seen (Figure 2-2B, lane 3) indicating the conformation of ERp57 is important for this activity. Additionally, the activity of ERp57 was lost upon pretreatment with the alkylating reagent N-ethylmaleimide (NEM) to modify free cysteine residues (Figure 2-2B, lane 4). We conclude that the catalytic cysteine residues of ERp57 can directly disrupt at least some disulfide bonds on mPyV to generate the virus-derived species.

During entry, mPyV traffics through the low pH endolysosome system before reaching the ER (6). As these conditions contribute subtle conformational changes we asked whether pretreatment of mPyV with low pH (i.e. pH 5) could affect the ability of ERp57 to generate the VP1-derived products. However, no significant differences in the amount or size of reaction products were detected (Figure 2-2C, compare lane 2 to 1).

The same pattern of VP1-derived products were also generated when PDI but not NEM-treated PDI (Figure 2-2D, compare lane 1 to 2) was incubated with (but not without) mPyV. PDI also acted on low pH-treated virus with similar efficiency as control virus (Figure 2-2E, compare lane 1 to 2). Finally, the VP1-derived products were produced when ERp72 but not NEM-treated ERp72 (Figure 2-2F, compare lane 1 to 2) was incubated with (but not without) mPyV. Again, pretreating mPyV with low pH did not significantly influence the ability of ERp72 to act on the virus (Figure 2-2G, compare lane 1 to 2). Therefore PDI and ERp72 also use their cysteines to produce the virus-derived products. The ER redox

conditions were mimicked in reactions containing a 1:1 molar concentration of oxidized glutathione (GSSG) and reduced glutathione (GSH) (17). Under these conditions, the VP1-derived products were also generated. We conclude that even under the relatively oxidizing ER conditions, PDI proteins can break disulfide bonds on the mPyV capsid.

**ERp57 and PDI function coordinately with ERp29 to induce conformational changes to mPyV *in vitro***

Previously, we developed an *in vitro* assay utilizing limited proteolysis to monitor conformational changes imparted to mPyV by an activity within an ER lumenal extract (11). Using this assay, a PDI-like protein called ERp29 was identified as a chaperone responsible for unfolding (exposing to protease) the VP1 C-terminal arms that stabilize the viral capsid. Importantly, this unfolding reaction was significantly more efficient upon addition of a reducing agent, presumably to disrupt viral disulfide bonds. To study the potential influence of ERp57, ERp72 and PDI in ERp29-mediated C-termini unfolding, we modified this assay by using an ER lumenal extract enriched with ERp29 and dilute in other PDI proteins.

When mPyV was incubated with bovine serum albumin (BSA) in the presence of DTT and EGTA (to remove the virus-bound calcium) followed by trypsin addition, a VP1-derived fragment, labeled as VP1a, was generated (Figure 2-3A, compare lane 2 to 1). However, when virus was instead incubated with ER lumenal extract, DTT, and EGTA, followed by trypsin addition, two VP1-derived tryptic digest products termed VP1a and VP1b formed (Figure 2-3A, compare lane 4 to 3). The VP1b fragment was previously identified as a fragment that lacks the C-terminus of VP1 and forms only when ERp29 is present within the extract (11).

Can ERp57, PDI, or ERp72 functionally replace the chemical reductant DTT? mPyV was pretreated with either the redox-inactive calmodulin, ERp57, ERp72, or PDI in the presence of EGTA. The samples were then incubated with an ER lumenal extract enriched for ERp29, followed by trypsin addition. Our results

show that VP1b was generated only when mPyV was pretreated with either ERp57 or PDI, but not with calmodulin or ERp72 (Figure 2-3B, compare lanes 2 and 4 versus lanes 1 and 3). The ERp29-enriched lumenal extract lacks ERp57 and PDI (Figure 2-3B, compare lane 6 to 5), explaining the requirement of these proteins in this reaction. NEM-alkylated ERp57 and PDI were not able to assist the lumenal extract in generating VP1b (Figure 2-3C, compare lane 2 to 1 and lane 4 to 3). As expected, the catalytic activities of ERp57 and PDI are required for replacing DTT to produce VP1b. We conclude that ERp57 and PDI act coordinately with ERp29 to extrude the VP1 C-terminal arm. We note that the lumenal extract used in this reaction was pretreated with DTT, and the excess DTT in the extract removed thoroughly by dialysis (see discussion).

We next investigated if these PDI family members could be isolated in cells as a complex or if they partition into distinct compartments within the ER. Cells expressing untagged or FLAG-tagged ERp29 were subjected to immunoprecipitation with anti-FLAG agarose beads. FLAG-ERp29 precipitates also contained detectable amounts of ERp57 (Figure 2-3D, lane 3 versus lane 1 and 3). PDI and ERp72 were detected similarly (Figure 2-3E). However, these interactions were only detected in cells treated prior to lysis with the membrane permeable crosslinker dithiobis succinimidylpropionate (DSP). This result indicates that the detected interactions are weak and transient or detergent-sensitive. Nevertheless, ERp29 may exist within a network of other PDI proteins to function coordinately.

**ERp57 principally isomerizes mPyV, while PDI and ERp72 reduce the virus *in vitro***

We next assessed the requirement of free thiol groups on the VP1 cysteines of mPyV during infection. To this end, mPyV was modified with the alkylating reagent NEM (NEM reacts with and irreversibly modifies free thiol groups) or mock treated prior to being subjected to a desalting spin column to remove the excess reagent. We found that the infection efficiency of the NEM-treated Py was

severely attenuated compared to mock, WT Py (Figure 2-4A). Protein unfolding or changes in structural integrity can result in an increased sensitivity to proteolysis. Limited proteolysis of NEM-treated and WT Py revealed almost identical sensitivity to proteinase K (Figure 2-4B, compare lanes 5-8 to lanes 1-4), suggesting that NEM did not grossly disrupt the structural integrity of the virions. Thus, similar to observations with SV40 (17), free cysteines in mPyV are critical for infection.

The requirement of free thiol groups on mPyV during entry prompted us to investigate if they are utilized by ERp57, PDI or ERp72 for isomerization reactions. In disulfide isomerization reactions the intermediate mixed disulfide formed between the enzyme and substrate is resolved by a thiol present on the substrate. By contrast, a reduction reaction only requires a free cysteine on the enzyme to resolve the intermediate. To test whether free cysteines on mPyV are required for ERp57 to disrupt viral disulfides, WT and NEM-treated virus were incubated with ERp57 and reaction products analyzed as before with nonreducing SDS-PAGE. Immunoblot detection of VP1 higher oligomer, pentamer, trimer, and to a lesser extent monomer, was diminished markedly when ERp57 was incubated with the NEM-treated Py compared to WT Py (Figure 2-4C, compare lane 4 to 2). DTT treatment of WT and NEM-treated virus produced a similar VP1 monomer level (Figure 2-4C, compare lane 5 to 6), demonstrating equivalent amounts of WT and NEM-treated virus was provided in the reactions and that both virus types display the same sensitivity to a small chemical reductant. We conclude that ERp57 primarily uses an isomerization reaction to disrupt VP1 disulfides.

PDI (Figure 2-4D, compare lane 4 to 2) and ERp72 (Figure 2-4E, compare lane 4 to 2) were observed to generate mPyV-derived species potently regardless of whether they were incubated with WT or NEM-treated virus. The prominent 72 kDa band that appeared in Figure 2-4E (lanes 2 and 4) was also present in a sample without Py, indicating that the VP1 antibody used in this immunoblot (i.e.

M1) cross-reacts with ERp72. As free cysteines in the Py were not necessary for the PDI- or ERp72-dependent reactions, PDI and ERp72 function here as reductases. Notably, ERp57 also functions as an isomerase on SV40 (17).

**Characterization of the C11A, C15A, and C11A:C15A Py mutants**

Our findings indicate that similar to SV40, mPyV requires free thiols for infection and can be isomerized by ERp57. Isomerization of SV40 results in the disruption of interpentameric C9-C9 bonds. We asked whether two uncharacterized analogous cysteines on mPyV, C11 and C15, were important for infection or contributed to capsid stability.

Mutant viruses were produced containing either single or double cysteine to alanine mutations of C11 and C15. We first compared their ability to cause infection with WT mPyV. When similar amounts of WT and mutant viruses were used (Figure 2-5A, lanes 1-4), infection by all three mutants was compromised by approximately 50% compared to WT Py (Figure 2-5A, right panel). Limited proteolysis demonstrated that all three mutant viruses displayed a similar protease sensitivity pattern as WT Py (Figure 2-5B, compare lanes 5-8, 9-12, and 13-16 to lanes 1-4). Additionally, when subjected to a native agarose gel system these mutant virions appeared large and intact as they migrated similarly to WT mPyV (Figure 2-5C, compare lanes 2-4 to 1). Next we analyzed the mutant and WT mPyV by nonreducing SDS-PAGE. Strikingly, only the C11A:C15A double mutant released higher oligomer VP1 products into the gel (Figure 2-5D, compare lanes 4 to 2-3). These findings demonstrate that C11 and C15 are important during infection and are collectively involved in interpentamer disulfides of at least a subset of pentamers.

## DISCUSSION

For successful infection of a target host, nonenveloped viruses must penetrate a biological membrane to gain access to the cytosol or nucleus. A common theme emerging is the role of conformational changes induced to the viral capsid at the site of membrane penetration (1, 3). These conformational changes can be imparted by a variety of cellular factors including low pH, proteases or chaperones. Multiple cellular factors in concert are hypothesized to be needed to accomplish structural changes that facilitate penetration. This current study provides evidence for multiple ER-resident PDI proteins inducing distinct conformational changes to mPyV necessary for ER membrane penetration.

We utilized an siRNA knockdown strategy to assess the importance of three PDI family members in mPyV infection of mouse fibroblasts. Loss of ERp57, ERp72 and PDI individually resulted in a moderate block in infection. Double knockdown of multiple PDI proteins blocked infection more severely, implicating these proteins as important for mPyV entry. The precise reason for only a moderate reduction of infection upon single knockdown is unclear but may be due to incomplete knockdown, functional redundancy among PDI proteins or as yet undescribed compensatory mechanisms. However, the loss of PDI proteins did not cause ER stress supporting their direct role in promoting infection as opposed perturbed infection due to global ER dysfunction.

Similar to mPyV, SV40 requires ERp57 and PDI for successful infection (17). Interestingly, there appears to be no requirement for ERp72 and ERp29 during SV40 infection. While mPyV and SV40 closely share structural characteristics, their disulfide bond arrangements are clearly different (14, 16, 25). SV40 contains two distinct interpentameric disulfide bonds and no intrapentameric bonds. The crystal structure of mPyV reveals only an intrapentameric bond. This difference between SV40 and mPyV may account for the use of different PDI proteins for conformational changes and partial capsid disassembly. The relative

concentration of specific PDI proteins within a cell type is also likely to contribute to the selection of these host-factors by Pys for membrane penetration.

Using purified components *in vitro*, we found that ERp57, ERp72 and PDI could engage mPyV directly by disrupting disulfide bonds within the capsid. Using a nonreducing SDS-PAGE system, VP1 reaction products released from intact viruses incubated with PDI proteins could be visualized. These products migrated at approximately the size of VP1 monomers, trimers, pentamers and higer oligomer species. VP1 monomers could be formed when each intrapentameric disulfide is disrupted within a pentamer. In reactions containing ERp57 and ERp72 we observed a doublet pattern for monomer sized VP1 products. It is unclear exactly how this monomer doublet is formed. The appearance of a doublet could represent newly formed intramonomeric disulfide bonds that occur during isomerization reactions that are mediated by the enzymes or incidentally by free thiols on other VP1 molecules released after initial disulfide disruption.

VP1 trimers but not dimers or tetramers were produced by PDI proteins. The VP1 trimers released from the viral particle could originate from a single pentamer with two intrapentameric disulfide disruptions. Similar to the doublet appearance of some monomer products, the trimer species does not migrate at a distinct molecular weight. This observation is indicative of a mixture of trimers containing different amounts of intramolecular disulfides. VP1 trimers may be more stable than tetramers and dimers. VP1 dimers and tetramers may be easily cleaved into monomers and trimers respectively by reactive cysteines on PDI proteins or newly freed thiols on VP1 itself. Initial disruption of mPyV disulfides may influence the accessiblity of other linkages or modify the VP1 surfaces where PDI proteins can interact.

Higher oligomer VP1 species may reflect relatively intact viral particles that have lost a subset of VP1 pentamers or clusters of VP1 pentamers that remain connected but are freed from the bulk of the particle. The latter scenario

suggests the presence of interpentameric disulfides, as SDS used in our analysis of released VP1 products would disrupt most noncovalent interactions. This hypothesis is supported by our mutagenesis study of the uncharacterized C11 and C15 residues on VP1 (discussed below).

Although each PDI family member analyzed in this study liberated nearly identical VP1 products when incubated with mPyV, we identified mechanistic differences in their activity. PDI and ERp72 act on mPyV with reductase activity while ERp57 principally uses isomerization, a reaction requiring free cysteines on the virus. The precise mechanisms used by PDI, ERp72 and ERp57 in promoting infection in cells is unknown. Cell based assays monitoring disulfide disruption during mPyV entry have been unsuccessful due to the low percentage of viruses (5%) reaching the ER from the plasma membrane (6). Alkylated mPyV, which cannot be isomerized by ERp57 *in vitro*, fails to infect cells. We hypothesize that ERp57, and possibly other PDI family members, isomerize mPyV in cells similar to the required ERp57-mediated isomerization during SV40 entry (17).

Despite the finding that ERp57, PDI, and ERp72 can individually engage mPyV to form the virus-derived species, only ERp57 and PDI cooperate with ERp29 to unfold the VP1 C-terminal arm (11). This ERp29-induced conformational change yields a hydrophobic viral particle competent for membrane binding to initiate penetration. Although PDI uses a chaperone activity to cause unfolding of cholera toxin (CT) to initiate the toxin's retrotranslocation into the cytosol (26), the catalytic activity of PDI (and ERp57) is instead required to assist ERp29 in unfolding the VP1 C-terminal arm. As there are both pentavalent and hexavalent pentamers, it is possible that the ERp57-PDI-ERp29 network acts on one of these two types, while ERp72 engages the other type. Detection of the ERp29-mediated conformational change relies on a limited proteolysis approach. Therefore, ERp72 may also appear to fail in cooperating with ERp29 if it binds and protects the region within VP1 that is normally exposed to trypsin digestion.

ERp72 appears to bind tightly to CT to prevent its proteolysis in a similar assay (27).

The necessity of multiple chaperone and enzymatic activities for capsid remodeling events may be due to the complexity of VP1 arrangement and pentamer interfaces on the capsid surface. This asymmetry likely allows the C11 and C15 residues, which are absent from structural data, to exist in a mixed population of oxidized and reduced states. This appears to be true for C104 of SV40 which exists in both reduced and disulfide bonded states. We produced mutant viruses to characterize C11 and C15 of mPyV. Both single and double mutants had reduced infection compared to WT virus. It is unclear why the double mutant did not have a more severe defect in infection compared to single mutants. This discrepancy may be related to a functional heterogeneity in these residues. For example, the double mutant may have a distinct defect from the single mutants while obtaining an advantage from bypassing the need to form an intermediate.

When analyzed by nonreducing SDS-PAGE, VP1 higher oligomers were generated only from the double C11A:C15A mutant. This finding demonstrates that C11 and C15 stabilize interpentamer interactions for a subset of the pentamers, possibly by forming interpentamer disulfide bonds. If these residues do not stabilize all interpentameric interactions because VP1 pentamers would appear instead of higher oligomers . Mutating a single cysteine did not generate the higher oligomers, indicating that the potential interpentamer disulfide linkages could exist between two C11 residues and two C15 residues. C11 on mPyV is analogous to C9 of SV40, which forms C9-C9 interpentamer disulfides. Due to the two types of pentamer geometries, some pentamers are situated in a different local environment than others. While it has not been formally ruled out, we consider it unlikely that C11 and C15 stabilize interpentamer contacts in a reduced state, coordinating $Mg^{2+}$ or $Ca^{2+}$ ions for example. Viruses alkylated with

NEM did not release these higher order species when subjected to nonreducing SDS-PAGE.

In addition to the PDI proteins described in this study, other ER components may act on mPyV to allow the virus to initiate membrane penetration. It is interesting to note that in the *in vitro* trypsin digestion assay, ERp57 or PDI added in combination with a reduced ERp29-enriched ER lumenal extract (which lacks ERp57 and PDI) generated VP1b. The need for reducing the ERp29-enriched lumenal extract in this reaction suggests that ERp29 in the extract must be in the reduced form to unfold Py (ERp29 contains one cysteine). Indeed, there is precedence for the redox state of a PDI protein controlling its chaperone unfolding activity (26, 28). Alternatively, additional reductases or isomerases in the extract may be involved in producing a penetration-competent viral particle. Further experiments are required to distinguish these possibilities.

In conclusion, our study highlights a complex interplay between viral cysteine residues of mPyV and host reductases, isomerases, and chaperones of the PDI family. These reactions promote transport of the virus from the ER into the cytosol, a pivotal infection step. The versatility of PDI family members to engage a complex endogenous proteome may be the reason why Pys have evolved to hijack their activities for successful infection.

## FIGURES

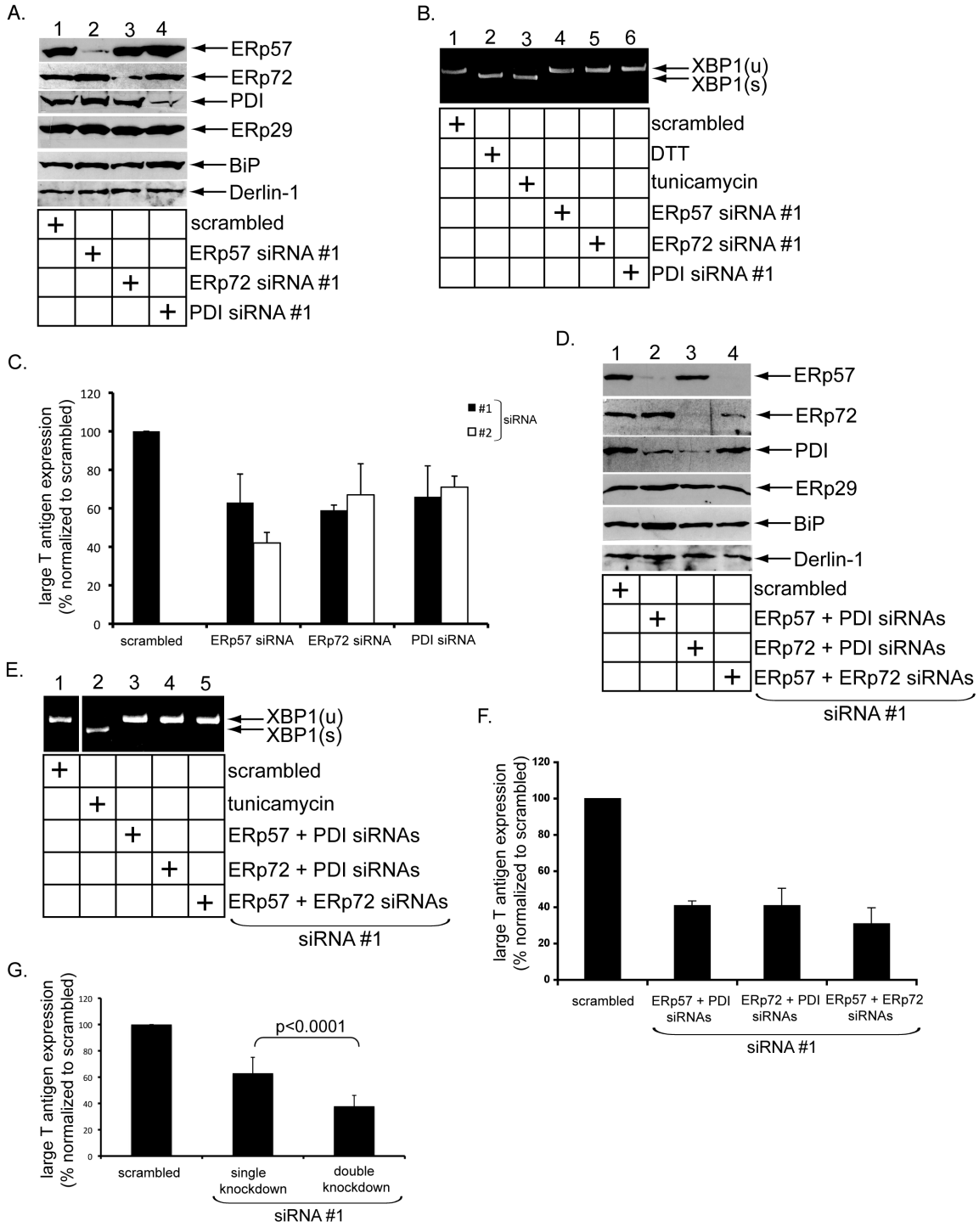
A.
1 2 3 4
ERp57
ERp72
PDI
ERp29
BiP
Derlin-1
scrambled
ERp57 siRNA #1
ERp72 siRNA #1
PDI siRNA #1
B.
1 2 3 4 5 6
XBP1(u)
XBP1(s)
scrambled
DTT
tunicamycin
ERp57 siRNA #1
ERp72 siRNA #1
PDI siRNA #1
C.
large T antigen expression (% normalized to scrambled)
#1
#2
siRNA
scrambled
ERp57 siRNA
ERp72 siRNA
PDI siRNA
D.
1 2 3 4
ERp57
ERp72
PDI
ERp29
BiP
Derlin-1
scrambled
ERp57 + PDI siRNAs
ERp72 + PDI siRNAs
ERp57 + ERp72 siRNAs
siRNA #1
E.
1 2 3 4 5
XBP1(u)
XBP1(s)
scrambled
tunicamycin
ERp57 + PDI siRNAs
ERp72 + PDI siRNAs
ERp57 + ERp72 siRNAs
siRNA #1
F.
large T antigen expression (% normalized to scrambled)
scrambled
ERp57 + PDI siRNAs
ERp72 + PDI siRNAs
ERp57 + ERp72 siRNAs
siRNA #1
G.
large T antigen expression (% normalized to scrambled)
p<0.0001
scrambled
single knockdown
double knockdown
siRNA #1

**Figure 2-1. Downregulation of ERp57, ERp72, and PDI Reduces mPyV Infection**

(A) Knockdown of PDI family members. NIH 3T3 cells were transfected with the indicated siRNA, and lysates derived from the cells subjected to SDS-PAGE and immunoblotted with the indicated antibodies.
(B) Induction of XBP1 splicing. RT-PCR analysis of the unspliced (u) and spliced (s) forms of the XBP1 mRNA from cells treated with DTT, tunicamycin, or transfected with the indicated siRNA.
(C) Py infection in the knockdown cells. Cells transfected with scrambled siRNA, or one of two independent siRNAs against ERp57, ERp72, and PDI (siRNA #1 and #2) were challenged with Py (100 PFU/cell), and the large T antigen expression was analyzed by standard immunofluorescence microscopy. Values were normalized to scrambled siRNA. Data represent the mean +/- SD of at least three independent experiments.
(D) As in A, except the indicated siRNAs were used.
(E) As in B, except the indicated siRNAs were used.
(F) As in C, except the indicated siRNAs were used.
(G) Average infection of single and double knockdown cells. A two-tailed t test was used.

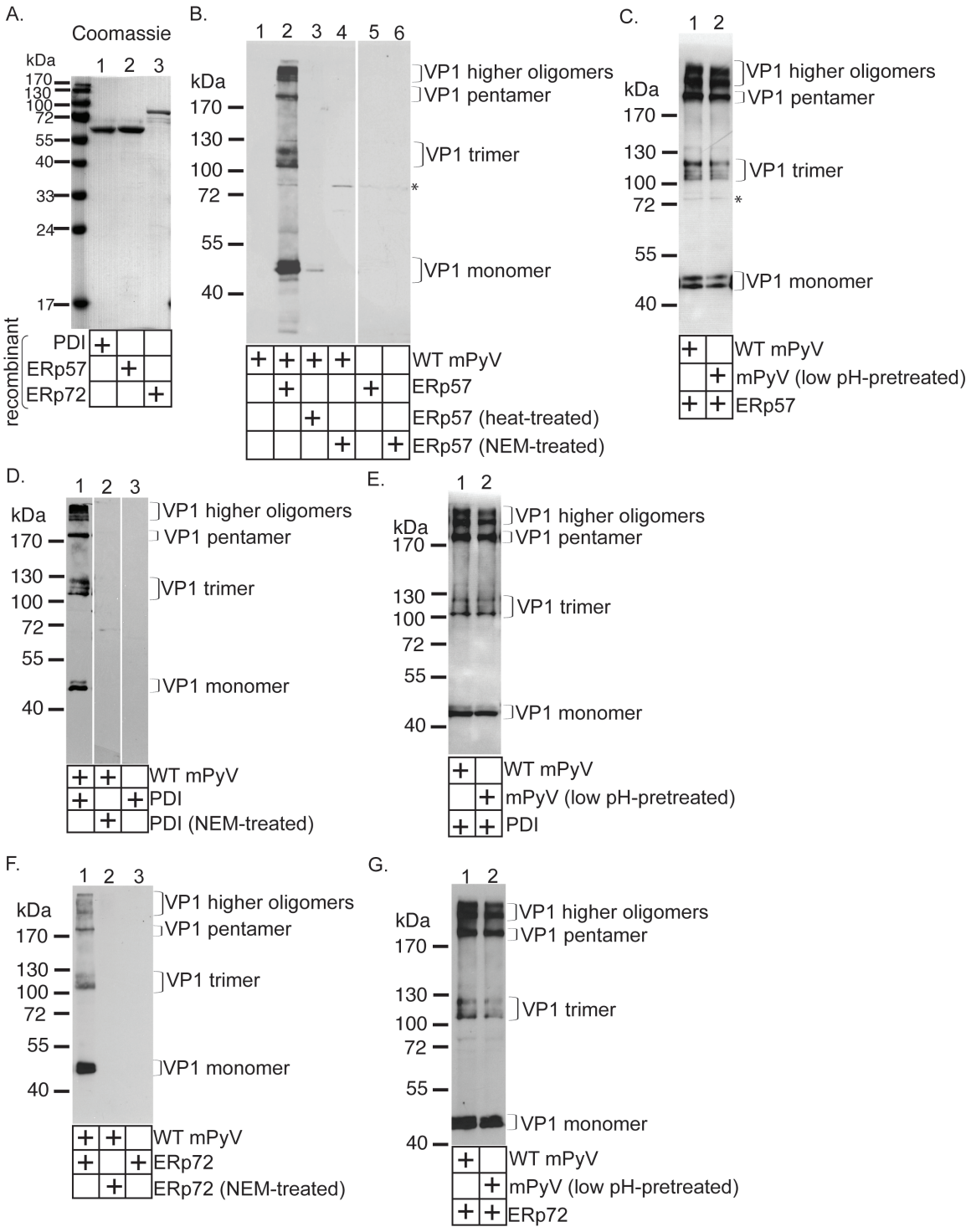
A.
Coomassie
kDa
1 2 3
170
130
100
72
55
40
33
24
17
recombinant
PDI
ERp57
ERp72
B.
1 2 3 4 5 6
kDa
170
130
100
72
55
40
VP1 higher oligomers
VP1 pentamer
VP1 trimer
*
VP1 monomer
WT mPyV
ERp57
ERp57 (heat-treated)
ERp57 (NEM-treated)
C.
1 2
kDa
170
130
100
72
55
40
VP1 higher oligomers
VP1 pentamer
VP1 trimer
*
VP1 monomer
WT mPyV
mPyV (low pH-pretreated)
ERp57
D.
1 2 3
kDa
170
130
100
72
55
40
VP1 higher oligomers
VP1 pentamer
VP1 trimer
VP1 monomer
WT mPyV
PDI
PDI (NEM-treated)
E.
1 2
kDa
170
130
100
72
55
40
VP1 higher oligomers
VP1 pentamer
VP1 trimer
VP1 monomer
WT mPyV
mPyV (low pH-pretreated)
PDI
F.
1 2 3
kDa
170
130
100
72
55
40
VP1 higher oligomers
VP1 pentamer
VP1 trimer
VP1 monomer
WT mPyV
ERp72
ERp72 (NEM-treated)
G.
1 2
kDa
170
130
100
72
55
40
VP1 higher oligomers
VP1 pentamer
VP1 trimer
VP1 monomer
WT mPyV
mPyV (low pH-pretreated)
ERp72

**Figure 2-2. ERp57, PDI, and ERp72 Disrupt Disulfide Bonds on mPyV *in vitro***

(A) Expression and purification of ERp57, PDI, and ERp72. N-terminally His-tagged ERp57, PDI, and ERp72 constructs were expressed in bacteria, purified to homogeneity, and subjected to Coomassie staining.
(B) ERp57 acts on mPyV directly. Where indicated, purified mPyV were incubated with ERp57, heat-treated ERp57, or NEM-treated ERp57. The samples were subjected to nonreducing SDS-PAGE and immunoblotted with an "I-58" VP1 antibody. * indicates a non-specific band recognized by the VP1 antibody.
(C) As in B, except mPyV was pretreated at pH 5.
(D) PDI acts on mPyV directly. PDI or NEM-treated PDI was incubated with or without purified mPyV and analyzed as in (B).
(E) As in D, except mPyV was pretreated at pH 5.
(F) ERp72 acts on mPyV directly. ERp72 or NEM-treated ERp72 was incubated with or without purified mPyV and analyzed as in (B).
(G) As in (F), except mPyV was pretreated at pH 5.

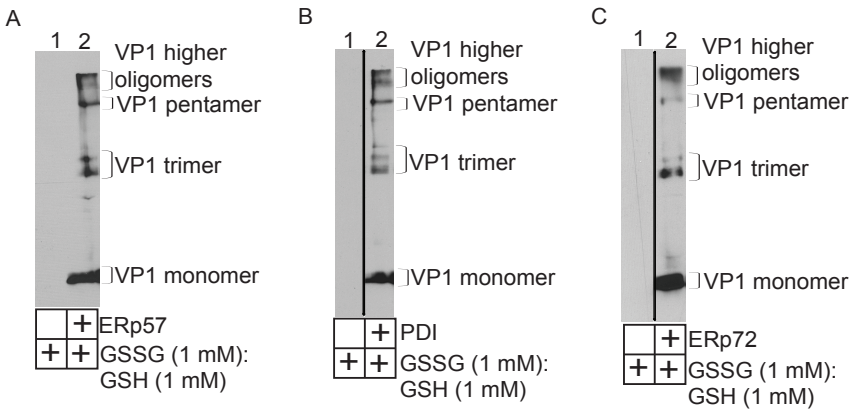


**Figure 2-S1. ERp57, PDI, and ERp72 can Disrupt Disulfide Bonds on mPyV Under Conditions Mimicking ER Redox**

(A-C) Reactions were carried out as in Figure 2-2, except GSSG and GSH were provided.

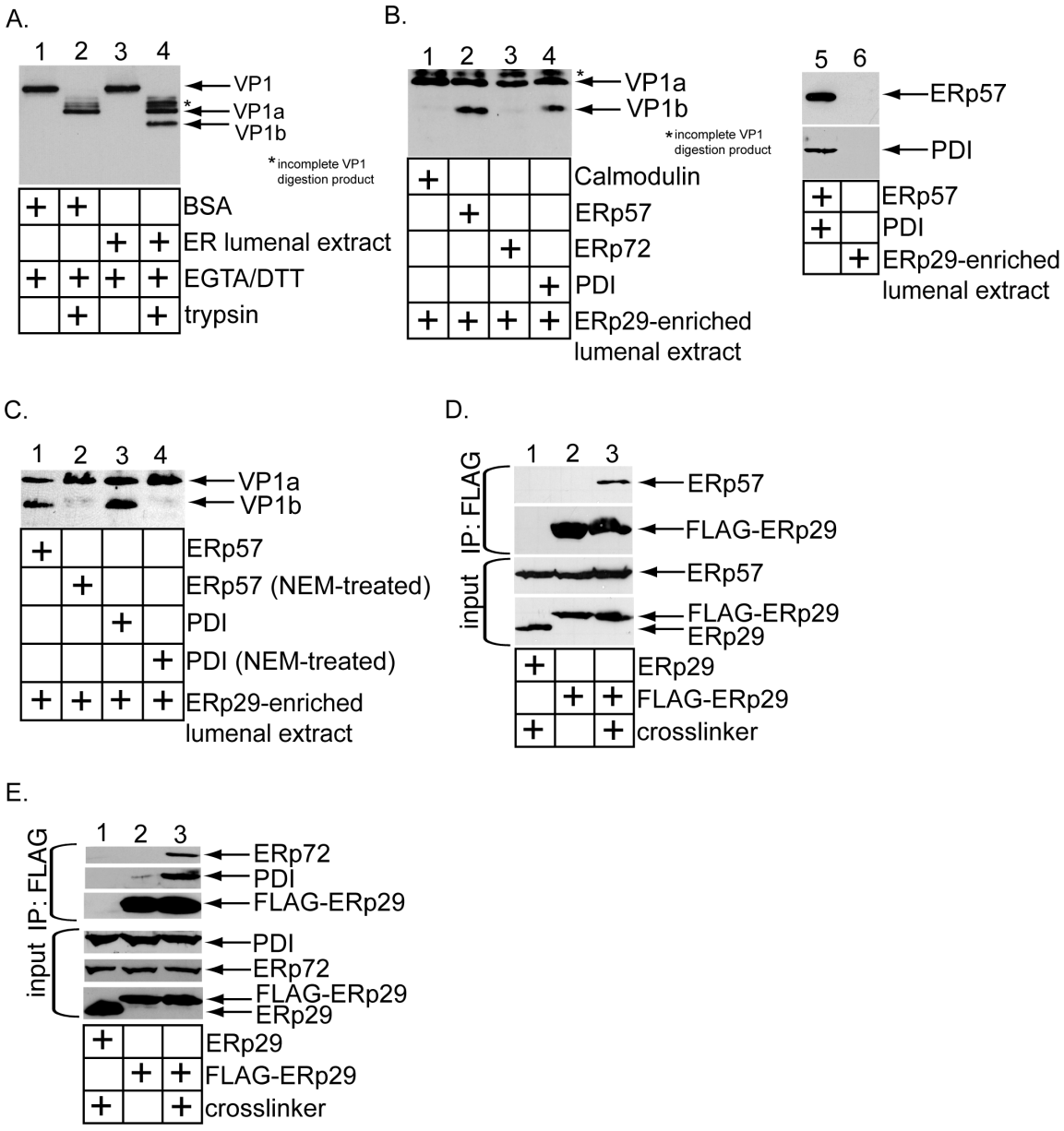
A.
1 2 3 4
VP1
VP1a
VP1b
*incomplete VP1 digestion product
BSA
ER lumenal extract
EGTA/DTT
trypsin
B.
1 2 3 4
VP1a
VP1b
*incomplete VP1 digestion product
Calmodulin
ERp57
ERp72
PDI
ERp29-enriched lumenal extract
5 6
ERp57
PDI
ERp57
PDI
ERp29-enriched lumenal extract
C.
1 2 3 4
VP1a
VP1b
ERp57
ERp57 (NEM-treated)
PDI
PDI (NEM-treated)
ERp29-enriched lumenal extract
D.
IP: FLAG
input
1 2 3
ERp57
FLAG-ERp29
ERp57
FLAG-ERp29
ERp29
ERp29
FLAG-ERp29
crosslinker
E.
input IP: FLAG
1 2 3
ERp72
PDI
FLAG-ERp29
PDI
ERp72
FLAG-ERp29
ERp29
ERp29
FLAG-ERp29
crosslinker

**Figure 2-3. ERp57 and PDI Function Coordinately with ERp29 to Unfold mPyV *in vitro***

(A) VP1 digestion pattern. Crude mPyV was incubated with DTT, EGTA and either BSA or an ER lumenal extract followed by trypsin addition, where indicated. The samples were subjected to SDS-PAGE followed by immunoblotting with a VP1 antibody.
(B) Purified mPyV was pretreated with either calmodulin, ERp57, ERp72, or PDI in the presence of EGTA. The samples were then incubated with an ERp29-enriched ER lumenal extract, added with trypsin, subjected to SDS-PAGE, and immunoblotted with a VP1 antibody. 10% input for the amount of ERp57, PDI, and the ERp29-enriched ER lumenal extract used are shown.
(C) As in B, except NEM-treated ERp57 and PDI were used where indicated.
(D) NIH 3T3 cells transfected with either a rat ERp29 or an N-terminally FLAG-tagged rat ERp29 construct were treated with or without the DSP crosslinker. The resulting cell lysates were subjected to immunoprecipitation using an antibody directed against the FLAG epitope conjugated to agarose. The precipitates, as well as the cell lysates (input), were subjected to SDS-PAGE and immunoblotted with antibodies against ERp57 and ERp29.
(E) As in (D), except antibodies against ERp72 and PDI were used instead of ERp57.

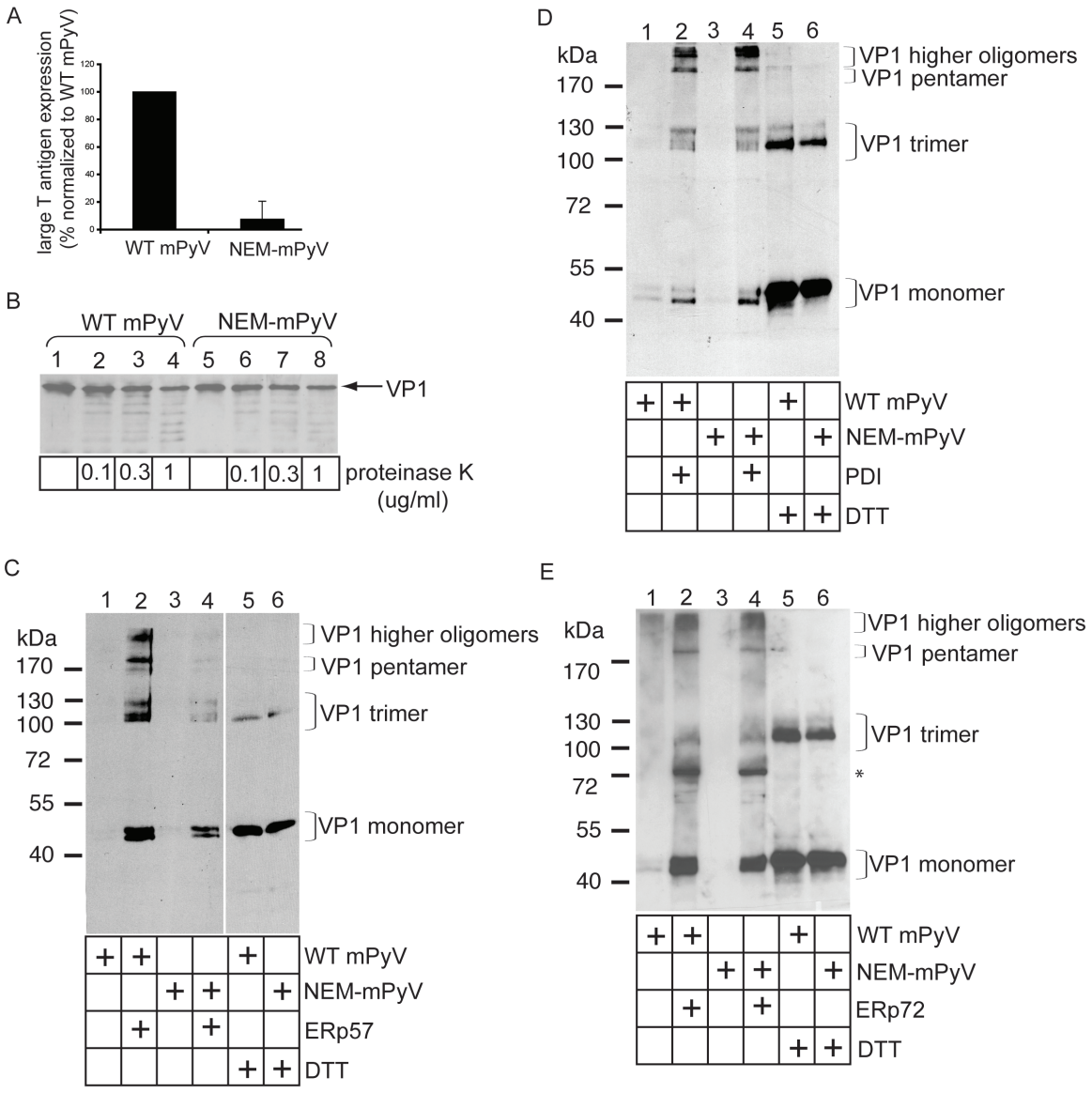
A
large T antigen expression
(% normalized to WT mPyV)
120
100
80
60
40
20
0
WT mPyV
NEM-mPyV
B
WT mPyV
NEM-mPyV
1 2 3 4 5 6 7 8
VP1
0.1 0.3 1 0.1 0.3 1
proteinase K
(ug/ml)
C
1 2 3 4 5 6
kDa
170
130
100
72
55
40
VP1 higher oligomers
VP1 pentamer
VP1 trimer
VP1 monomer
WT mPyV
NEM-mPyV
ERp57
DTT
D
1 2 3 4 5 6
kDa
170
130
100
72
55
40
VP1 higher oligomers
VP1 pentamer
VP1 trimer
VP1 monomer
WT mPyV
NEM-mPyV
PDI
DTT
E
1 2 3 4 5 6
kDa
170
130
100
72
55
40
VP1 higher oligomers
VP1 pentamer
VP1 trimer
*
VP1 monomer
WT mPyV
NEM-mPyV
ERp72
DTT

**Figure 2-4. ERp57 Principally Isomerizes mPyV, while PDI and ERp72 Reduce the Virus *in vitro***

(A) Free cysteines in mPyV are required for infection. NIH 3T3 cells were incubated with either WT or NEM-treated mPyV (100 PFU/cell), and the infection efficiency analyzed as in Figure 2-1C.
(B) NEM-treated virus is not grossly misfolded. WT and NEM-treated mPyV were incubated with the indicated concentrations of proteinase K, and the samples subjected to SDS-PAGE and immunoblotted with a VP1 antibody.
(C) ERp57 largely isomerizes mPyV. WT or NEM-treated mPyV was incubated with ERp57 or DTT (where indicated), and the samples analyzed by nonreducing SDS-PAGE followed by immunoblotting with a VP1 antibody.
(D) PDI reduces mPyV directly. As in (C), except PDI was used instead of ERp57.
(E) ERp72 reduces mPyV directly. As in (C), except ERp72 was used instead of ERp57. * indicates a non-specific band recognized by the “M1” VP1 antibody.

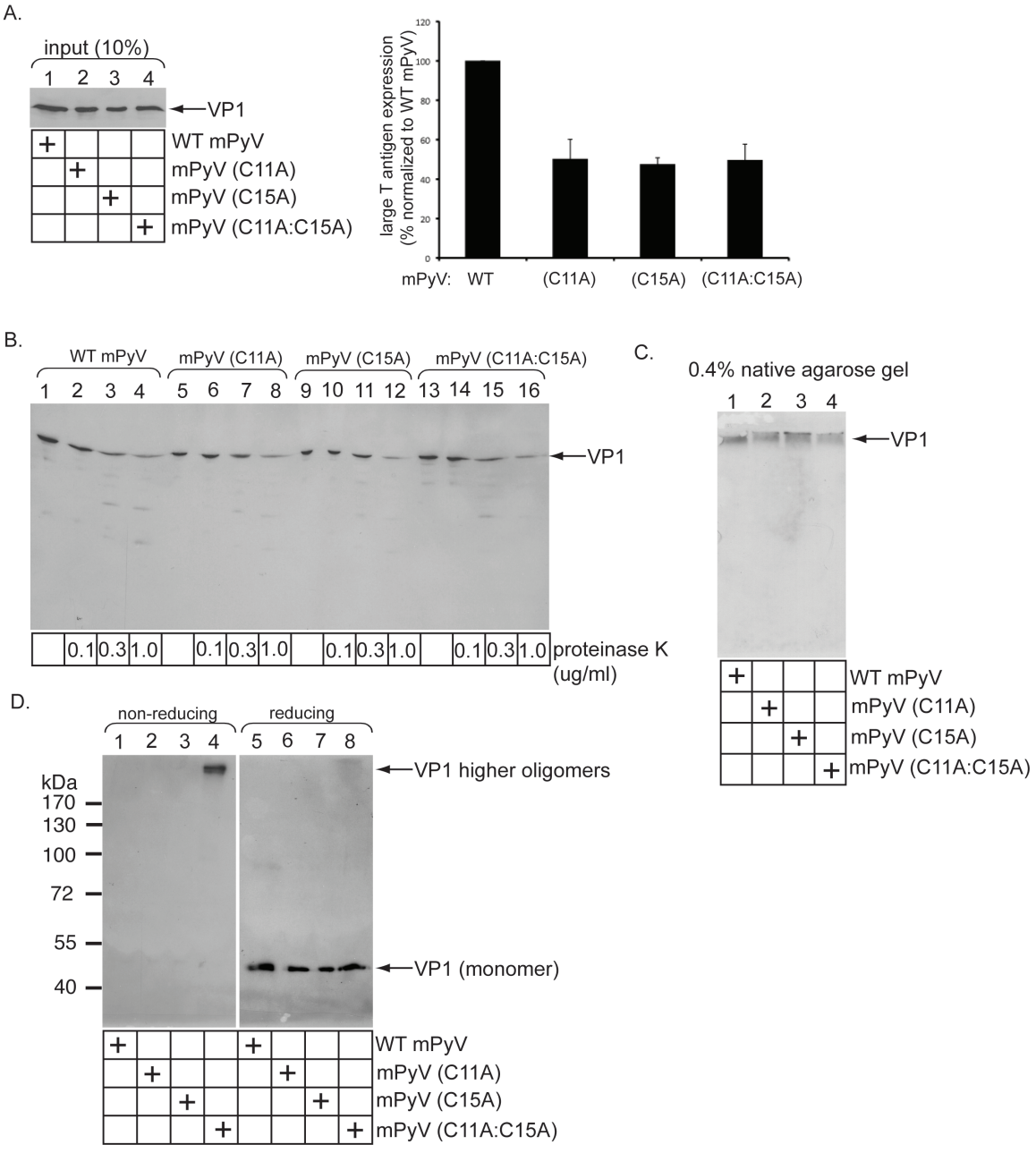
A.
input (10%)
1 2 3 4
VP1
WT mPyV
mPyV (C11A)
mPyV (C15A)
mPyV (C11A:C15A)
large T antigen expression
(% normalized to WT mPyV)
120
100
80
60
40
20
0
mPyV: WT (C11A) (C15A) (C11A:C15A)
B.
WT mPyV
mPyV (C11A)
mPyV (C15A)
mPyV (C11A:C15A)
1 2 3 4 5 6 7 8 9 10 11 12 13 14 15 16
VP1
0.1 0.3 1.0 0.1 0.3 1.0 0.1 0.3 1.0 0.1 0.3 1.0
proteinase K
(ug/ml)
C.
0.4% native agarose gel
1 2 3 4
VP1
WT mPyV
mPyV (C11A)
mPyV (C15A)
mPyV (C11A:C15A)
D.
non-reducing
reducing
1 2 3 4 5 6 7 8
kDa
170
130
100
72
55
40
VP1 higher oligomers
VP1 (monomer)
WT mPyV
mPyV (C11A)
mPyV (C15A)
mPyV (C11A:C15A)

**Figure 2-5. Characterization of the C11A, C15A, and C11A:C15A mPyV Mutants**

(A) VP1 C11 and C15 are important for mPyV infecion. NIH 3T3 cells were incubated with a similar level of crude WT mPyV, mPyV (C11A), mPyV (C15A), or mPyV (C11A:C15A), and the infection efficiency analyzed as in Figure 2-1C.
(B) Mutant viruses are not misfolded globally. Viruses in (A) were subjected to limited proteolysis as in Figure 2-4B.
(C) Native agarose gel analyses of mutant mPyV. Viruses in (A) were subjected to 0.4% native agarose gel, transferred to a nitrocellulose membrane, and immunoblotted with an antibody against VP1.
(D) VP1 C11 and C15 mediate inter-pentamer interaction for a subset of the pentamers. Viruses in (A) were subjected to nonreducing and reducing SDS-PAGE, followed by immunoblotting with an antibody against VP1.

## REFERENCES


1. Poranen MM, Daugelavicius R, & Bamford DH (2002) Common principles in viral entry. *Annual review of microbiology* 56:521-538.

2. Earp LJ, Delos SE, Park HE, & White JM (2005) The many mechanisms of viral membrane fusion proteins. *Curr Top Microbiol Immunol* 285:25-66.

3. Tsai B (2007) Penetration of nonenveloped viruses into the cytoplasm. *Annu Rev Cell Dev Biol* 23:23-43.

4. Tsai B*, et al.* (2003) Gangliosides are receptors for murine polyoma virus and SV40. *EMBO J* 22(17):4346-4355.

5. Gilbert J*, et al.* (2005) Ganglioside GD1a restores infectibility to mouse cells lacking functional receptors for polyomavirus. *J Virol* 79(1):615-618.

6. Qian M, Cai D, Verhey KJ, & Tsai B (2009) A lipid receptor sorts polyomavirus from the endolysosome to the endoplasmic reticulum to cause infection. *PLoS Pathog* 5(6):e1000465.

7. Gilbert J & Benjamin T (2004) Uptake pathway of polyomavirus via ganglioside GD1a. *J Virol* 78(22):12259-12267.

8. Smith AE, Lilie H, & Helenius A (2003) Ganglioside-dependent cell attachment and endocytosis of murine polyomavirus-like particles. *FEBS letters* 555(2):199-203.

9. Gilbert J, Ou W, Silver J, & Benjamin T (2006) Downregulation of protein disulfide isomerase inhibits infection by the mouse polyomavirus. *J Virol* 80(21):10868-10870.

10. Lilley BN, Gilbert JM, Ploegh HL, & Benjamin TL (2006) Murine polyomavirus requires the endoplasmic reticulum protein Derlin-2 to initiate infection. *J Virol* 80(17):8739-8744.

11. Magnuson B*, et al.* (2005) ERp29 triggers a conformational change in polyomavirus to stimulate membrane binding. *Mol Cell* 20(2):289-300.

12. Stehle T, Yan Y, Benjamin TL, & Harrison SC (1994) Structure of murine polyomavirus complexed with an oligosaccharide receptor fragment. *Nature* 369(6476):160-163.

13. Chen XS, Stehle T, & Harrison SC (1998) Interaction of polyomavirus internal protein VP2 with the major capsid protein VP1 and implications for participation of VP2 in viral entry. *EMBO J* 17(12):3233-3240.

14. Stehle T, Gamblin SJ, Yan Y, & Harrison SC (1996) The structure of simian virus 40 refined at 3.1 A resolution. *Structure* 4(2):165-182.

15. Liddington RC*, et al.* (1991) Structure of simian virus 40 at 3.8-A resolution. *Nature* 354(6351):278-284.

16. Stehle T & Harrison SC (1997) High-resolution structure of a polyomavirus VP1-oligosaccharide complex: implications for assembly and receptor binding. *EMBO J* 16(16):5139-5148.

17. Schelhaas M*, et al.* (2007) Simian Virus 40 depends on ER protein folding and quality control factors for entry into host cells. *Cell* 131(3):516-529.

18. Rainey-Barger EK, Magnuson B, & Tsai B (2007) A chaperone-activated nonenveloped virus perforates the physiologically relevant endoplasmic reticulum membrane. *J Virol* 81(23):12996-13004.

19. Uemura A, Oku M, Mori K, & Yoshida H (2009) Unconventional splicing of XBP1 mRNA occurs in the cytoplasm during the mammalian unfolded protein response. *Journal of cell science* 122(Pt 16):2877-2886.

20. Rainey-Barger EK, Mkrtchian S, & Tsai B (2009) The C-terminal domain of ERp29 mediates polyomavirus binding, unfolding, and infection. *J Virol* 83(3):1483-1491.

21. Forster ML, Mahn JJ, & Tsai B (2009) Generating an unfoldase from thioredoxin-like domains. *J Biol Chem* 284(19):13045-13056.

22. Rainey-Barger EK, Mkrtchian S, & Tsai B (2007) Dimerization of ERp29, a PDI-like protein, is essential for its diverse functions. *Mol Biol Cell* 18(4):1253-1260.

23. Oda Y*, et al.* (2006) Derlin-2 and Derlin-3 are regulated by the mammalian unfolded protein response and are required for ER-associated degradation. *J Cell Biol* 172(3):383-393.

24. Appenzeller-Herzog C & Ellgaard L (2008) The human PDI family: versatility packed into a single fold. *Biochimica et biophysica acta* 1783(4):535-548.

25. Yan Y, Stehle T, Liddington RC, Zhao H, & Harrison SC (1996) Structure determination of simian virus 40 and murine polyomavirus by a combination of 30-fold and 5-fold electron-density averaging. *Structure* 4(2):157-164.

26. Tsai B, Rodighiero C, Lencer WI, & Rapoport TA (2001) Protein disulfide isomerase acts as a redox-dependent chaperone to unfold cholera toxin. *Cell* 104(6):937-948.

27. Forster ML*, et al.* (2006) Protein disulfide isomerase-like proteins play opposing roles during retrotranslocation. *J Cell Biol* 173(6):853-859.

28. Tsai B & Rapoport TA (2002) Unfolded cholera toxin is transferred to the ER membrane and released from protein disulfide isomerase upon oxidation by Ero1. *J Cell Biol* 159(2):207-216.

Chapter 3: **Cytosolic Chaperones Complex with Dynamic Membrane J-proteins and Mobilizes Simian Virus 40 Out of the Endoplasmic Reticulum**

## INTRODUCTION

Nonenveloped viruses must penetrate a biological membrane to infect cells. As they lack a surrounding lipid bilayer, membrane penetration by nonenveloped viruses must be fundamentally different from enveloped viruses, which normally gain access to the host cell by membrane fusion. Although the precise membrane transport mechanism for nonenveloped viruses is not entirely clear, a general principle is emerging. These viruses enter host-cells by endocytic internalization in order to arrive at a precise cellular environment necessary for productive infection (1). Upon reaching this proper environment, important conformational changes are induced by specific cellular triggers including low pH, proteases, or chaperone activities (2). These conformational changes in turn generate a hydrophobic viral particle or cause the release of a lytic peptide hidden in the intact virus. Engagement of the hydrophobic particle or lytic peptide with the limiting membrane disrupts the membrane integrity and initiates membrane penetration. For example, the nonenveloped reovirus, parvovirus, and adenovirus become internalized and traffic to endosomes where the low pH or proteases trigger viral conformational changes that allow them to penetrate the endosomal membrane (3-6). In these cases, membrane penetration is thought to involve virus-induced pore formation or disruption of overall membrane integrity. Currently, absent in this model is a role for any cytosolic factors directly influencing membrane penetration.

Polyomaviruses are unique among nonenveloped viruses in that they traffic beyond the endosomal system to reach the endoplasmic reticulum (ER) for

membrane penetration (7-13). This virus family consists of a growing list of important human polyomaviruses known to cause devastating diseases in immunocompromised individuals (14, 15). Simian virus 40 (SV40) has traditionally served as an excellent model member of this family; it has genetic and structural similarity to human polyomaviruses, yet is easy to propagate and study in cells. To cause infection, SV40 engages the ganglioside receptor GM1 at the cell surface to initiate internalization (16, 17). Caveolae-dependent endocytosis brings SV40 particles attached to lipid rafts into the cell where they travel through endosomes before being sorted to the ER (7, 12). Once inside the ER lumen, SV40 is faced with the task of penetrating the ER membrane to reach the cytosol prior to nuclear import (18, 19). In the nucleus, transcription and replication of the viral genome take place, leading to production of new viral particles.

The ER provides an ideal environment for inducing important conformational changes to the structure of SV40. The outer surface of each viral particle contains 360 copies of the major coat protein VP1 arranged as 72 pentamers (20, 21). A single hydrophobic minor coat protein VP2 or VP3 resides beneath each VP1 pentamer (22). SV40 VP1 molecules are stabilized by interpentameric disulfide bonds, with bound calcium ions and hydrophobic interactions providing additional capsid support (20). Protein disulfide isomerase (PDI)-family members appear to be broadly important during entry of polyomaviruses for either their ability to disrupt viral disulfide bonds by using their redox/isomerase activities, or to impart conformational changes by using their chaperone functions (10, 23-26). PDI proteins exert these activities on SV40, likely in concert with other ER factors, resulting in VP2 exposure (11, 27, 28). Due to its hydrophobic N-terminus, exposure of VP2 renders the virus itself hydrophobic (28). As a result, the virus binds and integrates into the ER membrane to initiate membrane penetration.

In the next stage of the membrane penetration process, a critical Glu residue in VP2's N-terminus embedded in the ER membrane is hypothesized to act as a charged irregularity in the ER membrane and recruits cellular factors involved in ER-associated degradation (ERAD) (29). The ERAD pathway utilizes large multi-protein complexes to eliminate misfolded or incorrectly assembled ER proteins by facilitating their retro-translocation into the cytosol for degradation by the ubiquitin-proteasome system (30, 31). SV40 and other polyomaviruses co-opt several ERAD membrane components including the J-proteins DnaJB14 (B14) and DnaJB12 (B12) to reach the cytosol and infect cells (8, 26, 32, 33). B14 and B12 both span the ER membrane once and display their functional J domain in the cytosol (34-36). By virtue of this domain, J-proteins stimulate the ATPase activity of Hsp70 chaperones to promote substrate-Hsp70 interaction. However, the precise mechanism by which these membrane components facilitate ER-to-cytosol transport of a large viral particle is not clear. Whether any cytosolic components provide the driving force to extract the hydrophobic ER membrane-embedded SV40 into the cytosol is also unknown. In this context, the cytosolic ATPase p97 (also called VCP) involved in the mobilization of ERAD substrates into the cytosol was shown to be dispensable for SV40 infection (29, 37). Additionally, while chemical inhibition of the cytosolic proteasome perturbs SV40 infection (8, 26, 38, 39), this effect may be indirect (29). Thus, the potential roles of cytosolic factors that directly promote membrane penetration of polyomaviruses, as well as other nonenveloped viruses, remain enigmatic.

Here, we demonstrate that the cytosolic chaperone SGTA is critical for transport of SV40 from the ER membrane into the cytosol. SGTA associates with a chaperone complex containing B14 and B12 (B14-B12) at the ER membrane and is therefore positioned to act at the site of membrane penetration. Using a combination of cell-based and biochemical assays, we found that SGTA binds directly to SV40 and promotes its ER membrane penetration and infection. During membrane penetration, SGTA is released from the B14-B12 complex, suggesting SV40 alters localization or structural characteristics of these factors.

Consistent with this idea, we found that SV40 causes the B14-B12 complex to reorganize into discrete foci in the ER membrane. As formation of these foci coincides temporally with SV40's cytosolic arrival, they may represent ER exit sites where SGTA engages the virus to complete membrane penetration.

## MATERIALS AND METHODS

### Antibodies

Polyclonal DnaJB14, DnaJB12, ERdj5, SGTA, Hrd1 were purchased from Proteintech Group (Chicago, IL). An additional rabbit polyclonal against SGTA was provided by Yihong Ye (NIH). Monoclonal BAP31 and polyclonal Hsc70 and Bag6 antibodies were purchased from Pierce (Rockford, IL). Polyclonal Derlin-1 and Sec61$\alpha$ antibodies were provided by Tom Rapoport (Harvard University). Normal rabbit and mouse IgG, polyclonal Hsp90, PDI, and monoclonal SV40 Large T antigen antibodies were purchased from Santa Cruz Biotechnology (Santa Cruz, CA). Rabbit anti-VP1 antibody was a gift from Harumi Kasamatsu (UCLA). Monoclonal VP1 antibody was provided by Walter Scott (University of Miami). Monoclonal p97 was purchased from RDI/Fitzgerald (Concord, MA). Polyclonal BiP, mouse anti-GAPDH and rat anti-Hsc70 antibodies were purchased from Abcam (Cambridge, MA). Polyclonal calnexin antibodies were purchased from Stressgen. Polyclonal ERp29 was a gift from Souren Mkrtchian (Karolinska Institutet).

### Reagents

Dulbecco's modified Eagle's medium (DMEM), Opti-MEM, 0.25% trypsin-EDTA were purchased from Invitrogen (Carlsbad, CA). Fetal Clone III (FC) was from HyClone (Logan, UT). Complete-mini EDTA-free protease inhibitor cocktail tablets were purchased from Roche. Micro Bio-Spin P-30 Tris chromatography columns were purchased from Bio-Rad. Dithiothreitol (DTT), Dithiobis succinimidylpropionate (DSP), N-ethylmaleimide (NEM) and anti-FLAG M2 agarose beads were purchased from Sigma (St Louis, MO).

### Preparation of SV40

WT SV40 and $\Delta$VP2 SV40 were prepared using OptiPrep gradient system as described previously (39).

**Transfection of siRNA and DNA Plasmids**

Control siRNA (labeled as scrambled) is the All Star Negative purchased from Qiagen (Valencia, CA). Custom siRNA sequences were generated and purchased from Dharmacon (Pittsburgh, PA).

SGTA siRNA #1: 5'GGUAGAAGACAGUGACCUUUU3'
5'AAGGUCACUGUCUUCUACCUU3'
SGTA siRNA #2: 5'ACAAGAAGCGCCUGGCCUAUU3'
5'UAGGCCAGGCGCUUCUUGUUU3'
Bag6 siRNA #1: 5'GCUUGGAGGUGUUGGUGAAUU3'
5'UUCACCAACACCUCCAAGCUU3'
Bag6 siRNA #2: 5'GAUAAGAAGCUUCAGGAAUUU3'
5'AUUCCUGAAGCUUCUUAUCUU3'

Using Lipofectamine RNAiMAX (Invitrogen), 25 nM of control or custom siRNAs were reverse transfected into HeLa or CV-1 cells. Infection or biochemical assays were carried out 24 or 48 h.p.i.. A plasmid expressing human WT DnaJB14 was a gift from Daniel DaMaio (Yale) and cloned with an N-terminal FLAG tag into pcDNA3.1 minus (Invitrogen). Site-directed mutagenesis was performed on His136 to yield a H136Q mutant. The ∆lumenal FLAG-B14 contains residues 1-282 and ∆cytosol contains residues 226-379, and were generated using standard cloning methods. A plasmid expressing SGTA-myc/FLAG is from Origene (Rockville, MD) and double point mutants were derived similarly by site-directed mutagenesis. DNA was transfected into plated CV-1 cells (50-80% confluent) using FuGENE and allowed to express for 18-24 h prior to experimentation.

**B14-B12 and SGTA Co-immunoprecipitations**

Interactions detected between endogenous B14 and B12 utilized lysates derived from CV-1 or HeLa cells with buffer containing 50 mM Tris pH 7.4, 150 mM NaCl, 1 mM EDTA and protease inhibitors with 1% deoxyBigCHAP (Calbiochem, Billerica, MA). Cleared lysates were incubated with antibodies overnight at 4°C

with rotation. Antibodies were captured using protein A agarose beads and washed with lysis buffer containing 0.1% deoxyBigCHAP. SDS sample buffer was used for elution at 95°C. Interactions between endogenous SGTA and B14-B12 were detected similarly but with a different lysis buffer. 293T or CV-1 cells were lysed by resuspension and brief vortexing in 0.1% digitonin, 50 mM Tris, 150 mM NaCl, 1 mM EDTA and protease inhibitors followed by incubation on ice for 15 minutes. Cleared lysates were incubated with indicated antibodies, captured with protein A agarose beads and washed extensively with buffer lacking detergent. Immunoprecipitation of transfected SGTA-myc/FLAG was performed as above but with a buffer containing 0.2% digitionin and incubation with anti-FLAG M2 agarose beads.

**SGTA-SV40 Co-immunoprecipitations**

In 6 cm plates, 3 x $10^5$ CV-1 cells were transfected to express FLAG-tagged GFP or SGTA proteins for at least 18 h. SV40 particles (15 μg) were added to cells after synchronizing the entry at 4°C. Approximately 8 h.p.i., cells were harvested and cross-linked using 2 mM DSP at room temperature for 30 mins. After quenching, cells were lysed in 1% Triton X-100, 50 mM Tris pH 7.5, 150 mM NaCl, 1 mM EDTA, 20 mM NEM and protease inhibitors. Cleared lysates were immunoprecipitated with anti-FLAG agarose beads overnight and washed 3 times with lysis buffer. Bound material was analyzed by immunoblotting using rabbit anti-VP1 antibody.

**XBP1 Splicing Assay**

As previously described (25) using primers against human XBP1:
5'- CGCGGATCCGAATGTGAGGCCAGTGG-3' and
5'- GGGGCTTGGTATATATGTGG-3'.

**Gel Filtration Chromatography**

HeLa cells were lysed in 1% Triton, 30 mM Tris pH 8, 150 mM NaCl, and 4 mM $MgCl_2$. Cleared lysates were separated using lysis buffer and a Bio-Sil SEC 250

column (Bio-Rad, Hercules, CA). Forty fractions of 0.5 mL were collected and fractions 10-22 were analyzed by immunoblotting.

**Preparation of Purified Proteins**

For purification of FLAG-tagged GFP, WT and mutant SGTA, 293T cells were transfected to express proteins for 48 h. Cells were lysed in buffer containing 1% Triton X-100, 50 mM Tris, 150 mM NaCl, 1 mM EDTA and protease inhibitors. Cleared lysates were incubated with anti-FLAG agarose beads and bound proteins washed extensively with lysis buffer. Proteins were eluted with FLAG peptide overnight and concentrated using centrifugal filters that also removes residual FLAG peptides. Optiprep purified SV40 was treated with 3 mM DTT and 10 mM EGTA for 45 min at 37°C to mimic ER induced conformational changes. A spin column was used to exchange the buffer with PBS and to remove DTT and EGTA.

***In Vitro* Binding Assays**

Binding reactions were carried out in 50 mL PBS containing 250 ng of SV40 (pretreated with DTT and EGTA as described above) with or without 1 mg of purified protein. Reactions incubated for 1 h at 25°C followed by the addition of 0.25 mM DSP at 4°C for 30 min to stabilize transient interactions. After quenching with excess Tris, immunoprecipitation with anti-FLAG agarose beads was performed and bound material analyzed by immunoblotting.

**Immunofluorescence Microscopy for Foci Formation**

CV-1 cells were grown on 12 mm coverslips in 6 or 24-well plate for 24 h. Cells were treated with SV40 for the indicated time and then washed in PBS followed by fixation with 1% formaldehyde at room temperature. Cells were permeabilized with 0.2% Triton X-100 and blocked with 5% milk and 0.2% Tween. Primary antibodies were incubated for 1 h at room temperature, followed by fluorescent conjugated secondary antibodies for 30 min at room temperature. Cover slips were mounted with ProLong Gold (Invitrogen). Images were taken using an

inverted epifluorescence microscope (Nikon Eclipse TE2000-E) equipped with 60x and 100x 1.40 NA objective and a Photometrics CoolSnap HQ camera. For over-expression studies, cells were transfected with the desired plasmid with FuGene (Promega) at least 24 h prior to imaging. For live-cell imaging, cells are seeded on 35mm glass bottom tissue culture dishes (Greiner Bio-one, Germany). Imaging of the cells was performed from 2 to 20 h.p.i. using the microscope and objective mentioned above. The entire set-up was controlled by MetaMorph software (Molecular devices) and ImageJ software (NIH) was used for image processing, analysis, and assembly.

**SV40 and BKPyV Infection Assay**

CV-1 cells transfected with siRNA for 24 h were incubated with SV40 at 37°C (M.O.I. 3-10). At 20-24 h.p.i., cells were harvested for analysis by immunoblot or fixed and stained using antibodies against SV40 large T antigen as described previously (39). For each infection experiment, at least 500 cells were counted in each condition. Approximately 30-50% cells were positive for Large T antigen in the control conditions.

Purified BKPyV and pAb416 against BK large T antigen were provided by Michael Imperiale (University of Michigan). CV-1 cells transfected with siRNA for 24 h were infected at M.O.I. ≈ 1. Cells were harvested after 40 h.p.i., and immunoblot performed for large T antigen.

**ER-to-cytosol Transport and ER Arrival Assays**

Performed as in (39). SV40 was added (M.O.I ≈ 10) to CV-1 cells grown in 6 cm plates (~80% confluent). Where indicated, BFA (Epicenter, Madison, WI) was added to the media at 2.5 mg/mL. After fractionation, 40% of the supernatant fraction was compared alongside 10% of the pellet fraction for immunoblot analyses, as only a portion of SV40 reaches the cytosol. Fractionation markers were analyzed with equivalent amounts of supernatant and pellet. Image J

software was used for quantification of VP1 band intensities. ER arrival assays were performed as described previously (39).

**Immunopurification of B14 Binding Partners**

Flp-In T-REx 293 cells (Invitrogen) were transfected with a pcDNA5/FRT/TO plasmid expressing WT B14-3xFLAG along with pOG44 plasmid expressing a Flp recombinase. Selection was carried out with media containing hygromycin and blasticidin over several weeks. Expression of B14-3xFLAG to near endogenous levels was induced with 5 ng/mL of tetracycline provided to the media for 16 h. Three confluent 15 cm plates were collected in PBS and lysed for 30 mins on ice in 2.5 mL of buffer containing 0.1% digitonin, 50 mM Tris pH 7.4, 150 mM NaCl, 1 mM EDTA and protease inhibitor. Lysate was cleared with centrifugation at 20,000g for 15 min. Lysate divided in half was incubated for 2 h at 4°C with 30 mL of anti-FLAG M2 agarose beads that was pre-incubated with or without 3xFLAG peptide (100 mL, 0.25 mg/mL). Agarose beads were washed extensively with buffer lacking detergent. Bound proteins were eluted overnight at 4°C with 3xFLAG peptide (200 mL, 0.25 mg/mL). Three subsequent elutions were performed for 1 h each, pooled and concentrated using centrifugal filters (Amicon Ultra 0.5 mL 3K membrane). SDS sample buffer was added and heated for 30 min at 37°C followed by SDS-PAGE and silver staining or immunoblotting. Bands excised from a silver stained gel were analyzed by mass spectrometry at Taplin Biological Mass Spectrometry Facility (Harvard Medical School).

**Statistics**

Quantitative data is presented as the mean of at least three independent experiments with standard deviation. Paired two-tailed Student's t-tests were used to acquire *p*-values.

## RESULTS

### B14 Forms a High Molecular Weight Complex with B12

To clarify how B14 and B12 promote SV40 ER membrane penetration (32), we first characterized their biochemical properties. Gel-filtration analysis of detergent-solubilized cell extracts followed by subsequent immunoblotting of the individual fractions demonstrate that a substantial pool of B14 eluted in high-molecular weight fractions (>150 kDa), suggesting B14 is part of a complex larger than its monomeric size of 42 kDa (Figure 3-1A). Probing for Hrd1 and ERp29 confirmed the fractionation of large and small complexes, respectively. B12 co-fractionated identically with B14, raising the possibility that these proteins interact with each other. Co-immunoprecipitation experiments revealed that endogenous B14 and B12 bind to each other with high efficiency in both HeLa and CV-1 cells (Figure 3-2B and 3-2C). These data demonstrate that these J-proteins interact with each other and are likely part of a stable membrane complex.

### The Cytosolic Chaperone SGTA Binds to the B14-B12 Complex in a Hsc70-dependent Manner

To identify other components of the B14 complex, we used an unbiased strategy of immunoprecipitation followed by mass spectrometry (MS). We constructed 293T cells that allowed for tetracycline-inducible expression of B14-3xFLAG. To minimize overexpression artifacts, B14-3xFLAG expression was maintained at a level similar to endogenous B14 by providing a low concentration of tetracycline (Figure 3-2A). Under this condition, cells were lysed with a low concentration of digitonin to maintain protein-protein interactions during immunoprecipitation with anti-FLAG conjugated agarose beads. To control for nonspecific binding to the agarose beads, an identical lysate was incubated with anti-FLAG conjugated agarose beads pre-blocked with 3xFLAG peptide. After washing and elution by addition of 3xFLAG peptide, the eluted material was concentrated and subjected to SDS-PAGE followed by silver staining (Figure 3-2B). Co-immunoprecipitated proteins reproducibly observed by silver staining were excised and analyzed by

MS. Not surprisingly, a band migrating at approximately 72 kDa was identified as Hsc70, a common interacting partner of J-proteins. Interestingly, another band corresponding to approximately 38 kDa was identified as the cytosolic chaperone SGTA. We focused our study on this protein as it was recently implicated in the ERAD pathway (40). While several components of the SMN complex involved in spliceosomal snRNP assembly and pre-mRNA processing were also identified during MS analyses, they remain to be tested as authentic B14 binding partners. Eluted samples prepared as in Figure 3-2B were immunoblotted with specific antibodies to confirmed the presence of SGTA, Hsc70, and B14-3xFLAG (Figure 3-2C). Importantly, when endogenous SGTA was immunoprecipitated from standard 293T or CV-1 cells, endogenous B14 but not the abundant membrane protein BAP31 was detected in the precipitate (Figure 3-2D, left and right panels). As B12 complexes with B14 (Figure 3-1), we asked whether endogenous B12 also binds SGTA. Indeed, B12 also co-precipitated with SGTA. (Figure 3-2D, right panels).

We asked whether B14-B12 binding to SGTA was mediated by any known interacting partners of SGTA. Previously SGTA has been observed to interact with Hsc70 as a co-chaperone (41, 42). Additionally, a more recent study demonstrated that SGTA binds to the cytosolic Bag6 (BAT3, scythe)-Ubl4a-Trc35 complex via Ubl4a (40). We therefore tested whether SGTA mutants defective in their ability to bind to either Hsc70 (K160E/R164E) or Ubl4a (D27R/E30R) could interact with B14. CV-1 cells were transfected to express FLAG-tagged WT or a mutant form of SGTA. Lysates derived from these cells were immunoprecipitated with anti-FLAG conjugated agarose beads. Endogenous B14 was observed to precipitate with WT-SGTA and the Ubl4a-binding defective mutant (D27R/E30R) (Figure3- 2E). By contrast, the Hsc70-binding defective mutant (K160E/R164E) was unable to interact with B14, despite substantially more mutant in the precipitation when compared to WT SGTA (Figure 3-2E). This interaction was specific to B14's cytosolic J-domain as ERdj5, a lumenal J-protein, did not precipitate with any form of SGTA (Figure 3-2E). We performed the converse

analysis by transfecting FLAG-tagged WT B14 or a mutant B14 defective in coupling to Hsc70 (H136Q)(34). WT B14 but not H136Q B14 precipitated endogenous SGTA (Figure 3-2F). Together these data demonstrate SGTA interacts with the B14-B12 complex in a Hsc70-dependent manner.

**Downregulation of SGTA Perturbs SV40 and BKPyV Infection**

B14 and B12 are two key ER membrane components crucial for SV40 and human BK polyomavirus (BKPyV) infection (32). Since our findings revealed SGTA is a binding partner of the B14-B12 complex, we first asked whether SGTA was important for SV40 infection. Expression of the virally-encoded large T antigen protein in the host nucleus reflects successful viral infection. We monitored infection in this way by scoring cells for the presence or absence of large T antigen using immunofluorescence microscopy. Two distinct siRNA oligonucleotides effectively downregulated SGTA expression in both CV-1 and HeLa cells (Figure 3-3A). Under these knockdown conditions, cells appeared healthy as determined by their overall morphology and number when compared to cells transfected with scrambled siRNA. Downregulation of SGTA in both cell types reduced SV40 infection by approximately 50% when compared to cells transfected with a scrambled siRNA (Figure 3-3B). Similarly, these knockdown conditions markedly reduced the expression of BKPyV large T antigen as assessed by immunoblot analyses (Figure 3-3C). Neither upregulation of the ER stress markers BiP, PDI, and Derlin-1 (Figure 3-3C), nor pronounced stimulation of XBP-1 slicing (Figure 3-3D) was observed when SGTA was silenced, indicating no significant induction of ER stress occurred within the time frame of our experiments. This result varies from a recent report where a cell line stably expressing SGTA shRNA exhibits an ER stress response. This difference may be due to our use of a transient knockdown. We conclude that SGTA plays an important and specific role during SV40 and BKPyV infection.

SGTA is involved in multiple aspects of protein quality control. Recent evidence suggests one function of SGTA is to facilitate ERAD substrate loading on Bag6, a

holdase that prevents substrate aggregation prior to proteasomal degradation. Based on these findings, we tested whether Bag6 was important for SV40 infection and found that Bag6 knockdown did not block expression of SV40 large T antigen (Figure 3-S1), indicating that SGTA promotes SV40 infection independent of Bag6.

**SGTA Promotes ER-to-cytosol Transport of SV40**

As SGTA is a cytosolic chaperone complexed with the ER membrane J-proteins B14 and B12, we asked whether this chaperone facilitates the arrival of SV40 into the cytosol from the ER. Our laboratory previously developed a cell-based assay to monitor SV40 ER-to-cytosol transport (39). A similar assay has also been reported (29). Briefly, cells infected with SV40 are harvested, selectively permeabilized with a low digitonin concentration, and centrifuged to generate a supernatant and a pellet fraction; the supernatant harbors cytosolic material while the pellet contains intracellular membranes including the ER. These fractions are subsequently analyzed by immunoblotting for fractionation markers and VP1. VP1 in the supernatant therefore represents SV40 that reached the cytosol, and VP1 in the pellet reflects virus within intracellular organelles. We applied this assay to cells transfected with scrambled or SGTA siRNAs. The cytosolic markers GAPDH and Hsp90 were predominantly detected in the supernatant whereas the ER lumenal markers PDI and ERp29 were found exclusively in the pellet (Figure 3-3E), confirming the integrity of the fractionation procedure. Strikingly, the VP1 level in the supernatant was significantly reduced in cells with SGTA downregulated when compared to scrambled control (Figure 3-3E; quantified in 3-3F). We note that the severity in the ER-to-cytosol transport defect appears to be greater than the perturbation in infection (Figure 3-3B). This difference is likely attributed to the low virus level present in the cytosol under SGTA knockdown conditions that is sufficient to reach the nucleus and express large T-antigen(43).

We also assessed whether downregulating SGTA affects arrival of SV40 to the ER. Successful SV40 ER arrival can be monitored by examining the amount of Triton X-100 soluble VP1 present in the pellet (i.e. membrane fraction). We previously found that only viruses which arrive in the ER are released from Triton X-100 insoluble lipid rafts into the ER lumen whose content can be extracted by Triton X-100. As expected, when cells were infected in the presence of Brefeldin A (BFA), there was a robust block in ER arrival of SV40 due to disruption of intracellular retrograde trafficking (Figure 3-3G). However, no detectable loss of SV40 ER arrival was found using SGTA siRNA #2 while only a modest loss in the ability of SV40 to reach the ER when SGTA siRNA #1 was used (Figure 3-3G). Thus SGTA does not significantly regulate retrograde trafficking of SV40 to the ER. Given that a pool of SGTA resides on the cytosolic side of the ER membrane due to its interaction with B14 and B12, we propose this factor facilitates SV40 infection primarily by completing the membrane penetration step during entry.

**SGTA Dissociates From the B14-B12 Complex During SV40 Entry**

If SGTA extracts SV40 from the ER membrane into the cytosol, we reasoned that SGTA itself might dissociate from the B14-B12 complex during virus transport. We first monitored SGTA-B14 interaction using co-immunoprecipitation assays during SV40 entry. Cells were uninfected or infected for 2 or 8 h, harvested, followed by cross-linking of the intact cells. Similar to previous experiments (Figure 3-2D), when endogenous SGTA was immunoprecipitated, a significant amount of B14 was detected (Figure 3-4A). This interaction remained intact at 2 h post infection (h.p.i.) (Figure 3-4A), a time point when SV40 particles are largely present in endosomes and have not yet reached the ER. By contrast, a stable SGTA-B14 interaction was completely lost at 8 h.p.i. (Figure 3-4A) when SV40 has reached the ER and initiated ER-to-cytosol transport. When Hsc70 was immunoprecipitated under similar conditions, a loss of stable B14 interaction was also detected (Figure 3-4B). However, the interaction between Hsc70 and SGTA was mostly preserved. These data indicate that during time points of entry

where SV40 is undergoing membrane penetration, SGTA and Hsc70 are being released from the B14-B12 complex at the ER membrane.

This phenomenon held true in CV-1 cells transfected to express FLAG-tagged GFP or FLAG-tagged SGTA (Figure 3-4C); when cells uninfected or infected for 16 h were lysed and immunoprecipitated using anti-FLAG agarose beads, stable interactions between transfected SGTA and endogenous B14 as well as B12 remained disrupted at this later time point. While membrane penetration is observed to begin between 6 and 8 h.p.i., this process likely continues at later times due to the asynchronous nature of SV40 entry.

Our time point analyses suggested that SV40 penetration across the ER membrane is required to release SGTA from the B14-B12 complex. To further test this hypothesis, we utilized a mutant SV40 lacking VP2 (i.e. ΔVP2 SV40). This mutant virus becomes internalized but fails to penetrate the ER membrane to reach the cytosol. When compared to WT SV40, ΔVP2 SV40 did not disrupt the interaction of SGTA and B14-B12 (Figure 3-4D). Together, our findings indicate that the initiation of ER membrane penetration by SV40 is required for release of SGTA from the B14-B12 complex.

We assessed whether this dissociation event was general for ER bound cytosolic chaperones or specific to SGTA. The cytosolic p97 chaperone is well documented to link to ERAD complexes at the ER membrane and facilitate retro-translocation of ERAD substrates. In cells infected with SV40, p97's interaction with the ERAD membrane component Derlin-1 was unchanged (Figure 3-4E). This result is consistent with the recent finding that p97 is not required for SV40 entry and infection(29). SV40 infection also did not disrupt endogenous B14-B12 interaction (Figure 3-4E). We conclude SV40 specifically triggers SGTA to be released from the B14-B12 complex without globally disrupting the connection of cytosolic factors to the ER membrane.

**SGTA Associates with SV40 During Entry in Cells and *In Vitro***

An additional explanation to account for the release of SGTA from B14-B12 is that SGTA disengages from B14-B12 in order to engage SV40 as it becomes exposed in the cytosol. To test this possibility, CV-1 cells were transfected to express FLAG-tagged SGTA and infected for 8 h followed by cross-linking and immunoprecipitation with anti-FLAG agarose beads. Indeed, VP1 was detected in the immunoprecipitate of infected cells (Figure 3-4F). By contrast, VP1 was not detected in infected cells treated with BFA, which blocks ER arrival and subsequent transport to the cytosol (11, 39) (Figure 3-4F). Thus, SGTA binds to SV40 upon cytosolic arrival. We next investigated whether this SV40-SGTA interaction required the Hsc70-dependent localization of SGTA to the B14-B12 complex. When cells transfected with FLAG-tagged GFP, WT SGTA or the K160E/R164E SGTA mutant were infected and subjected to immunoprecipitation, VP1 was observed to co-precipitate only with WT SGTA and not GFP or K160E/R164E SGTA (Figure 3-4G). This result suggests that localization of SGTA to the B14-B12 complex via Hsc70 is required for SGTA to engage the virus during entry.

Hsc70 has been reported to associate with polyomaviruses *in vitro* and in cells during both entry and de novo capsid assembly. To assess whether SGTA binds to SV40 directly or requires Hsc70, we tested whether the SGTA-SV40 interaction could be recapitulated *in vitro* using purified components. FLAG-tagged GFP, WT SGTA and K160E/R164E SGTA were purified from transfected 293T cells. WT but not GFP or K160E/R164E SGTA copurified Hsc70 (Figure 3-4H). These purified components were incubated with purified SV40 pretreated with DTT and EGTA to partially mimic conformational changes that occur in the ER. When GFP or SGTA proteins were immunoprecipitated from these reactions, VP1 was detected only in reactions containing SGTA (Figure 3-4I). WT SGTA pulled down moderately more VP1 when compared to K160E/R164E SGTA, likely due to the presence of Hsc70 in the WT SGTA preparation. Nonetheless,

the observation that purified K160E/R164E SGTA lacking copurified Hsc70 binds to VP1 demonstrates that SGTA can directly interact with SV40.

**SV40 Induces the B14-B12 Complex to Form Foci on the ER Membrane**

Our finding that SV40 liberates SGTA and Hsc70 from the B14-B12 complex suggests that the virus may restructure B14-B12 within the ER membrane. To assess whether SV40 imparts any reorganization of B14-B12, we stained endogenous proteins in fixed cells uninfected or infected with SV40 for analysis by immunofluorescence microscopy. In uninfected cells, both B14 and B12 co-localized extensively with the ER membrane protein BAP31 (Figure 3-5A and 3-5B, top panels), as expected. Strikingly, in infected cells, a significant portion of B14 and B12 was observed to concentrate into discrete foci within the ER (Figure 3-5A and 3-5B, lower panels). Some cells were observed to contain a single focus, while others contained several. Notably, B14 and B12 foci co-localized with VP1 (Figure 3-5C and 3-5D), suggesting that SV40 is responsible for foci formation. As reported previously, BAP31 also reorganizes into foci during SV40 infection (29). We found that virus-induced BAP31 foci co-localized with the B14 and B12 foci (Figure 3-5A and 3-5B). These results indicate that, while B14-B12 and BAP31 were identified independently to be critical for SV40 membrane penetration, they are likely to be unified in facilitating this entry step rather than functioning in distinct parallel pathways.

The localization of Sec61$\alpha$, a major translocon component reported to associate with BAP31 (44), remained diffuse and unchanged by addition of SV40 (Figure 3-S2A, top panels). Similarly, Hrd1 staining revealed it did not form foci upon SV40 infection (Figure 3-S2A, middle panels). Although Hrd1 is a central component of ERAD machinery (45, 46), it is dispensable for SV40 entry and infection. Consistent with our observation that SGTA disengages from B14-B12 during entry, we did not detect any SV40-induced enrichment of SGTA in the B14-B12-BAP31 foci (Figure 3-S2A, bottom panels). These data indicate that SV40

induces the reorganization of only a specific subset of ER membrane proteins into a discrete region.

We observed that knockdown of SGTA did not inhibit foci formation (Figure 3-S2B), indicating that SGTA acts independently or downstream of foci formation. We further characterized SV40-induced foci formation by performing time course experiments where the presence or absence of this structure was monitored during infection by staining with specific antibodies after fixation (Figure 3-5E). When cells were infected for 2 h, foci were not detected. After 8 and 12 h of SV40 infection, approximately 25-70% of cells contained B12, B14, and BAP31 foci. By 16 h, nearly every cell was positive for B12, B14, and BAP31 foci. BFA strongly inhibited foci formation. Moreover, we used live cell imaging to monitor foci formation in cells transiently transfected to express GFP-tagged B14 (GFP-B14). GFP-B14 was observed to gradually re-organize into clear foci at approximately 5-6 h after the addition of SV40 (Figure 3-5F). We conclude that SV40-induced reorganization of B14-B12 and other membrane components is dependent on ER arrival of the virus, occurs approximately 5-6 h.p.i., and is largely irreversible. The timing of SV40's cytosolic arrival (39) correlates strongly with our detection of foci in the ER membrane, therefore we postulate that these virus-induced structures are ER exit/cytosol entry sites for the virus.

**B14 Requires its Lumenal Domain for SV40-induced Foci Formation**

We sought to identify the molecular determinants of B14 necessary for SV40-induced B14 foci formation. When full length FLAG-tagged B14 was transfected into CV-1 cells and stained as before, the transfected protein co-localized extensively with BAP31 in a diffuse manner (Figure 3-6A, left panels). When cells were infected, the ectopically expressed FLAG-B14 formed foci similar to the behavior of endogenous B14 (Figure 3-6A, right panels), with variable number of foci per cell observed. Comparable to endogenous B14 foci (Figure 3-5A), the ectopically expressed B14 foci also co-localized extensively with endogenous BAP31 foci.

As transfected WT B14 forms foci in response to SV40, we then asked whether transfected mutant forms of B14 are capable of forming foci during SV40 infection. Transfected H138Q B14, which does not interact with Hsc70 or SGTA, formed foci identical to WT B14 (Figure 3-6B, first and second row). Truncating most of B14's lumenal domain (97 amino acids) to generate Δ lumenal B14 strongly restricted it's ability to form foci, despite this mutant co-localizing normally with BAP31 in the absence of SV40 (Figure 3-6B, third row and quantified in Figure 3-6C). In addition to the normal ER expression pattern, this mutant also precipitated endogenous B12 and SGTA, demonstrating the overall integrity of this variant (Figure 3-S3). By contrast, a severe truncation of B14's cytosolic residues (i.e. Δ cytosol B14) did not restrict foci formation, acting similar to the full length WT B14 (Figure 3-6B, fourth row). Expression of the FLAG-B14 variants had minimal influence on the ability of endogenous BAP31 to form foci and did not perturb infection, likely due to the presence of endogenous B14 (Figure 3-6D). We conclude that the lumenal domain of B14 is required for its SV40-triggered reorganization into foci and potentially acts as a sensor for the virus directly.

**B14-mediated Chaperone Recruitment and Foci Formation is Required to Promote Infection.**

We assessed the molecular requirements of B14 in promoting SV40 infection by performing rescue experiments. HeLa cells were chosen for these experiments because of their high transfection efficiency. DNA plasmids were first transfected for expression from an empty vector, WT B14, H138Q B14 or Δ lumenal B14. Subsequently siRNA transfections were carried out using an siRNA oligo targeting the 3' UTR sequence of B14 to ensure depletion of only endogenous B14. After 48 h of siRNA treatment, cells were incubated with SV40 and successful infection measured 2 days later by immunoblotting for TAg (Figure 3-7). Infection of cells expressing empty vector as a control presented a complete loss of TAg expression upon B14 knockdown compared to scrambled siRNA.

This phenotype was reversed significantly in cells expressing WT B14. By contrast, H138Q B14 and Δ lumenal B14, while expressed at appropriate levels, failed to support infection in cells depleted of endogenous B14 (Figure 3-7). These data support a model whereby B14's ability to recruit Hsc70-SGTA is necessary for SV40 infection. The inability of Δ lumenal B14 to form foci and promote infection suggests that foci are functionally important for SV40 as well.

## DISCUSSION

To cause infection, nonenveloped viruses penetrate a biological membrane to gain access into the target cell. While host cues priming these viruses for membrane penetration are well-characterized, cytosolic factors co-opted to complete this membrane penetration event remain unknown. In this study, we pinpoint SGTA as a cytosolic chaperone that promotes membrane penetration of SV40 and likely other polyomaviruses. A model depicting SGTA-dependent SV40 ER membrane penetration is presented in Figure 3-8.

Our initial finding revealed that a pool of SGTA binds to the cytosolic surface of the ER membrane by engaging two transmembrane J-proteins called B14 and B12 (Figure 3-8A), essential factors for SV40 ER-to-cytosol transport and infection (32). Interaction between SGTA and the B14-B12 complex requires Hsc70, a cytosolic chaperone central to global cellular proteostasis, and is consistent with previous reports demonstrating that SGTA interacts with Hsc70 (42). The interaction of SGTA with the B14-B12 complex prompted us to ask whether it might serve to dislocate SV40 into the cytosol from the ER membrane. Indeed, our functional studies demonstrated that SGTA downregulation disrupts SV40 and BKPyV infection by blocking virus ER-to-cytosol transport, with subsequent binding experiments establishing a direct SGTA-SV40 physical interaction. These results suggest that SGTA engages the virus on the cytosolic surface of the ER membrane to mobilize it into the cytosol.

The use of SGTA to liberate SV40 into the cytosol from the ER membrane resolves a previous enigma in the mechanism of ER membrane penetration by SV40(47). Structural alterations occuring within the ER render the virus hydrophobic, enabling it to bind to and integrate into the ER membrane(28, 29). Despite these remodeling events, SV40 remains a large and intact particle when it penetrates the ER membrane (39). How this large and hydrophobic viral particle avoids aggregation in the aqueous cytosolic environment is unclear. Particle aggregation would clearly prevent SV40 from successfully reaching the

nucleus to cause infection. One possibility entails cytosolic chaperones positioned next to the ER membrane binding to and extracting the hydrophobic virus into the cytosol, and by use of this interaction, protecting the hydrophobic viral surfaces. Our results support this scenario by implicating SGTA, a cytosolic chaperone that binds to hydrophobic proteins (40), in mobilizing the virus into the cytosol and concomitantly protecting the viral hydrophobic surfaces.

Although SGTA has been recently linked to the ER-to-cytosol transport process known as ERAD, its apparent role in this instance is to assist the Bag6 complex in capturing ERAD substrates in the cytosol and preventing their aggregation prior to proteasomal degradation (40, 48). By contrast, a separate study found that SGTA antagonizes Bag6 function during protein quality control in the cytosol (49). Regardless of their relationship, SGTA appears to promote SV40 infection independently of Bag6. Our data reveals that SGTA likely serves additional undocumented roles in ER biology, possibly in cooperation with B14-B12.

We observed that SGTA and Hsc70 disengage from the B14-B12 complex, an event that coincides with the drastic reorganization of the B14-B12 complex into concentrated foci on the ER membrane (Figure 3-8B). It is possible that smaller foci structures, which are not clearly detected by microscopy, also exist to mediate viral transport. This would explain why a stable SGTA-B14 interaction appears fully disrupted at time points where not all cells have visible foci.
The energy source driving release of the virus-SGTA-Hsc70 complex into the cytosol is not known. It is possible that virus-induced B14-B12 foci formation imparts a conformational change that weakens the affinity between B14-B12 and SGTA-Hsc70. Alternatively, foci formation may simply be used to transiently increase the local chaperone concentration at the penetration site, allowing efficient engagement of the virus. While SGTA itself does not harbor ATPase activity, it can modulate the ATPase activity of Hsc70 (41). Thus, if SV40 binding to SGTA promotes SGTA to drive Hsc70 preferentially to the ADP-bound state, ADP-bound Hsc70 would have lower affinity for its cognate J-proteins B14 and

B12 (50, 51). This postulated scenario could explain how SV40 triggers release of SGTA-Hsc70 from B14-B12. Future experiments will clarify the precise mechanism by which SV40 induces SGTA and Hsc70 to disengage from the B14-B12 complex. Nonetheless, discharge of the SV40-SGTA-Hsc70 complex into the cytosol from the ER membrane (Figure 3-8C) is conceptually consistent with SV40's requirement to reach the cytosol in preparation for nuclear import during infectious entry. As Hsc70 proteins are observed to disassemble murine polyomavirus *in vitro* (52), polyomaviruses entering a host-cell could in principle co-opt both SGTA and Hsc70 activities to couple the cytosol release and viral disassembly reactions, with the latter likely being necessary for subsequent nuclear import.

The B14-B12 foci were positive for VP1, similar to a previous report that found VP1 co-localizes with BAP31 foci (29). Foci likely contain multiple viruses and future work will attempt to assess the presence of VP1 quantitatively. As ER membrane penetration is an inefficient process (39), only a small fraction of virus in the foci are expected to be released into the cytosol, explaining why VP1 accumulates in the foci even at later time points. These foci unlikely represent nonproductive, aggregation structures as no dramatic changes in the solubility of the B14 and B12 membrane proteins were observed during foci formation. Moreover, B14-B12 foci co-localize with BAP31, another ER membrane factor involved in SV40 ER membrane penetration, but not with other membrane proteins dispensable for SV40 infection such as a core ERAD component Hrd1 (29). Thus foci consist of specific ER factors that conduct SV40 across the ER membrane but not ER components irrelevant to this process. Intriguingly, there was a strong temporal correlation between foci formation and virus arrival in the cytosol. Foci formation can be readily identified prior to 8 h.p.i. and SV40 cytosol arrival occurs between approximately 6-8 h.p.i (29, 39). We therefore propose that the B14-B12 foci represent cytosol entry sites that function to increase the local SV40 concentration precisely at the membrane penetration site where the properly positioned SGTA can efficiently bind to and extract the virus into the

cytosol. This model is supported by our findings that B14 requires its ability to recruit chaperones and form foci to promote infection.

Virus-induced foci formation and other changes to ER morphology is likely to be common among Pys. BKPyV was recently observed to localize to specific subdomains within the ER (38). Addition of proteasome inhibitor blocked infection by BKPyV and caused viruses to localize away from BiP-rich regions of the ER and instead colocalize with Calnexin. These results suggest that engagement by BiP may be critical for productive infection by BKPyV.

A direct interaction between SV40 and B14-B12 or BAP31 has yet to be demonstrated, possibly due to a weak affinity of these factors to the particle within the membrane. This weak physical interaction could also explain the necessity of foci formation, which would facilitate multivalent interactions among several membrane components functioning to promote membrane penetration. At present, the relationship between B14-B12 and BAP31 remains obscure. Although these membrane proteins form foci in response to SV40 entry, no obvious physical interaction between B14-B12 and BAP31 can be isolated. Moreover, while BAP31 is thought to recognize membrane integrated SV40 with exposed VP2 via charge-pairing (29), both B14 and B12 lack charged residues within their transmembrane domains and thus recognize SV40 differently. In this regard, by evaluating different B14 mutants, we found that the lumenal portion of B14 is required for its SV40-induced reorganization. This region of B14, which lacks any clear protein-protein interaction domains, could therefore act as a sensor for engaging SV40 complementarily with BAP31.

An outstanding question is whether a bona fide protein-conducting channel exists to accommodate SV40 transport across the ER membrane. If this is the case, it is unlikely that a native channel can support the transport of such a large viral particle whose diameter is approximately 45-50 nm. Instead, the hydrophobic virus might initially integrate into the membrane and subsequently recruit and

oligomerize ER membrane proteins such as B14, B12, and BAP31. The oligomerized structure (i.e. foci) would surround the viral particle until SGTA-Hsc70 extracts it into the cytosol.

In conclusion, this study identifies a novel cytosolic chaperone complex that completes ER membrane penetration of a nonenveloped virus, and utilizes dramatic rearrangement of ER membrane elements in the process. Viral entry, replication, and assembly are defining steps during the infection course. While diverse viruses are known to rearrange the ER membrane to facilitate viral replication and assembly, essentially nothing is known regarding how viruses reorganize the ER membrane during entry (53). The possibility that SV40 and other polyomavirus family members might reorganize components of the ER membrane to fashion its own entry site would demonstrate that viruses have the capacity to restructure the ER membrane to accommodate the early events of infection.

## FIGURES

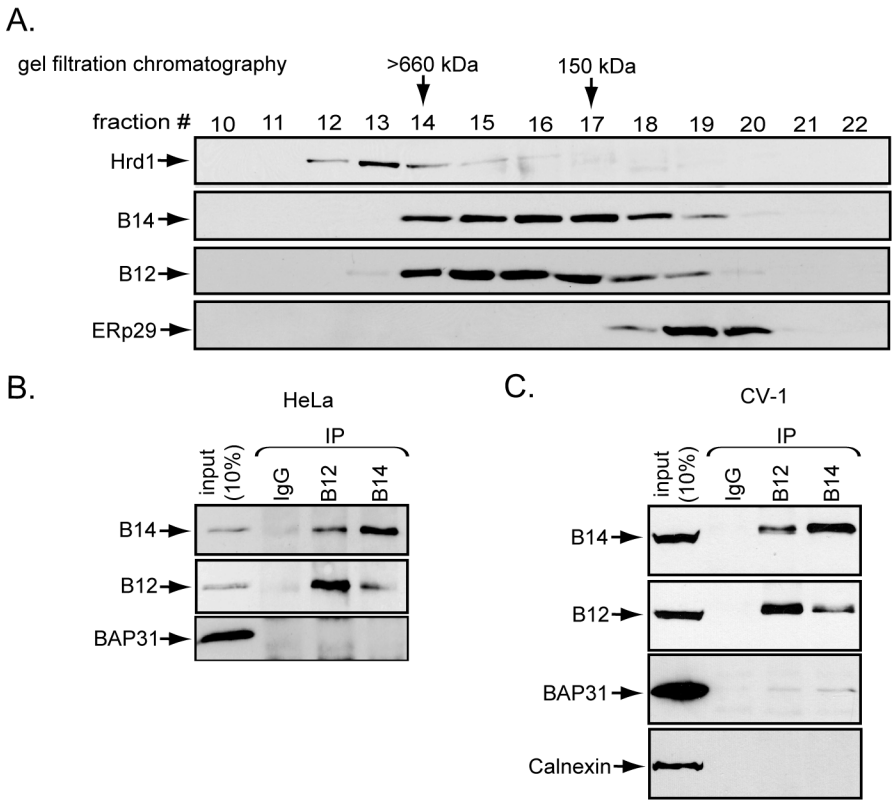


**Figure 3-1. B14 complexes with B12.**

(A) Lysates prepared from HeLa cells were subjected to gel filtration chromatography. Collected fractions were analyzed by immunoblot with the indicated antibodies.
(B) B14 and B12 interact. HeLa cell lysates were used for immunoprecipitation with control IgG or antibodies against endogeneous B12 or B14.
(C) as in (B) except CV-1 cell lysate was used.

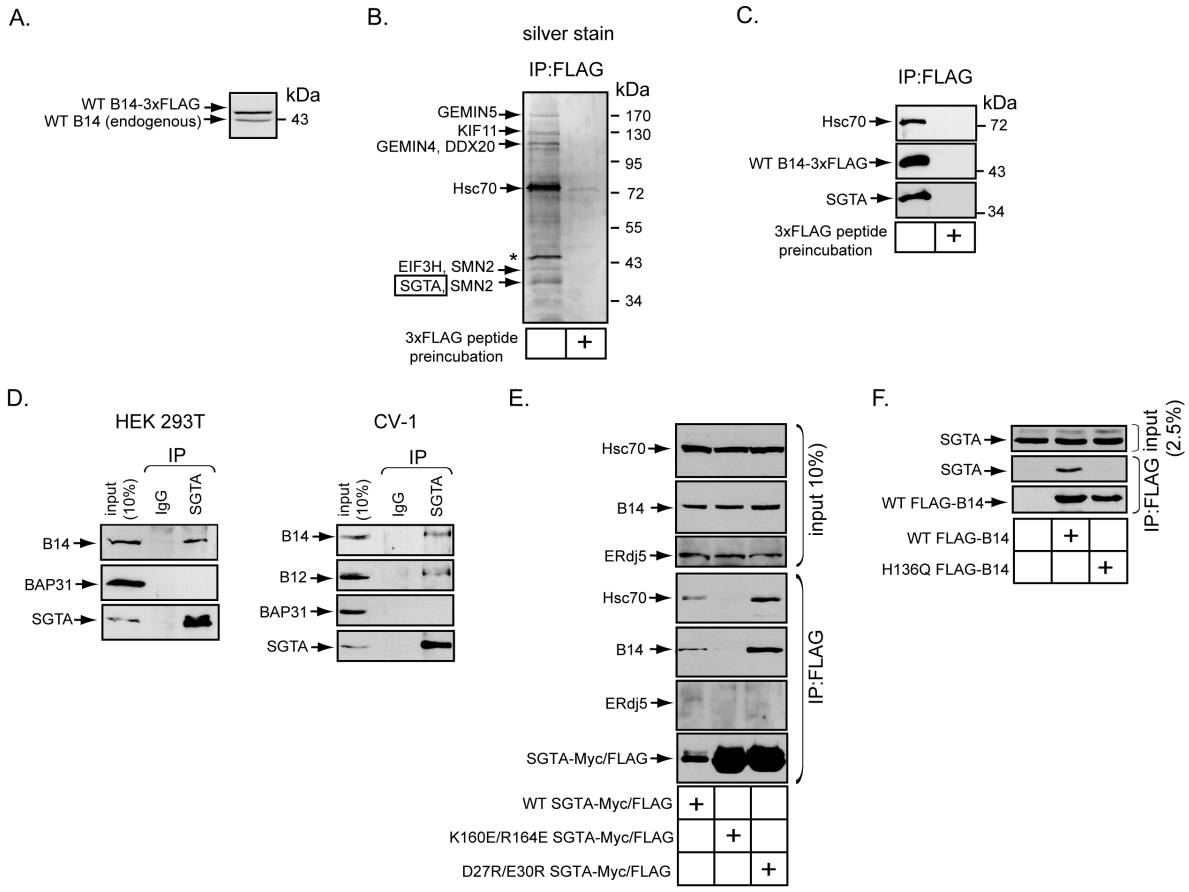
A.
WT B14-3xFLAG
WT B14 (endogenous)
kDa
43
B.
silver stain
IP:FLAG
kDa
GEMIN5
KIF11
GEMIN4, DDX20
Hsc70
EIF3H, SMN2
SGTA, SMN2
*
170
130
95
72
55
43
34
3xFLAG peptide preincubation
+
C.
IP:FLAG
kDa
Hsc70
WT B14-3xFLAG
SGTA
72
43
34
3xFLAG peptide preincubation
+
D.
HEK 293T
CV-1
IP
input (10%)
IgG
SGTA
B14
BAP31
SGTA
B12
E.
Hsc70
B14
ERdj5
input 10%
IP:FLAG
SGTA-Myc/FLAG
WT SGTA-Myc/FLAG
K160E/R164E SGTA-Myc/FLAG
D27R/E30R SGTA-Myc/FLAG
F.
SGTA
WT FLAG-B14
H136Q FLAG-B14
IP:FLAG input (2.5%)

**Figure 3-2. The Cytosolic Chaperone SGTA Binds to the B14-B12 Complex in a Hsc70-dependent Manner**.

(A) B14-3xFLAG is expressed at a level near endogenous B14. Whole cell lysates derived from Flpn-293 TREx(B14-3xFLAG) were analyzed by SDS-PAGE and immunoblotted with an antibody against B14. Relative molecular weight markers in kDa are shown on the right.
(B) SGTA identified by MS as a binding partner of B14. Immunopurified B14-3xFLAG complexes from lysate in (A) was eluted by 3xFLAG peptide and subjected to SDS-PAGE and silver staining. A control experiment was performed in which lysate was incubated with anti-FLAG agarose beads pre-incubated with 3xFLAG peptide. Indicated proteins were identified after band excision using MS. * indicates a protein migrating at the size of B14-3xFLAG.
(C) As in (B) except immunoblotting was performed with the indicated antibodies.
(D) Endogenous interaction between SGTA and B14-B12. Lysates derived from 293T (left) or CV-1 cells (right) were used for immunoprecipitation with the indicated antibodies.
(E) SGTA's interaction with B14 requires coupling to Hsc70. CV-1 cells were transfected with plasmids expressing FLAG-tagged WT or SGTA mutants. Immunoprecipitation was performed from the cell lysates using anti-FLAG agarose beads with subsequent immunoblot analysis.
(F) As in (E) except cells were transfected with plasmids encoding WT or mutant B14.

.

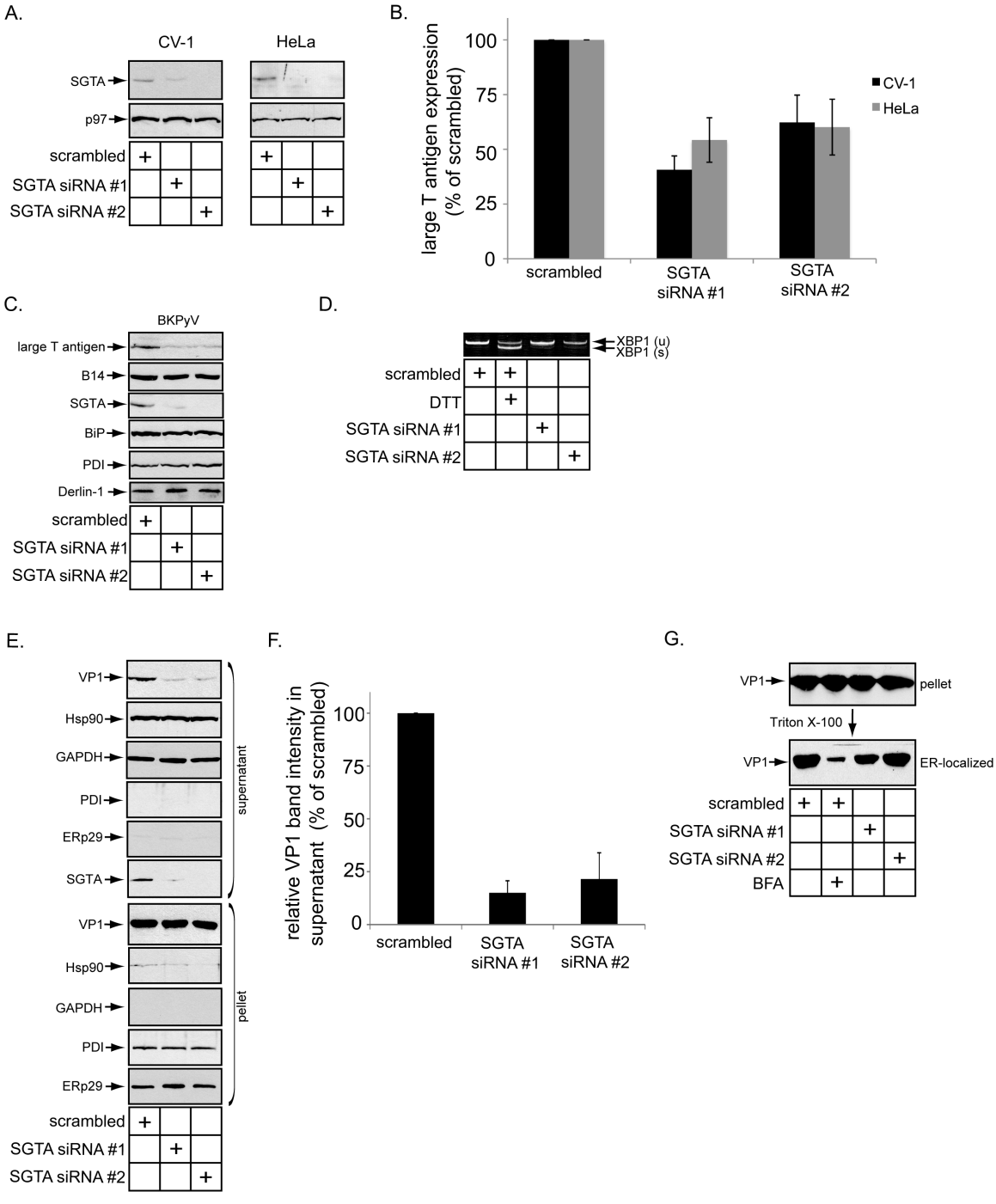
A.
CV-1
HeLa
SGTA
p97
scrambled
SGTA siRNA #1
SGTA siRNA #2
B.
large T antigen expression (% of scrambled)
100
75
50
25
0
CV-1
HeLa
scrambled
SGTA siRNA #1
SGTA siRNA #2
C.
BKPyV
large T antigen
B14
SGTA
BiP
PDI
Derlin-1
scrambled
SGTA siRNA #1
SGTA siRNA #2
D.
XBP1 (u)
XBP1 (s)
scrambled
DTT
SGTA siRNA #1
SGTA siRNA #2
E.
VP1
Hsp90
GAPDH
PDI
ERp29
SGTA
supernatant
VP1
Hsp90
GAPDH
PDI
ERp29
pellet
scrambled
SGTA siRNA #1
SGTA siRNA #2
F.
relative VP1 band intensity in supernatant (% of scrambled)
100
75
50
25
0
scrambled
SGTA siRNA #1
SGTA siRNA #2
G.
VP1
pellet
Triton X-100
VP1
ER-localized
scrambled
SGTA siRNA #1
SGTA siRNA #2
BFA

**Figure 3-3. SGTA Knockdown Perturbs SV40 and BKPyV Infection by Blocking Viral ER-to-cytosol Transport**

(A) CV-1 (left) or HeLa cells (right) were transfected with scrambled or siRNAs targeting SGTA for 24 h before being harvested and analyzed by immunoblotting with the indicated antibodies.
(B) SGTA knockdown blocks SV40 infection. Cells transfected for 24 h as in (A) were infected with SV40 for 20-24 h, fixed, and stained for large T antigen. Infection was scored using immunofluorescence microscopy (counting ≥500 cells for each condition). CV-1 cells were infected at a MOI ≈ 3, resulting in 30-50% cells positive for large T antigen. HeLa cells were infected with SV40 at a MOI≈10, resulting in 3-5% cells infected for the control condition. Infection was normalized to scramble siRNA and represents the mean ± SD of at least three independent experiments. A statistically significant ($p < 0.05$) difference was observed with all SGTA knockdown conditions compared to scrambled.
(C) SGTA is important for BKPyV infection. CV-1 cells transfected as in (A) were infected with BKPyV at a MOI ≈1. Lysates were subjected to immunoblotting with the indicated antibodies 40 h.p.i.
(D) XBP1 splicing does not occur with transient SGTA knockdown. RT-PCR analysis of the unspliced (u) and spliced (s) forms of XBP1 mRNA in cells transfected with scrambled or SGTA siRNAs. Where indicated, cells were treated with DTT as a positive control for UPR induction.
(E) SGTA promotes ER-to-cytosol transport of SV40. CV-1 cells transfected as in (A) were incubated with SV40 at a MOI ≈10, harvested 12 h.p.i. and subjected to ER-to-cytosol transport assay (see experimental procedures).
(F) Relative VP1 band intensities in the supernatant fractions were determined using ImageJ (NIH). Data are normalized to scrambled siRNA. Only experiments with equal loading (Hsp90 or GAPDH) were considered. Values represent the mean ± SD of four independent experiments. A statistically significant ($p < 0.05$) difference was observed with all SGTA knockdown conditions compared to scrambled.
(G) Loss of SGTA does not significantly block ER arrival of SV40. Pellet fraction produced from cells as in (E) were solubilized in a buffer containing 1% Triton X-100. After centrifugation, the soluble fraction was analyzed by VP1 immunoblotting. As a positive control, where indicated, cells were treated with BFA to block ER arrival.

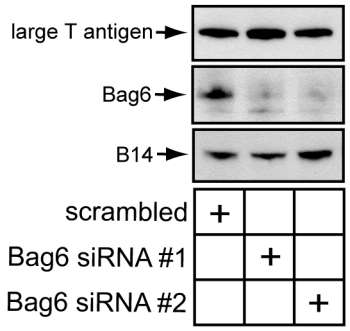


**Figure 3-S1. Bag6 Knockdown does not Block SV40 Infection, Related to Figure 3-3**

CV-1 cells were transfected with the indicated siRNAs for 24 h before being infected with SV40 for an additional 24 h and harvested. Immunoblot analysis was performed with the indicated antibodies.

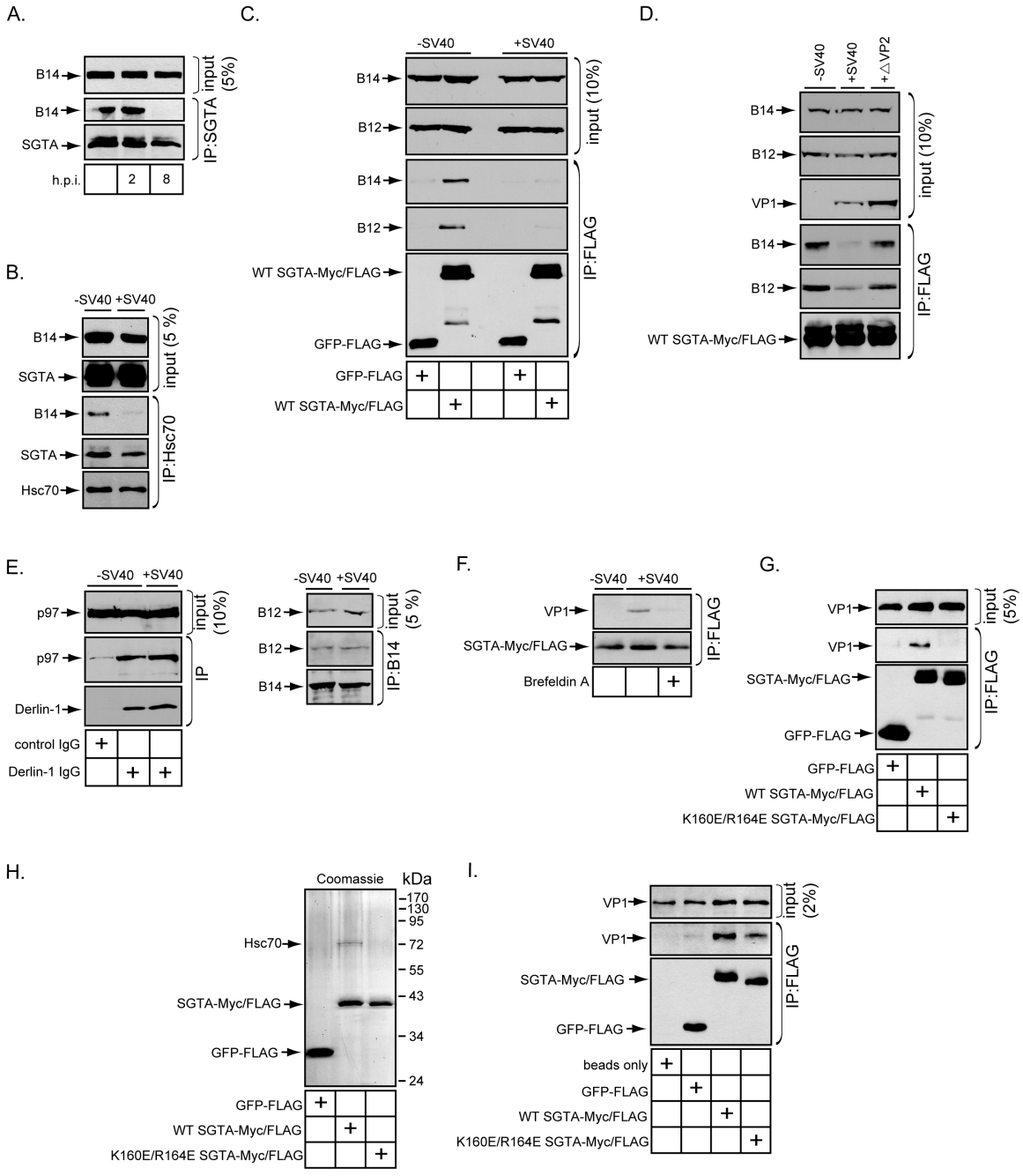
A.
B14
B14
SGTA
h.p.i.
2
8
IP:SGTA input (5%)
B.
-SV40 +SV40
B14
SGTA
B14
SGTA
Hsc70
input (5 %)
IP:Hsc70
C.
-SV40
+SV40
B14
B12
B14
B12
WT SGTA-Myc/FLAG
GFP-FLAG
GFP-FLAG
WT SGTA-Myc/FLAG
input (10%)
IP:FLAG
D.
-SV40
+SV40
+△VP2
B14
B12
VP1
B14
B12
WT SGTA-Myc/FLAG
input (10%)
IP:FLAG
E.
-SV40 +SV40
p97
p97
Derlin-1
control IgG
Derlin-1 IgG
input (10%)
IP
-SV40 +SV40
B12
B12
B14
input (5 %)
IP:B14
F.
-SV40 +SV40
VP1
SGTA-Myc/FLAG
Brefeldin A
IP:FLAG
G.
VP1
VP1
SGTA-Myc/FLAG
GFP-FLAG
GFP-FLAG
WT SGTA-Myc/FLAG
K160E/R164E SGTA-Myc/FLAG
input (5%)
IP:FLAG
H.
Coomassie
kDa
170
130
95
72
55
43
34
24
Hsc70
SGTA-Myc/FLAG
GFP-FLAG
GFP-FLAG
WT SGTA-Myc/FLAG
K160E/R164E SGTA-Myc/FLAG
I.
VP1
VP1
SGTA-Myc/FLAG
GFP-FLAG
beads only
GFP-FLAG
WT SGTA-Myc/FLAG
K160E/R164E SGTA-Myc/FLAG
input (2%)
IP:FLAG

**Figure 3-4. SGTA-Hsc70 Dissociates from the B14-B12 Complex and Engages SV40 During Entry**

(A) Endogenous SGTA is released from B14 during entry. CV-1 cells were uninfected or infected with SV40 at a high MOI (≈100) for the indicated time. Cells were harvested, cross-linked, and lysed in buffer containing 1% Triton X-100 followed by immunoprecipitation with SGTA antibodies and immunoblotting.
(B) Endogenous Hsc70 is released from B14 during entry. CV-1 cells were infected or uninfected for 12 h and immunoprecipitated as in (A) except Hsc70 antibodies were used.
(C) Transfected SGTA is released from B14-B12 during entry. CV-1 cells transfected to express FLAG-tagged GFP or SGTA were infected with SV40 for 16h. Immunoprecipitation was performed without cross-linking and the precipitated material analyzed by immunoblotting.
(D) SV40 lacking VP2 fails to trigger dissociation of SGTA from B14-B12. As in (B) except cells were also infected with ΔVP2 SV40.
(E) p97-Derlin-1 interaction is unaffected by SV40. Cells infected with virus as in (A) were lysed without cross-linking and immunoprecipitated with the indicated antibodies with subsequent immunoblotting of the precipitated material.
(F) SGTA interacts with SV40 in cells during entry. CV-1 cells transfected to express FLAG-tagged WT SGTA were infected with SV40 at high MOI. Where indicated, cells were treated with BFA. Cells were cross-linked, lysed, and immunoprecipitated with anti-FLAG agarose beads. Precipitated proteins were analyzed by immunoblotting with the indicated antibodies.
(G) SGTA requires localization to B14-B12 for interaction with SV40. As in (E) except cells were transfected to express either FLAG-tagged GFP, WT SGTA or mutant SGTA.
(H) Coomassie staining of purified proteins isolated from transfected 293T cells.
(I) Direct binding of SGTA and SV40 *in vitro*. Purified proteins were incubated with DTT/EGTA-treated SV40. Reactions were cross-linked, and the sampled precipitated using anti-FLAG agarose beads. Bound material was analyzed by immunoblotting.

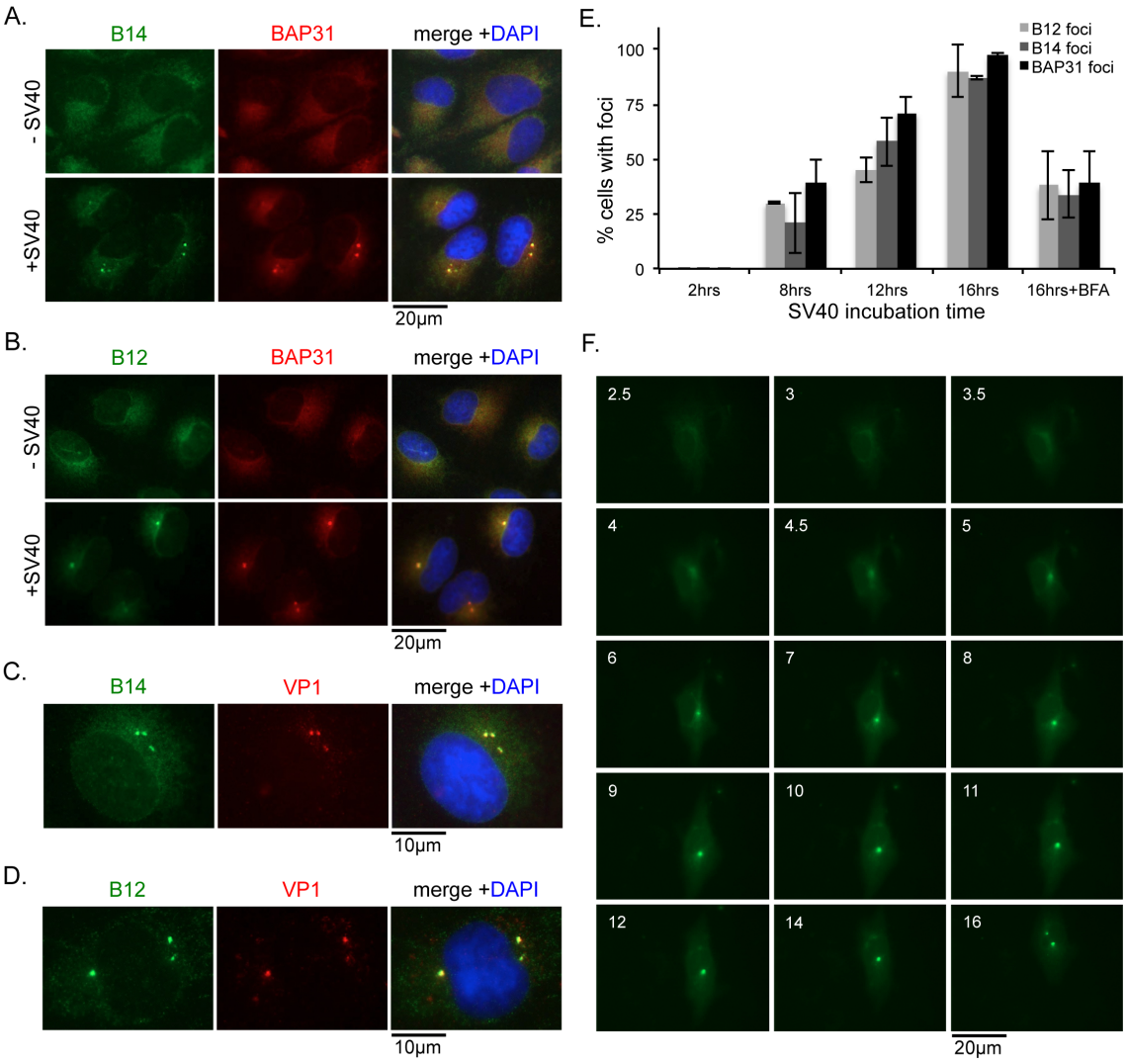
A.
B14
BAP31
merge +DAPI
- SV40
+SV40
20μm
B.
B12
BAP31
merge +DAPI
- SV40
+SV40
20μm
C.
B14
VP1
merge +DAPI
10μm
D.
B12
VP1
merge +DAPI
10μm
E.
B12 foci
B14 foci
BAP31 foci
% cells with foci
100
75
50
25
0
2hrs
8hrs
12hrs
16hrs
16hrs+BFA
SV40 incubation time
F.
2.5
3
3.5
4
4.5
5
6
7
8
9
10
11
12
14
16
20μm

**Figure 3-5. SV40 Induces the B14-B12 Complex to Form Foci on the ER Membrane**

(A) B14 reorganizes into foci upon SV40 infection. CV-1 cells uninfected or infected with SV40 (MOI ≈ 30-50) for 16 h were fixed and stained with the indicated antibodies for immunofluorescence microscopy.
(B) B12 reorganizes into foci upon SV40 infection. As in (A) except B12 antibodies were used.
(C) VP1 is present in B14-B12 foci. As in (A) using B14 and VP1 antibodies.
(D) As in (C) except using B12 antibodies.
(E) Time course experiment monitoring foci formation. Cells were infected as in (A). Where indicated, BFA was added during entry. Cells were fixed at different time points after infection and stained with antibodies against BAP31, B14, or B12. Cells were scored positive if at least one focus is present in the cell. Values represent mean ± SD of three independent experiments.
(F) Live cell imaging of GFP-B14 foci formation. Cells were transfected to express B14 with an N-terminal GFP tag. Cells were infected with SV40 and live cell imaging performed beginning at 2.5 h.p.i. Numbers in each frame indicate time is h.p.i.

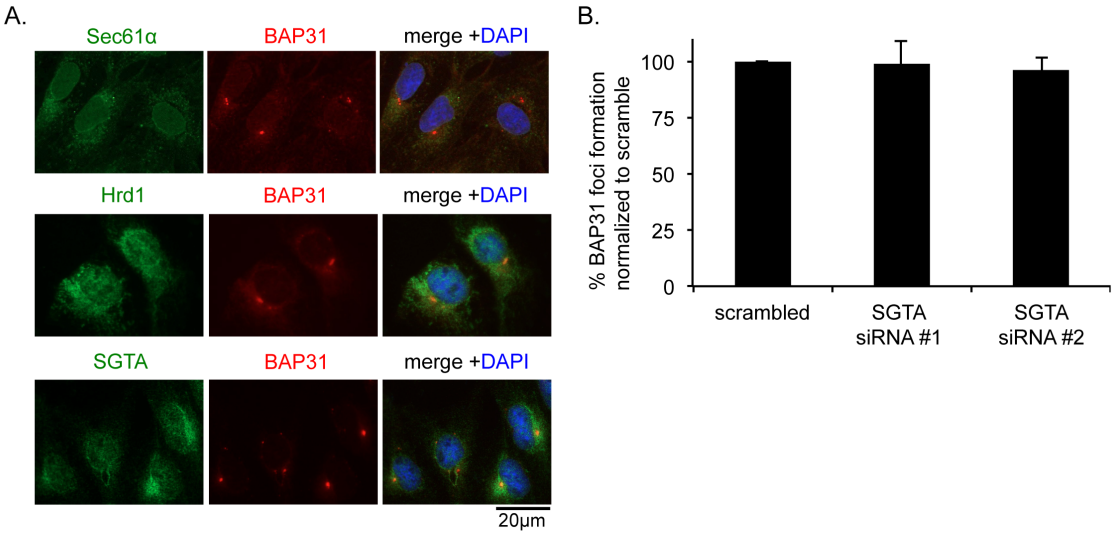


**Figure 3-S2. Foci do not Contain Sec61α, Hrd1 and SGTA, and are Unaffected by Loss of SGTA, Related to Figure 3-5.**

(A) CV-1 cells were infected with SV40 for 16 h before being fixed and stained with the indicated antibodies for immunofluorescence microscopy.
(B) CV-1 cells were transfected with scramble or SGTA siRNAs prior to addition of SV40. 16 h.p.i., cells were fixed and stained for BAP31. Cells were scored for the presence or absence of foci. Data are normalized to the scramble condition and represent the mean ± SD of three independent experiments. No statistical differences were found, $p > 0.05$.

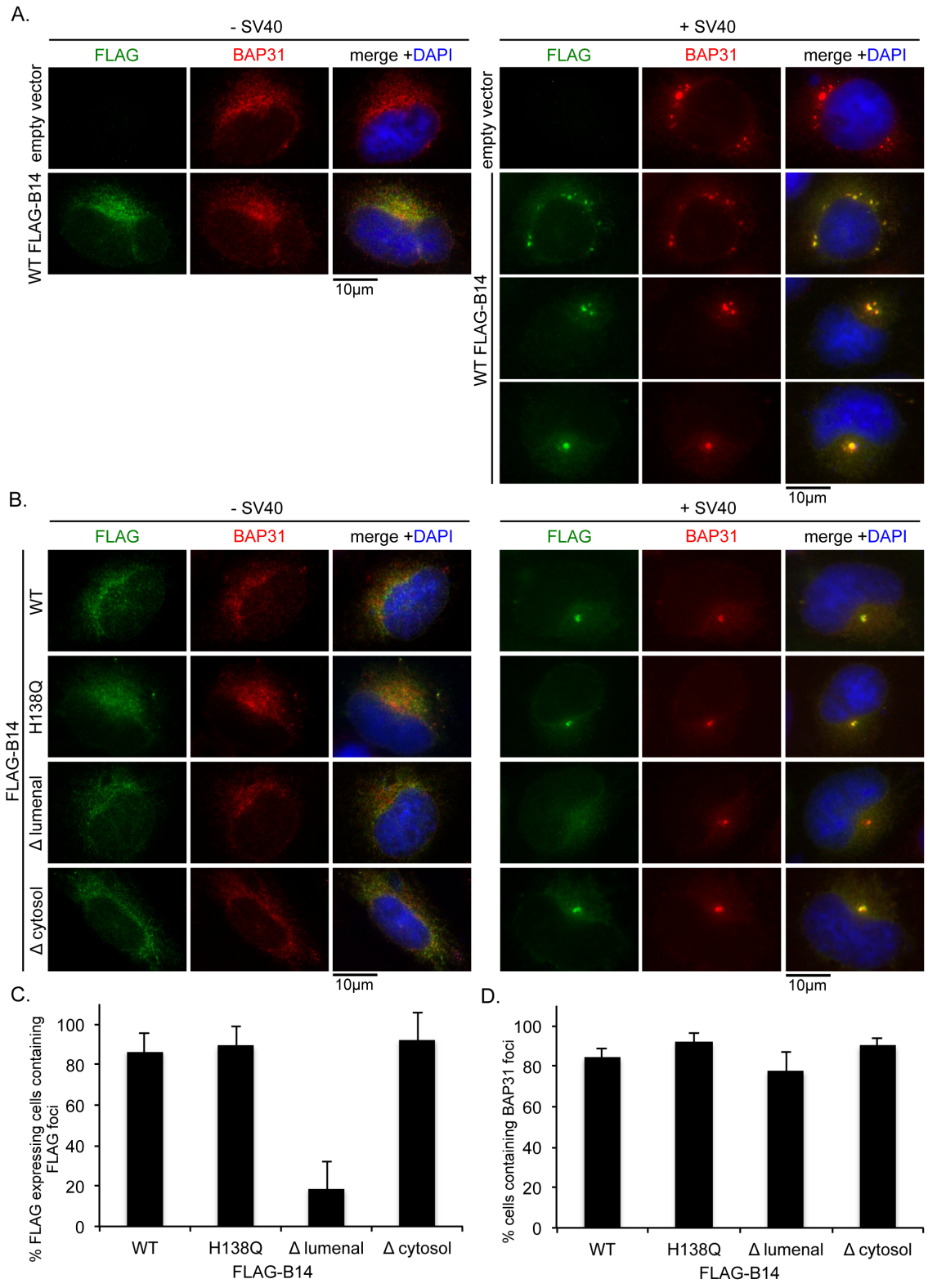
A.
- SV40
+ SV40
FLAG
BAP31
merge +DAPI
empty vector
WT FLAG-B14
10μm
B.
FLAG-B14
WT
H138Q
Δ lumenal
Δ cytosol
C.
% FLAG expressing cells containing FLAG foci
100
80
60
40
20
0
WT
H138Q
Δ lumenal
Δ cytosol
FLAG-B14
D.
% cells containing BAP31 foci

**Figure 3-6. B14 Requires Its Lumenal Domain for SV40-induced Foci Formation**

(A) Transfected WT FLAG-B14 forms SV40-induced foci. Cells were transfected with empty vector or a plasmid expressing WT FLAG-B14. Cells were uninfected or infected with SV40 for 16 h, fixed, and stained with antibodies for immunofluorescence microscopy.
(B) ∆lumenal FLAG-B14 fails to reorganize into foci. Cells were transfected with WT or mutant FLAG-B14 and analyzed as in (A).
(C) Quantification of (B). Fixed cells were scored for the presence or absence of FLAG-foci in cells expressing the respective FLAG-tagged protein. Values represent mean ± SD of three independent experiments. A statistically significant ($p < 0.05$) difference was observed with ∆lumenal FLAG-B14 when compared to all other versions of FLAG-B14.
(D) BAP31 foci formation is not disrupted by expression of WT or mutant B14. As in (C) except cells were scored for BAP31 foci in cells expressing the indicated FLAG-tagged protein. Values represent mean ± SD of three independent experiments. No statistical differences were found, $p > 0.05$.

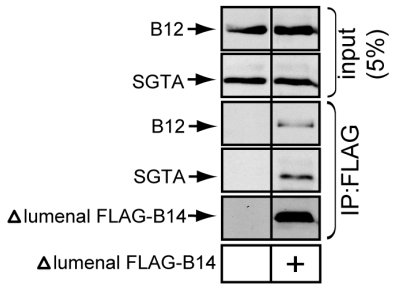


**Figure 3-S3. B14 Mutant Lacking Lumenal Domain Interacts with B12 and SGTA, Related to Figure 3-6**

CV-1 cells were transfected to express FLAG-tagged B14 mutant or left untransfected. Lysates were prepared and immunoprecipitation carried out using anti-FLAG agarose beads. Bound material was analyzed by immunoblotting.

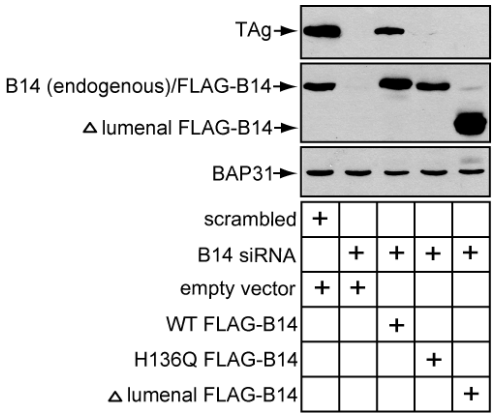


**Figure 3-7. B14-mediated Chaperone Recruitment and Foci Formation is Required to Promote Infection.** HeLa cells were transfected with the indicated DNA plasmids for approximately 18 h prior to transfection with scrambled or B14 siRNA. SV40 was incubated with cells for 2 days before preparing whole cell lysates for immunoblot analysis with the indicated antibodies.

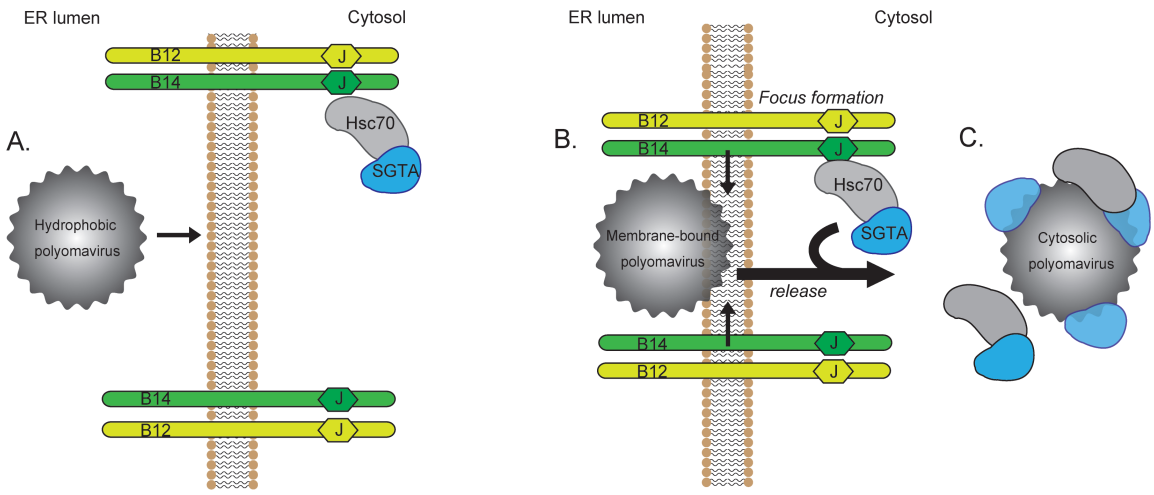


**Figure 3-8. Model for ER-to-Cytosol Transport of Polyomaviruses Mediated by Foci Formation and Cytosolic SGTA**

(A) Polyomaviruses become hydrophobic due to conformational changes imposed upon them by ER lumenal chaperones and PDI proteins. This hydrophobicity allows for membrane binding and integration by the viral particle.
(B) Membrane-bound viruses recruit the B14-B12 complex causing their reorganization into discrete foci, which may serve to transiently increase the local concentration of chaperones at the site of membrane penetration.
(C) Polyomaviruses are mobilized out of the ER into the cytosol in a SGTA-dependent manner. SGTA and Hsc70 are released from the B14-B12 complex as SGTA physically interacts with the virus.

## REFERENCES


1. Mercer J, Schelhaas M, & Helenius A (2010) Virus entry by endocytosis. *Annual review of biochemistry* 79:803-833.

2. Tsai B (2007) Penetration of nonenveloped viruses into the cytoplasm. *Annu Rev Cell Dev Biol* 23:23-43.

3. Baer GS & Dermody TS (1997) Mutations in reovirus outer-capsid protein sigma3 selected during persistent infections of L cells confer resistance to protease inhibitor E64. *J Virol* 71(7):4921-4928.

4. Chandran K, Farsetta DL, & Nibert ML (2002) Strategy for nonenveloped virus entry: a hydrophobic conformer of the reovirus membrane penetration protein micro 1 mediates membrane disruption. *J Virol* 76(19):9920-9933.

5. Farr GA, Zhang LG, & Tattersall P (2005) Parvoviral virions deploy a capsid-tethered lipolytic enzyme to breach the endosomal membrane during cell entry. *Proc Natl Acad Sci U S A* 102(47):17148-17153.

6. Wiethoff CM, Wodrich H, Gerace L, & Nemerow GR (2005) Adenovirus protein VI mediates membrane disruption following capsid disassembly. *J Virol* 79(4):1992-2000.

7. Engel S*, et al.* (2011) Role of endosomes in simian virus 40 entry and infection. *J Virol* 85(9):4198-4211.

8. Jiang M, Abend JR, Tsai B, & Imperiale MJ (2009) Early events during BK virus entry and disassembly. *J Virol* 83(3):1350-1358.

9. Kartenbeck J, Stukenbrok H, & Helenius A (1989) Endocytosis of simian virus 40 into the endoplasmic reticulum. *J Cell Biol* 109(6 Pt 1):2721-2729.

10. Nelson CD, Derdowski A, Maginnis MS, O'Hara BA, & Atwood WJ (2012) The VP1 subunit of JC polyomavirus recapitulates early events in viral trafficking and is a novel tool to study polyomavirus entry. *Virology* 428(1):30-40.

11. Norkin LC, Anderson HA, Wolfrom SA, & Oppenheim A (2002) Caveolar endocytosis of simian virus 40 is followed by brefeldin A-sensitive transport to the endoplasmic reticulum, where the virus disassembles. *J Virol* 76(10):5156-5166.

12. Qian M, Cai D, Verhey KJ, & Tsai B (2009) A lipid receptor sorts polyomavirus from the endolysosome to the endoplasmic reticulum to cause infection. *PLoS Pathog* 5(6):e1000465.

13. Richards AA, Stang E, Pepperkok R, & Parton RG (2002) Inhibitors of COP-mediated transport and cholera toxin action inhibit simian virus 40 infection. *Mol Biol Cell* 13(5):1750-1764.

14. DeCaprio JA & Garcea RL (2013) A cornucopia of human polyomaviruses. *Nat Rev Microbiol* 11(4):264-276.

15. Jiang M, Abend JR, Johnson SF, & Imperiale MJ (2009) The role of polyomaviruses in human disease. *Virology* 384(2):266-273.

16. Ewers H*, et al.* (2010) GM1 structure determines SV40-induced membrane invagination and infection. *Nat Cell Biol* 12(1):11-18; sup pp 11-12.

17. Tsai B*, et al.* (2003) Gangliosides are receptors for murine polyoma virus and SV40. *EMBO J* 22(17):4346-4355.

18. Nakanishi A, Shum D, Morioka H, Otsuka E, & Kasamatsu H (2002) Interaction of the Vp3 nuclear localization signal with the importin alpha 2/beta heterodimer directs nuclear entry of infecting simian virus 40. *J Virol* 76(18):9368-9377.

19. Nakanishi A, Clever J, Yamada M, Li PP, & Kasamatsu H (1996) Association with capsid proteins promotes nuclear targeting of simian virus 40 DNA. *Proc Natl Acad Sci U S A* 93(1):96-100.

20. Stehle T, Gamblin SJ, Yan Y, & Harrison SC (1996) The structure of simian virus 40 refined at 3.1 A resolution. *Structure* 4(2):165-182.

21. Liddington RC*, et al.* (1991) Structure of simian virus 40 at 3.8-A resolution. *Nature* 354(6351):278-284.

22. Chen XS, Stehle T, & Harrison SC (1998) Interaction of polyomavirus internal protein VP2 with the major capsid protein VP1 and implications for participation of VP2 in viral entry. *EMBO J* 17(12):3233-3240.

23. Magnuson B*, et al.* (2005) ERp29 triggers a conformational change in polyomavirus to stimulate membrane binding. *Mol Cell* 20(2):289-300.

24. Gilbert J, Ou W, Silver J, & Benjamin T (2006) Downregulation of protein disulfide isomerase inhibits infection by the mouse polyomavirus. *J Virol* 80(21):10868-10870.

25. Walczak CP & Tsai B (2011) A PDI family network acts distinctly and coordinately with ERp29 to facilitate polyomavirus infection. *J Virol* 85(5):2386-2396.

26. Schelhaas M*, et al.* (2007) Simian Virus 40 depends on ER protein folding and quality control factors for entry into host cells. *Cell* 131(3):516-529.

27. Kuksin D & Norkin LC (2012) Disassembly of simian virus 40 during passage through the endoplasmic reticulum and in the cytoplasm. *J Virol* 86(3):1555-1562.

28. Rainey-Barger EK, Magnuson B, & Tsai B (2007) A chaperone-activated nonenveloped virus perforates the physiologically relevant endoplasmic reticulum membrane. *J Virol* 81(23):12996-13004.

29. Geiger R*, et al.* (2011) BAP31 and BiP are essential for dislocation of SV40 from the endoplasmic reticulum to the cytosol. *Nat Cell Biol* 13(11):1305-1314.

30. Hirsch C, Gauss R, Horn SC, Neuber O, & Sommer T (2009) The ubiquitylation machinery of the endoplasmic reticulum. *Nature* 458(7237):453-460.

31. Olzmann JA, Kopito RR, & Christianson JC (2012) The Mammalian Endoplasmic Reticulum-Associated Degradation System. *Cold Spring Harbor perspectives in biology*.

32. Goodwin EC*, et al.* (2011) BiP and Multiple DNAJ Molecular Chaperones in the Endoplasmic Reticulum Are Required for Efficient Simian Virus 40 Infection. *MBio* 2(3).

33. Lilley BN, Gilbert JM, Ploegh HL, & Benjamin TL (2006) Murine polyomavirus requires the endoplasmic reticulum protein Derlin-2 to initiate infection. *J Virol* 80(17):8739-8744.

34. Sopha P*, et al.* (2012) A novel mammalian ER-located J-protein, DNAJB14, can accelerate ERAD of misfolded membrane proteins. *Cell Struct Funct* 37(2):177-187.

35. Grove DE, Fan CY, Ren HY, & Cyr DM (2011) The endoplasmic reticulum-associated Hsp40 DNAJB12 and Hsc70 cooperate to facilitate RMA1 E3-dependent degradation of nascent CFTRDeltaF508. *Mol Biol Cell* 22(3):301-314.

36. Yamamoto YH*, et al.* (2010) A novel ER J-protein DNAJB12 accelerates ER-associated degradation of membrane proteins including CFTR. *Cell Struct Funct* 35(2):107-116.

37. Ye Y, Meyer HH, & Rapoport TA (2001) The AAA ATPase Cdc48/p97 and its partners transport proteins from the ER into the cytosol. *Nature* 414(6864):652-656.

38. Bennett SM, Jiang M, & Imperiale MJ (2013) Role of cell-type-specific endoplasmic reticulum-associated degradation in polyomavirus trafficking. *J Virol* 87(16):8843-8852.

39. Inoue T & Tsai B (2011) A large and intact viral particle penetrates the endoplasmic reticulum membrane to reach the cytosol. *PLoS Pathog* 7(5):e1002037.

40. Xu Y, Cai M, Yang Y, Huang L, & Ye Y (2012) SGTA recognizes a noncanonical ubiquitin-like domain in the Bag6-Ubl4A-Trc35 complex to promote endoplasmic reticulum-associated degradation. *Cell Rep* 2(6):1633-1644.

41. Angeletti PC, Walker D, & Panganiban AT (2002) Small glutamine-rich protein/viral protein U-binding protein is a novel cochaperone that affects heat shock protein 70 activity. *Cell stress & chaperones* 7(3):258-268.

42. Tobaben S*, et al.* (2001) A trimeric protein complex functions as a synaptic chaperone machine. *Neuron* 31(6):987-999.

43. Diacumakos EG & Gershey EL (1977) Uncoating and gene expression of simian virus 40 in CV-1 cell nuclei inoculated by microinjection. *J Virol* 24(3):903-906.

44. Wang B*, et al.* (2008) BAP31 interacts with Sec61 translocons and promotes retrotranslocation of CFTRDeltaF508 via the derlin-1 complex. *Cell* 133(6):1080-1092.

45. Carvalho P, Stanley AM, & Rapoport TA (2010) Retrotranslocation of a misfolded luminal ER protein by the ubiquitin-ligase Hrd1p. *Cell* 143(4):579-591.

46. Christianson JC*, et al.* (2012) Defining human ERAD networks through an integrative mapping strategy. *Nat Cell Biol* 14(1):93-105.

47. Inoue T, Moore P, & Tsai B (2011) How viruses and toxins disassemble to enter host cells. *Annual review of microbiology* 65:287-305.

48. Wang Q*, et al.* (2011) A ubiquitin ligase-associated chaperone holdase maintains polypeptides in soluble states for proteasome degradation. *Mol Cell* 42(6):758-770.

49. Leznicki P & High S (2012) SGTA antagonizes BAG6-mediated protein triage. *Proc Natl Acad Sci U S A* 109(47):19214-19219.

50. Ahmad A*, et al.* (2011) Heat shock protein 70 kDa chaperone/DnaJ cochaperone complex employs an unusual dynamic interface. *Proc Natl Acad Sci U S A* 108(47):18966-18971.

51. Suh WC, Lu CZ, & Gross CA (1999) Structural features required for the interaction of the Hsp70 molecular chaperone DnaK with its cochaperone DnaJ. *The Journal of biological chemistry* 274(43):30534-30539.

52. Chromy LR, Oltman A, Estes PA, & Garcea RL (2006) Chaperone-mediated in vitro disassembly of polyoma- and papillomaviruses. *J Virol* 80(10):5086-5091.

53. Miller S & Krijnse-Locker J (2008) Modification of intracellular membrane structures for virus replication. *Nat Rev Microbiol* 6(5):363-374.

## Chapter 4. **Conclusions and Future Directions**

A conceptual overview of this thesis is presented in Figure 4-1. The membrane penetration events that allow Pys to infect a host-cell relies on multiple PQC networks existing in the ER lumen, membrane and cytosol. Py transport to the cytosol appears analogous in many ways to the pathway used for the elimination of misfolded ER proteins.

The hijacking of cellular PQC systems by nonenveloped viruses and other pathogens has evolved as a strategy for several reasons. First, PQC systems exist with a functional versatility that allows for the proper folding, translocation, and degradation of a diverse and complex proteome. This versatility is highly suitable for recognition of foreign viruses during both entry and assembly, as productive protein-protein interactions and conformational changes are often critical for these events. Secondly, chaperones and other quality control factors are positioned in nearly every cellular space to maintain proteostasis with high efficiency. In the context of membrane penetration by viruses, the utilization of membrane-localized chaperone networks existing normally for translocation into or out of organelles may be underappreciated.

The use of ER resident PDI proteins by polyomaviruses during entry (Chapter 2) illustrates how PQC factors can be exploited for their versatility. PDI proteins are involved in both the biogenesis and destruction of proteins (1, 2). Many PDIs have established chaperone activity (2-5), allowing them to bind hydrophobic stretches of proteins to minimize aberrant interactions to promote proper folding. The oxidoreductase activity of PDI proteins is carried out by thioredoxin domains containing C-x-x-C motifs (6). This enzymatic activity permits the disulfide oxidation, reduction and isomerization of newly synthesized or misfolded proteins. Formation or rearrangement of disulfides (i.e. oxidation and

isomerization) can confer stability and proper folding of newly synthesized proteins entering the ER. By contrast, reduction of disulfides can correct mistakes in disulfide formation and is hypothesized to maximize the efficiency of retrotranslocation and degradation of some misfolded ER proteins. In these cases, the disruption of disulfide bonds exposes a degradation signal or produces a more unstable substrate allowing recognition by degradation machinery (7-9). For interchain linkages, disulfide bond disruption reverses the multimerized state of a substrate prior to retrotranslocation (10).

mPyV appears to use enzymatic and chaperone activities of PDI proteins to become ‘activated’ for the initiation of membrane penetration (11-13). Previous studies, together with research described in Chapter 2, suggest that activation occurs in a series of reactions. ERp57, ERp72 and PDI can disrupt disulfides that stabilize the mPyV capsid structure. According to crystallographic data, a disulfide bond between two cysteines serves to reinforce the interpentameric interaction between VP1 C-termini (14). Disruption of this bond is likely a prerequisite for ERp29-induced conformational changes, which involves the extrusion of VP1 C-termini from neighboring pentamers and ultimately the exposure of hydrophobic VP2 proteins (12, 13). Consistent with this, the assay utilized for monitoring ERp29-dependent VP1 conformational changes requires addition of a reductant such as DTT for full activity(13). *In vitro* experiments presented in Chapter 2 demonstrate that catalytic activities of ERp57 and PDI can functionally replace DTT. From these results it appears that isomerase (ERp57) or reductase (PDI) activity allows for chaperone (ERp29) conformational changes that lead to a hydrophobic viral particle. Chaperone activities of these PDI proteins, as well as other factors, could also be used to maintain the solubility of the hydrophobic virus during targeting to the ER membrane. Thus, the various actions of PDI proteins working in a coordinated fashion leads to productive membrane penetration by mPyV.

The precise actions of ERp57, PDI and ERp29 which facilitate mPyV infection have not yet been demonstrated *in vivo*. Furthermore, the specific role of ERp72 (which does not functionally replace DTT *in vitro*) in promoting mPyV infection is unclear but may involve its chaperone or catalytic activity or both. Cell based assays that monitor conformational changes would prove useful for dissecting specific PDI roles during mPyV entry. However, the low percentage of viral particles reaching the ER limits the sensitivity and robustness of this strategy (15). Another unanswered question is whether PDI proteins also act to release the ganglioside-bound Pys into the lumen of the ER. Is this an upstream event or one concomitant with VP2 exposure? A Py particle must be released from the ganglioside receptors prior to reaching the cytosol. Optimally, this receptor-detachment step would involve the same conformational changes required for transport across the ER membrane. An assay that exploits detergent solubility differences between ganglioside-bound viruses in lipid rafts and released lumenal viruses is suitable for exploring this nuance.

ERp29 downregulation does not inhibit SV40 infection in HeLa cells (16). It is unknown what factor(s) within the ER cause VP2 exposure for SV40. It is possible that the interpentameric disulfide disruption is sufficient for VP2 exposure and membrane binding. Future studies should examine if ERp57 or other factors are involved in SV40 VP2 exposure using *in vitro* and cell based approaches. Nevertheless, the versatility of PDI family members appears to be utilized extensively during Py entry.

Cellular proteins require their correct conformation and localization to function properly. To achieve and supervise this, PQC systems assisting in the protein folding, transport and appropriate turnover are distributed widely throughout the cell. This ubiquity serves pathogens an opportunity to utilize these systems wherever needed for conformational changes or transport events. For example, Pys encounter PDI proteins in the ER lumen for conformational changes and ERAD machinery localized at the ER membrane for transport to the cytosol. The

findings presented in Chapter 3 reveal that cytosolic chaperones recruited by ER membrane proteins also function in the membrane penetration of SV40 and likely other polyomaviruses. This is the first report providing evidence that cytosolic chaperones can be utilized by nonenveloped viruses for membrane penetration.

Chaperone networks could also be utilized for membrane penetration by other nonenveloped viruses that are not trafficked to the ER but instead penetrate from the endolysosomes. For example, it is speculated that reovirus uses Hsc70 during endosomal membrane penetration (17), however this remains to be formally tested. A population of Hsc70 is described to reside on the cytosolic side of the lysosomal membrane to function in recruiting and translocating substrates of chaperone-mediated autophagy (CMA) into this digestive compartment (18). Cochaperones, including J-proteins, are not yet described in CMA but could also be co-opted with Hsc70, analogous to SV40 utilizing B14-B12 and SGTA at the ER membrane.

SGTA appears to have a variety of cellular functions as a cochaperone of heat shock proteins (19-21). Likely to be the most relevant for Py entry is the recent observation that SGTA is active during ERAD (22). Again as part of a complex, SGTA functions to promote solubility of dislocated ER proteins. This is achieved by aiding in substrate capture by the cytosolic holdase Bag6, which interacts with gp78, a core membrane component of ERAD (23). Cells with reduced levels of SGTA or Bag6 contain large aggregates of the canonical ERAD substrate TCR$\alpha$, an unassembled transmembrane protein. Additionally, *in vitro* experiments reveal that SGTA and Bag6 preferentially bind unfolded proteins and can suppress the aggregation of denatured luciferase. Currently there is no clear evidence that SGTA promotes the solubility of cytosol-localized Pys. Future research should attempt to examine this possibility further.

Upon discovering that SGTA promotes ER-to-cytosol transport of SV40, the possibility that Bag6 was important for this process was also tested. Unlike SGTA

the downregulation of Bag6 by siRNA did not affect infection. This result may indicate that a pool of SGTA has a normal cellular function at the ER membrane outside of the Bag6-associated role and that Bag6 is not important for infection. Analogously, when ERp57 was identified to be important for SV40 infection (16), it too appeared to be acting outside of its canonical function (i.e. in association with CNX and CRT, both of which are dispensable for SV40 infection).

While recently described to function in ERAD as a holdase, Bag6 was initially discovered to mediate cytosolic proteostasis. Specifically, Bag6 is central to the transmembrane recognition complex (TRC)-mediated biosynthetic pathway for membrane insertion of tail-anchored (TA) proteins and may provide a function similar to Sgt2p in the analogous GET (guided entry of TA proteins) pathway in yeast (24). These factors are involved in a cascade of hand-off reactions between chaperones that ultimately target and insert hydrophobic TA proteins into the ER membrane. As knockdown of Bag6 did not perturb SV40 infection, newly synthesized TA proteins may also be dispensable for SV40 entry. However, stable preexisting TA proteins could still be utilized by the virus for various steps of entry, including internalization, vesicular transport or membrane penetration.

The native function of SGTA-Hsc70 complexed with B14 and B12 is unknown and an important question. B14 and B12 are both implicated as factors promoting ERAD of the membrane substrate CFTR. SGTA's role in protein degradation is currently limited to recruiting dislocated substrates to the Bag6 holdase. It is possible that SGTA is functioning with B14-B12 during ERAD in parallel to its role with Bag6. In experiments monitoring ERAD, the utilization of SGTA mutants that favor interaction with one complex over another could help resolve this question. Alternatively, as GEMIN proteins and related factors were identified as putative binding partners of B14 there may be a functional connection with RNA biology and spliceosome assembly. A more rigorous screen for overlapping binding partners of B14-B12 and SGTA will provide additional insight.

Considering the ubiquity of PQC factors, what determines which factors are selected for use by an evolving Py? The answer to this question is not entirely clear. One possibility is related to one hypothesis regarding the selection of misfolded proteins for degradation among others that are unfolded but *en route* to a proper conformation. Importantly, some factors involved in folding also moonlight with a role in degradation. This suggests a mechanism where some proteins can be targeted for degradation stochastically. For example, PDI aids in the productive folding and degradation of proteins yet interacts weakly with membrane bound ERAD component Derlin-1(25). If a substrate is terminally misfolded it will have prolonged interactions with PDI and therefore have an increased chance of remaining bound to PDI during complex formation with Derlin-1. This might explain why toxins and viruses that breach the ER membrane co-opt soluble PQC units that have direct physical interactions with membrane bound retrotranslocation machinery (7). Determining whether the specific PDI-Derlin interaction (or other examples including BiP and Sel1L (26, 27)) is necessary for Py infection would formally test this hypothesis.

The selection of PQC factors that have physical linkages between the membrane and cytosol may also apply. Rescue experiments presented in Chapter 3 reveal that B14 must be able to interact with Hsc70-SGTA to promote SV40 infection. Future work could investigate the possibility that other ER membrane components used by Pys recruit distinct cytosolic factors for viral transport.

The highly abundant cytosolic AAA ATPase p97 provides the critical driving force for the mobilization of ERAD substrates into the cytosol (28). Due to several interactions with membrane-bound ERAD machinery, p97 is positioned on the cytosolic side of the ER membrane (29, 30). Together with cofactors Ufd1 and Npl4, p97 uses ATP driven chaperone activity to extract proteins and shuttle them to the proteasome. Why does SV40 require SGTA-Hsc70 and not p97-Ufd1-Npl4 for membrane penetration? One possibility is that unlike canonical

ERAD substrates, SV40 is not observed to be ubiquitinated. While p97 can engage non-ubiquitinated protein moieties, its cofactors Ufd1 and Npl4 assist in ERAD by recognizing polyubiquitin chains, rendering p97 function largely ubiquitin-selective (31). Another molecular pathogen produced by *Vibrio cholera*e, cholera toxin, disguises itself also as noncanonical ERAD substrate that is not ubiquitinated and does not require p97 for retrotranslocation (32-35). A second explanation stems from the finding that ER membrane components that recruit p97, such as Hrd1 and Derlin-1, do not reorganize into SV40-induced foci structures. Consequently, foci formation does not increase the local concentration of p97 at the site of membrane penetration where it can be co-opted.

The SV40 induced foci described previously and in Chapter 3 may represent ER exit structures for the virus, however direct evidence is still lacking. Once formed, these foci containing B14-B12, BAP31 and BiP are mostly static and contain deposits of multiple virions. Several lines of evidence from our studies suggest that foci formation has a functional role during infection. First, only factors involved in ER-to-cytosol transport of SV40 are detected within the foci. Secondly, foci formation can be detected within the time frame previously observed for cytosol arrival. Thirdly, a B14 mutant lacking most of its lumenal domain fails to reorganize into foci and also fails to promote infection in cells depleted of endogenous B14. Furthermore, BKPyV appears to localize to discrete regions within the ER, suggesting this phenomenon could be general for Pys (36).

Virus induced foci are in some ways reminiscent of a number of distinct PQC structures that have been observed in yeast and mammalian cells. Some of these PQC structures, including aggresomes, IPOD and JUNQ, are proposed to be a strategy for the cell to compartmentalize misfolded proteins and aggregates in a cytoprotective manner (37-39). These inclusions occur particularly under stress conditions where autophagy or proteasome systems are temporarily

saturated. Perhaps cellular machinery is attempting to sequester membrane-bound Pys, which appear as large aggregates. This scenario is not mutually exclusive with the putative function of foci as viral ER exit sites. In the case of the JUNQ compartment, the compartmentalized misfolded proteins are capable of diffusing out of the inclusion for refolding (38). Future studies must thoroughly examine and compare the composition of the SV40 foci with other PQC structures and investigate any potential interplay with the ubiquitin-proteasome or autophagy systems.

SGTA interacts with the B14-B12 complex in a manner dependent on Hsc70. Whether Hsc70 is directly important in mobilizing Pys into the cytosol is not known. B14 variants which cannot recruit Hsc70 (and consequently SGTA) are not able to promote infection of SV40. Minimally, Hsc70 is important for allowing SGTA to engage the virus during membrane penetration. Knockdown strategies have not been attempted due to the global role of Hsc70 in proteostasis. Although technically challenging, one essential goal of future research should be to reconstitute these later steps of membrane penetration *in vitro*. The ATP-dependence and role of Hsc70 could then be assessed directly.

In summary, the working model of membrane penetration by Pys can be elaborated in light of the presented findings. ER arrival of viral particles is met with engagement by multiple PDI family members. In the case of mPyV, ERp57 and PDI work directly to disrupt key disulfide bonds on VP1. The disruption of the C19-C114 disulfides, which clamp down the interlocking C-terminal arms, would allow ERp29 access to impart conformational changes to unlock the C-terminal arms. This ERp29-mediated reaction also results in the exposure of hydrophobic VP2, which is otherwise hidden beneath VP1 pentamers. With VP2 exposed the intact viral particle can bind to the ER membrane to initiate the penetration. VP2 embedded in the membrane triggers the reorganization of BAP31, B14 and B12 in the ER membrane. These factors, along with lumenal BiP, cluster in close proximity to viral particles to form foci. Conformational changes induced by BiP

binding and release cycles may allow the virus to become exposed to the cytosol. The J-domains of complexed B14-B12 recruit cytosolic chaperones, including SGTA, to bind and mobilize some particles out of the membrane. The foci therefore serve to transiently increase the concentration of cytosolic chaperones at the site of ER exit. SGTA-Hsc70 may also promote the disassembly of cytosol localized Pys to facilitate viral genome exposure and nuclear transport.

## FIGURES

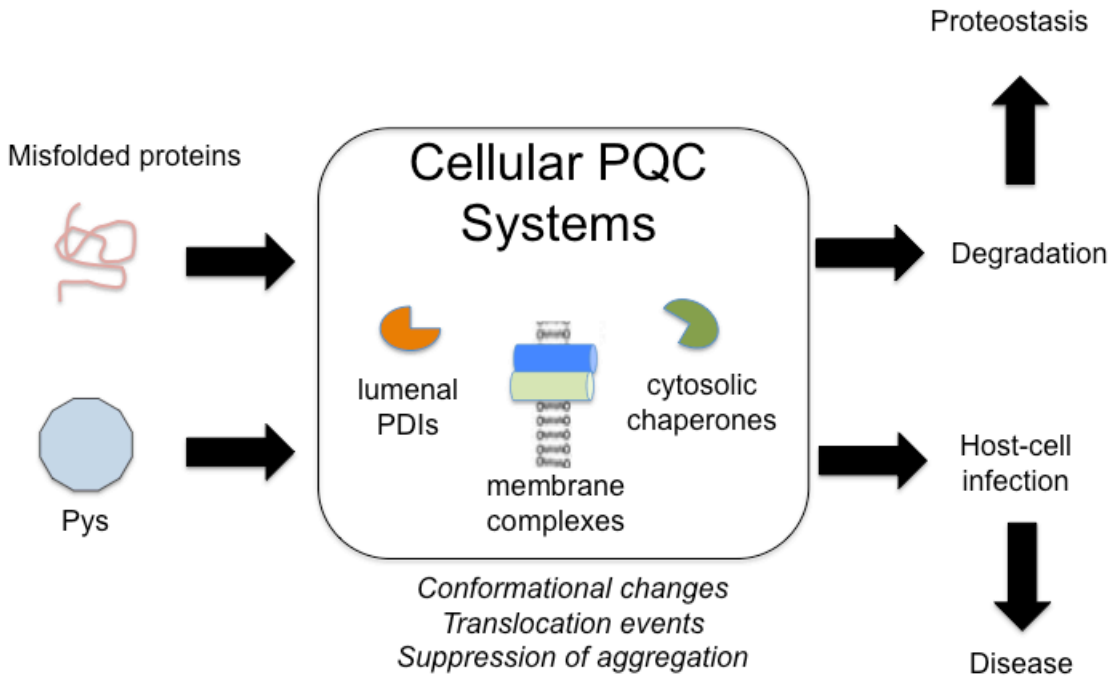


**Figure 4-1. Conceptual Overview of PQC in Py Entry and Proteostasis**

Several similarities are evident between the elimination of misfolded proteins and ER membrane penetration by Pys. Both require multiple networks of PQC machinery that contribute distinct functions during the process. While the destruction of misfolded proteins maintains cellular proteostasis, Py infection can ultimately lead to cell lysis or transformation.

## REFERENCES


1. Appenzeller-Herzog C & Ellgaard L (2008) The human PDI family: versatility packed into a single fold. *Biochimica et biophysica acta* 1783(4):535-548.

2. Forster ML*, et al.* (2006) Protein disulfide isomerase-like proteins play opposing roles during retrotranslocation. *J Cell Biol* 173(6):853-859.

3. Tsai B, Rodighiero C, Lencer WI, & Rapoport TA (2001) Protein disulfide isomerase acts as a redox-dependent chaperone to unfold cholera toxin. *Cell* 104(6):937-948.

4. Spee P, Subjeck J, & Neefjes J (1999) Identification of novel peptide binding proteins in the endoplasmic reticulum: ERp72, calnexin, and grp170. *Biochemistry* 38(32):10559-10566.

5. Meunier L, Usherwood YK, Chung KT, & Hendershot LM (2002) A subset of chaperones and folding enzymes form multiprotein complexes in endoplasmic reticulum to bind nascent proteins. *Mol Biol Cell* 13(12):4456-4469.

6. Bulleid NJ & Ellgaard L (2011) Multiple ways to make disulfides. *Trends Biochem Sci* 36(9):485-492.

7. Walczak CP, Bernardi KM, & Tsai B (2012) Endoplasmic Reticulum-Dependent Redox Reactions Control Endoplasmic Reticulum-Associated Degradation and Pathogen Entry. *Antioxid Redox Sign* 16(8):809-818.

8. Okuda-Shimizu Y & Hendershot LM (2007) Characterization of an ERAD pathway for nonglycosylated BiP substrates, which require Herp. *Mol Cell* 28(4):544-554.

9. Chen X*, et al.* (2011) Processing and turnover of the Hedgehog protein in the endoplasmic reticulum. *J Cell Biol* 192(5):825-838.

10. Ushioda R*, et al.* (2008) ERdj5 is required as a disulfide reductase for degradation of misfolded proteins in the ER. *Science* 321(5888):569-572.

11. Walczak CP & Tsai B (2011) A PDI family network acts distinctly and coordinately with ERp29 to facilitate polyomavirus infection. *J Virol* 85(5):2386-2396.

12. Rainey-Barger EK, Magnuson B, & Tsai B (2007) A chaperone-activated nonenveloped virus perforates the physiologically relevant endoplasmic reticulum membrane. *J Virol* 81(23):12996-13004.

13. Magnuson B*, et al.* (2005) ERp29 triggers a conformational change in polyomavirus to stimulate membrane binding. *Mol Cell* 20(2):289-300.

14. Stehle T, Yan Y, Benjamin TL, & Harrison SC (1994) Structure of murine polyomavirus complexed with an oligosaccharide receptor fragment. *Nature* 369(6476):160-163.

15. Qian M, Cai D, Verhey KJ, & Tsai B (2009) A lipid receptor sorts polyomavirus from the endolysosome to the endoplasmic reticulum to cause infection. *PLoS Pathog* 5(6):e1000465.

16. Schelhaas M*, et al.* (2007) Simian Virus 40 depends on ER protein folding and quality control factors for entry into host cells. *Cell* 131(3):516-529.

17. Ivanovic T, Agosto MA, Chandran K, & Nibert ML (2007) A role for molecular chaperone Hsc70 in reovirus outer capsid disassembly. *J Biol Chem* 282(16):12210-12219.

18. Kaushik S & Cuervo AM (2012) Chaperone-mediated autophagy: a unique way to enter the lysosome world. *Trends in cell biology* 22(8):407-417.

19. Tobaben S*, et al.* (2001) A trimeric protein complex functions as a synaptic chaperone machine. *Neuron* 31(6):987-999.

20. Leznicki P*, et al.* (2013) The association of BAG6 with SGTA and tail-anchored proteins. *PloS one* 8(3):e59590.

21. Leznicki P & High S (2012) SGTA antagonizes BAG6-mediated protein triage. *Proc Natl Acad Sci U S A* 109(47):19214-19219.

22. Xu Y, Cai M, Yang Y, Huang L, & Ye Y (2012) SGTA recognizes a noncanonical ubiquitin-like domain in the Bag6-Ubl4A-Trc35 complex to promote endoplasmic reticulum-associated degradation. *Cell Rep* 2(6):1633-1644.

23. Wang Q*, et al.* (2011) A ubiquitin ligase-associated chaperone holdase maintains polypeptides in soluble states for proteasome degradation. *Mol Cell* 42(6):758-770.

24. Denic V (2012) A portrait of the GET pathway as a surprisingly complicated young man. *Trends Biochem Sci* 37(10):411-417.

25. Bernardi KM, Forster ML, Lencer WI, & Tsai B (2008) Derlin-1 facilitates the retro-translocation of cholera toxin. *Mol Biol Cell* 19(3):877-884.

26. Hagiwara M*, et al.* (2011) Structural basis of an ERAD pathway mediated by the ER-resident protein disulfide reductase ERdj5. *Mol Cell* 41(4):432-444.

27. Williams JM, Inoue T, Banks L, & Tsai B (2013) The ERdj5-Sel1L complex facilitates cholera toxin retrotranslocation. *Mol Biol Cell* 24(6):785-795.

28. Ye Y, Meyer HH, & Rapoport TA (2001) The AAA ATPase Cdc48/p97 and its partners transport proteins from the ER into the cytosol. *Nature* 414(6864):652-656.

29. Ye Y*, et al.* (2005) Recruitment of the p97 ATPase and ubiquitin ligases to the site of retrotranslocation at the endoplasmic reticulum membrane. *Proc Natl Acad Sci U S A* 102(40):14132-14138.

30. Lilley BN & Ploegh HL (2005) Multiprotein complexes that link dislocation, ubiquitination, and extraction of misfolded proteins from the endoplasmic reticulum membrane. *P Natl Acad Sci USA* 102(40):14296-14301.

31. Ye Y, Meyer HH, & Rapoport TA (2003) Function of the p97-Ufd1-Npl4 complex in retrotranslocation from the ER to the cytosol: dual recognition of nonubiquitinated polypeptide segments and polyubiquitin chains. *J Cell Biol* 162(1):71-84.

32. Bernardi KM, Williams JM, Inoue T, Schultz A, & Tsai B (2013) A deubiquitinase negatively regulates retro-translocation of nonubiquitinated substrates. *Mol Biol Cell* 24(22):3545-3556.

33. Kothe M*, et al.* (2005) Role of p97 AAA-ATPase in the retrotranslocation of the cholera toxin A1 chain, a non-ubiquitinated substrate. *J Biol Chem* 280(30):28127-28132.

34. Rodighiero C, Tsai B, Rapoport TA, & Lencer WI (2002) Role of ubiquitination in retro-translocation of cholera toxin and escape of cytosolic degradation. *EMBO reports* 3(12):1222-1227.

35. Moore P, He K, & Tsai B (2013) Establishment of an In Vitro Transport Assay That Reveals Mechanistic Differences in Cytosolic Events Controlling Cholera Toxin and T-Cell Receptor alpha Retro-Translocation. *PloS one* 8(10):e75801.

36. Bennett SM, Jiang M, & Imperiale MJ (2013) Role of cell-type-specific endoplasmic reticulum-associated degradation in polyomavirus trafficking. *J Virol* 87(16):8843-8852.

37. Bagola K & Sommer T (2008) Protein quality control: on IPODs and other JUNQ. *Current biology : CB* 18(21):R1019-1021.

38. Kaganovich D, Kopito R, & Frydman J (2008) Misfolded proteins partition between two distinct quality control compartments. *Nature* 454(7208):1088-1095.

39. Kopito RR (2000) Aggresomes, inclusion bodies and protein aggregation. *Trends in cell biology* 10(12):524-530.